Ecole polytechnique federale de Lausanne

School of Life Sciences

Master's project in Life Sciences and Technology

Intracardiac organization indices for the monitoring of atrial fibrillation

Done by

Sarah Volorio

Under the direction of

Dr. Jean-Marc Vesin and Andrea Buttu

In the Signal Treatment Laboratory LTS 1

EPFL

External expert: Dr. Etienne Pruvot from the Cardiology Department of CHUV

LAUSANNE, EPFL, 2010-2011

Acknowledgements

I would like to thank the director of my master thesis, Dr. Jean-Marc Vesin for giving me the possibility of working at the Laboratory of Signal Treatment. I would like to thank Dr. Jean-Marc Vesin and Andrea Buttu for their availability, their patience and their kindness during the master thesis.

I would like also to thank Dr. Etienne Pruvot, and Dr. Andrei Forclaz for the time they spent to follow my work and the medical staff of the CHUV for their kindness during the ablation procedures.

A special thank to Dr. Laurent Uldry and Jérôme Van Zaen who were always available for any question on matlab or latex. I would like to thank the other collaborators of the research group, Maîtresse Aline Cabasson, Anne Piatti, Dr. Cédric Duchêne, Dr. Florian Jousset, Dr. Mathieu Lemay, Dr. Yann Prudat, and Alain Viso for their kindness and their good mood.

Abstract

Atrial fibrillation (AF) is the most common arrhythmia observed in clinical practice. It is responsible for about one third of hospitalizations related to problems of arrhythmia. AF is an important clinical entity due to the increased risk of morbidity and mortality. The consequences of AF most frequently found are hemodynamic function impairment (loss of atrial synchronized contraction, irregular and inadequately rapid ventricular rate), atriogenic thromboembolic events and tachycardia induced atrial and ventricular cardiomyopathy. With the present increase of life expectancy, AF prevalence is expected to double in the next fifty years, in particular in western countries.

In collaboration with the Division of Cardiology of CHUV, a catheter ablative protocol mainly based on pulmonary vein isolation (PVI) and complex fractionated elctrograms ablations was defined in order to develop new strategies to decrease procedural time and ablation extent. More precisely, surface EGC as intracardiac electrogram (EGM) signals were recorded from different catheters at specific locations before ablation during and after PVI. The purpose of this project is to evaluate the ability of known (AF cycle length) and new intracardiac organization indices based on recorded surface ECGs and EGM signals to monitor AF organization during stepwise ablation of persistent AF.

Contents

List of Figures

List of Tables

Chapter 1

Physiology of the heart

The heart is one of the most important organs. It is considered as the human body motor, essential to a normal developement and life. More precisely, the heart is a cardiac striated muscle localized in the mediastinum which functions like a pump. Venous return arrives into heart by the inferior and superior cava vena in order to be re-oxygenated in the lungs. The oxygenated blood comes back into the heart and is ejected into the systemic circulation via the aorta. The mean cardiac rate is between 60 and 100 beats per minute which represents a blood flow of about 5 litres. The heart has the characteristic to be independent from the central nervous system but its modulation can be controlled by the autonomic nervous system. Acetylcholine released by parasympathetic innervations has the capacity to decrease heart rate while adrenaline as noradrenaline liberation from sympathetic nerves increases heart rhythm (see figure 1.1).

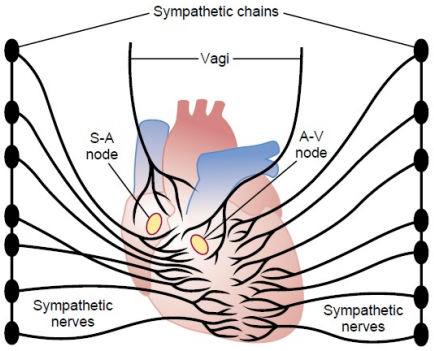

Figure 1.1: *The heart with the parasympathetic and sympathetic nerves.* [15]

1.1 Cellular biology

1.1.1 Pacemaker cells

Pacemaker (P) cells are specific cardiomyocytes responsible for heart depolarization and cardiac frequency. They are principally localized in small amount

at the sinusoatrial (SA) and atrioventricular (AV) nodes. They rhythmically and spontaneously elicit action potentials and orderly propagate them throughout the heart.

P cells resting membrane voltage is approximatively -60 mV. It is due to a continuous efflux of K^+ ions via the K^+ channels. Depolarization is initiated by a decrease of K^+ permeability. The consequences are an entry of a slow influx of Na^+ into P cells via Na^+ channels and a generation a slow depolarization called pre-potential. When the pre-potential reaches the exciting threshold of -40 mV, Ca^{2+} enter into P cells via Ca^{2+} channels. In these conditions, an action potential is elicited and the generated electrical current is further propagated. P cells return to their resting potential because Ca^{2+} permeability decreases while K^+ permeability increases (see figure 1.2).

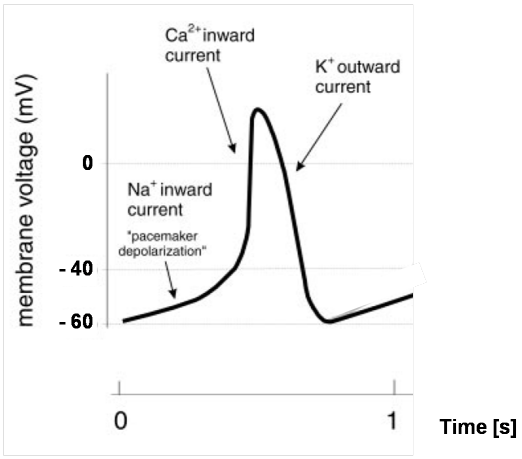

Figure 1.2: *Pacemaker action potential at the sinusoatrial node.* [25]

1.1.2 Cardiomyocytes

Transmission of P cells depolarization to cardiomyocytes produces a voltage change. Indeed, cardiomyocytes resting membrane potential which is normally -90 mV becomes positive and reaches +20 mV. The consequence is the eliciting of an action potential which is caused by a large ions influx of two specific types of channels:

- Fast Na^+ channels. These channels are described as fast because the time between their opening and their closure is very short.
- Slow Ca^{2+} channels. They are described as slow because they need more time to open but also they remain longer open.

Cardiomyocytes depolarization is characterized by a plateau during which cardiomyocytes are in a refractory period. In others words, during this period, others stimulations cannot be processed before the end of the ongoing excitation. At the end of an action potential, Ca^{2+} permeability becomes weaker while

K^+ permeability becomes stronger. This leads to Ca^{2+} channels closure, K^+ channels opening and so, a return of cardiomyocytes to their resting membrane potential (see figure 1.3).

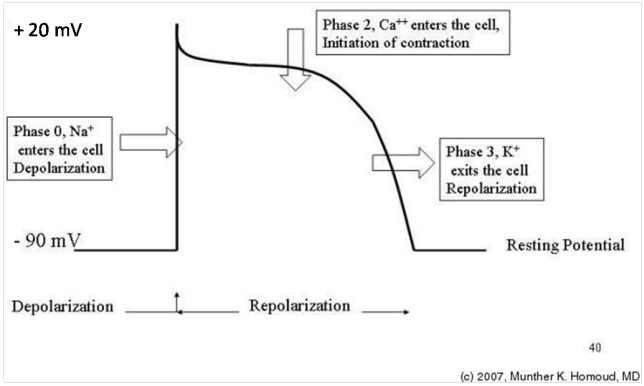

Figure 1.3: *Cardiomyocyte action potential.* [2]

Action potential generated in cardiomyocytes propagates quickly in neighboring cardiac cells. The propagation is facilitated because cardiomyocytes form a syncytium through which communication is done via electrical synapses called gap-junctions. Due to their very small resistance, gap-junctions improve efficiently cell to cell conduction of intracellular current. The final heart response to this whole electrical activity is the heart contraction.

1.1.3 Contraction

Cardiomyocytes cytoskeleton is composed of thin and thick filaments. Thin filaments are constituted of double-stranded α-helical polymer of actin molecules. Two helical α filaments coiling around each other formed tropomyosin which is localized on actin filaments. Troponin molecules interact not only with tropomyosin but also with actin filaments. Thick filaments are composed of two intertwinded α-helices of myosin-II molecules at the end of which two heads are capable to interact with actin filament at specific binding sites (see figure 1.4).

As mentionned previously, depolarization of P cells permits the opening of Ca^{2+} channels localized inside P cells and more precisely in the membrane of the sarcoplasmic reticulum which is an intracellular Ca^{2+} reserve. As consequence, a large flow of Ca^{2+} ions goes out of the sarcoplasmic reticulum into the cytosol. This leads to a strong increase of intracellular Ca^{2+} concentration. By binding troponin, Ca^{2+} involves a conformation change of tropomyosin on actin filaments permitting the liberation of binding sites for myosin heads (see figure 1.5).

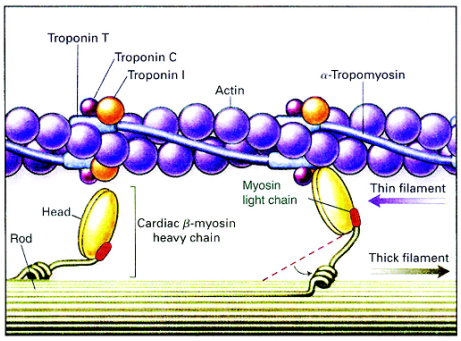

Figure 1.4: *Thin and thick filaments involved in the cardiac muscle contraction.* [1]

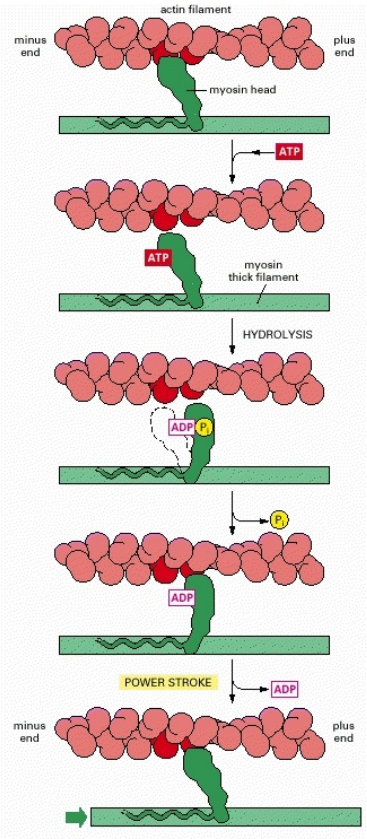

Figure 1.5: *Contraction cycle.* [5]

At the end of the contraction cycle, myosin heads are tightly bound on actin filaments. Very rapidly, molecules of adenosine triphosphate (ATP) bind myosin heads. Like this, myosin affinity for actin filaments becomes weaker.

The consequence is myosin heads and actin filaments dissociations. In these conditions, heart muscle is relaxed. However, when ATP on myosin heads is hydrolyzed, it is transformed into adenosine diphosphate (ADP) and inorganic phosphate (Pi). This biochemical transformation involves a weak binding of myosin heads onto actin filaments new sites. Simultaneously with the Pi release, myosin heads strengthen their position by binding tightly actin filaments. It generates the "power stroke". This generated force coordinates contraction of all heart muscle fibers. Finally, myosin heads change position to recover their original conformation on actin filaments and loose ADP molecules. In these conditions, myosin heads remain tightly bound to actin filaments and a new contraction cycle can begin (see figure 1.5).

1.2 Propagation of cardiac action potential

P cells frequency discharge is not homogenous in heart tissue. P cells with the fastest discharge are localized in the SA node. This region is called the primary heart rhythmogen center. The action potential generated in the SA node propagates into the AV node via the internodal pathways. AV node is described as the second heart rhythmogen center also capable to generate spontaneously and regularly action potentials. It can replace SA node only if the latter fails in its discharge activity. However, frequency discharge is slower at the AV node than at the SA node. After the AV node excitation, the action potential reaches the bundle of His. The latter is divided in two parts, the right and the left bundle branches.The generated electrical current follows its path along the septum, passing through the right and left branches until the heart apex. Once the action potential reaches heart apex, it propagates along the ventricular walls via the Purkinje fibers (see figure 1.6).

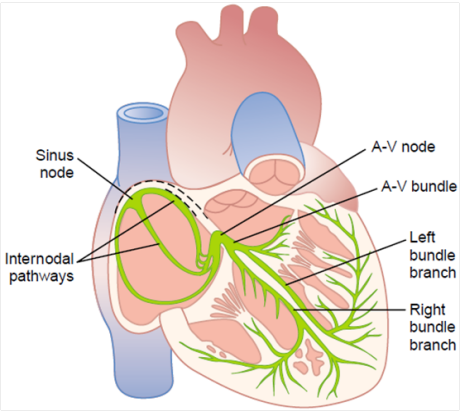

Figure 1.6: *Propagation of the cardiac action potential through the conductive system of the heart.* [15]

1.3 Cardiac cycle

The cardiac cycle is composed of two periods. The first one is called the diastole which is a relaxation periode during which heart is passively filled with blood. The second period is called the systole which is the active state characterized by the heart contraction.

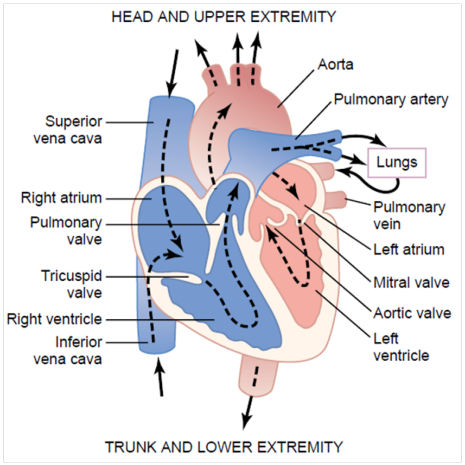

Figure 1.7: *The heart structure and course of blood flow through the heart.* [15]

Heart is principally composed of four main cavities:

- Right atrium (RA)
- Left atrium (LA)
- Right ventricle (RV)
- Left ventricle (RL)

During diastole, venous return coming from the superior and the inferior cava vein fills directly the right ventricle passing through the RA and the tricuspid valve. The atrial contraction permits a supplementary ventricular filling. At the end of the atrial contraction the tricuspid valve closes and the ventricles contract. Pulmonary valve opening permits deoxygenated blood to reach lungs via the pulmonary arteries in order to be purified. Blood re-oxygenation takes place at the alveolo-capillary membrane by gas diffusion.

From the pulmonary veins, the re-oxygenated blood returns directly into the left ventricle passing through the LA and the mitral valve. The ventricular contraction pushes the blood into the aorta via the aortic valve. From the aorta, the blood is ejected out of the heart and vascularizes all the tissues (see figure 1.7).

1.4 Normal electrocardiogram

The heart electrocardiogram (ECG) is defined as a voltage recording of heart electrical activity. By placing electrodes on the patient chest, the physician can read the potential travelling through the heart.

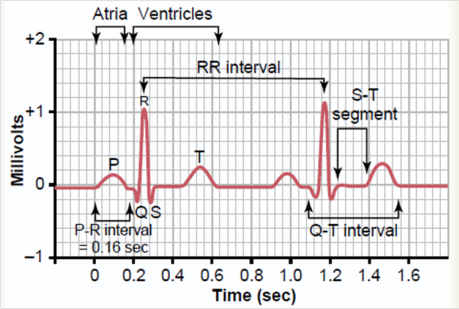

Figure 1.8: *Normal electrocardiogram of two heart beats.* [15]

First, there is the depolarization of atria characterized by the P wave. The QRS complex represents the depolarization and the contraction of ventricles. Because electrical activity is more sustained in the ventricular muscles than in the atria muscles, atria repolarisation is hidden in the QRS wave. Finally, the T wave characterizes the repolarization of ventricles (see figure 1.8).

The PR interval gives the time necessary for the electrical wave to travel from the SA node to the AV node. The heart rate is given by the RR interval which should be between 60 and 100 beats per minute as mentionned previously. The QT interval represents the depolarization and the repolarization of ventricles while the ST segment characterizes the beginning and the end of ventricles repolarization.

Chapter 2

The pathology of atrial fibrillation

2.1 Definition

Atrial fibrillation (AF) is characterized by rapid and irregular activations of the atrial cells with a rate between 400 to 600 times per minute [31]. The consequence of this high rate of discharge is the presence of irregular fibrillatory waves and uncoordinated contractions in atria [11]. At long term, one of the main consequences is an electrical remodelling of the atria promoting the self-sustaining of the AF [9].

2.2 Epidemiology

AF is the most common caridac arrhythmia. Its prevalence and incidence become larger with age [7] [38]. In Switzerland, AF affects 4% of people aged 60 and more. It increases by 10% for people aged more than 85 [4]. Other risk factors as male sex, a history of stroke, diabetes, hypertension, congestive heart failure, rheumatic and nonreuhmatic valve disease, and myocardial infarction seem to play important roles as predictors of AF [7] [38]. The consequences of this disease are an increase of morbidity and frequent hospital admissions of patients. In these conditons, life quality can be severly reduced [11] [42]. High risk of mortality in both sexes is associated with AF [7] [38] [42].

2.3 Classification

After a first detected episode, AF is classified according to three types [11] :

- Paroxysmal AF is defined as recurrent AF ($\geq$ 2 episodes) that terminates spontaneously within seven days.
- Persistent AF is defined as AF which is sustained beyond seven days, or lasting than seven days but necessitating pharmacologic or electrical cardioversion.

- Longstanding persistent AF is defined as continous AF of greater than one-year duration.

2.4 Mechanisms

AF mechanisms are still not yet well understood. Initiators and AF propagation modes especially remain partially unknown. There are conceptual models which attempt to explain AF mechanisms.

In 1964, Moe and al. suggested the multiple wavelet hypothesis as dominant AF mechanism. According their theory, AF is initiated by unidirectionnal propagation of impulses about an obstacle and is sustaining by a minimal number of random re-entrant wavelets in both atria. The number of wavelets and so AF maintenance depends on the mass of the tissue, the duration of refractory period and the conduction velocity. From these features, the wavelength can be defined as the product of the refractory period and the conduction velocity. It means that a pathlength circuit shorter than the wavelength elicits its disappearance and so, AF termination. Therefore, the wavelength is considered as the shortest distance travelled by the wave in one refractory period which can sustain a re-entry. [11] [28] [31]

In 1976, Allessie and al. developed the "leading circle" concept. Without the presence of an anatomical obstacle, the center of a circle movement (mother wavelet) is maintening by a continuously and naturally re-entering of centripetal wavelets (daugther wavelets). The global effect is a persistent rotating of the mother wavelets in clockwise or couterclockwise direction. Because the "leading circle" center is too small to sustain the rotating movement, the daughter wavelets collide at the center and travel from the center to the periphery increasing the length of the circular pathway. Size circuit is not fixed, it can change with electrophysiological properties. Therefore, the minimal circuit size can be described as the "leading circle" in which the head of the mother wavelet is capable to excite its tail in refraction period. [6] [31]

In opposition to Moe and Allessie concepts, Berenfeld and Jalife research group suggested a periodic mechanism. Micro-entrant sources of high frequency periodic activity are present during AF. They are described as mother rotors. The latter propagate in both atira and collide each other or with anatomical obstables. The consequences are fragmentation and daugther wavelets formation leading to an aperiodic process charcterizing AF. [24] [27] [31]

The landmark observation in AF mechanisms comes from the study of Haïssaguerre and his colleagues in 1994. They suggested that AF is elicited by single focal mechanisms that can be treated by radiofrequency (RF) catheter ablations. They reported three cases where AF presented localized mechanisms [11] [16] [22]. Further investigations in patients with paroxysmal AF demonstrated that focal sources were characterized with a very fast firing activity [22]. In 1998, Haïssaguerre and al. found the earliest sources of ectopic beats in the pulmonary veins of nine patients affected with paroxysmal AF. The pul-

monary veins were considered as th main initiators of AF and also the dominant re-initiating triggers of AF in patients with chronic AF [18]. These foci can be efficiently eliminate by discrete RF catheter abaltions [11] [17] [31]. Moreover, electron microscopy studies of human pulmonary veins with AF history demonstrated presence of P cells, transitional cells and Purkinje cells in human pulmonary veins of patients with AF. This discovery tends to confirm the AF initiator role of the pulmonary veins [35].

In conclusion, AF is a complex illness which does not only arise from one mechanism. The focal mechanism demonstrated by Haïssaguerre and al. is now well accepted by the medical and research community. However, multiple re-entry mechanisms remain partially unclear and need further investigations. There is still the possibility that the mechanisms presented above are all involved in AF [31].

2.5 Treatments

Treatments depend on the type and the severity of AF. They can be used to increase survival and improve life quality of patient.

First lines of treatment are antiarrythmic drugs (AAD) which are often combined with anticoagulant drug in order to prevent blood clot formation. AAD attempt to cease AF activity by prolonging the refractory period. Another treatment is the cardioversion which attempts to restore sinusal rhythm by focal electrical shocks on patient chest. It is also often conjugated with AAD and anticoagulant drugs. If heart rate is too slow in patients with AF, there is also the possibility to implant a pacemaker in order to control the cardiac frequency. The main disadvantage of AAD and cardioversion treatments is their short-term duration which is not the case with an ablation procedure. [4]

When patients becomes AAD resistant or AAD intolerant and are good potential candidates, an AF ablation strategy is undertaken. Increase of AF cycle length with discrete RF catheter ablations is highly correlated with AF termination [19]. However, pulmonary veins isolation is sometimes insufficient to cure efficacy patients affected with persistent and longstanding persistent AF. In this case, additionnal substrate ablations in left atrial after pulmonary veins isolation are necessary to completely restore sinusal rhythm. Mitral isthmus, left artial roof, left superior vena cava and coronary sinus are also known as arrythmogenic sources in patients with AF. Their isolation conjugated with pulmonary veins disconnection demonstrate better cure rate [13] [20] [21] [23].

Catheter ablation becomes a more and more frequent procedure to treat AF [12]. It seems to be more efficient than AAD therapy. Indeed, ablation strategy increases survival, improves life quality, and drecreases the need for a re-hospitalization [30] [32] [37] [34]. Therefore, should ablation strategy become first-line therapy for some patients? Opinions diverge about this question [40]. Today, it is not possible to reply to this question by a simple yes or no. It remains parameters that are yet not well understood and controlled. Therefore,

further investigations comparing the cost and the efficacy between AAD therapy and ablation strategy on long term are necessary [26].

2.6 Complex fractionated atrial electrograms

Complex fractionated atrial electrograms (CFAEs) are specific waves susceptible to be at the origin of AF maintenance. They are correlated with areas of slowed conduction and pivot points of re-entrant wavelets, and characterized by a relatively short cycle length (120 msec on average). However, the exact mechanism of CFAEs is poorly understood yet. Nademanee and al. suggested to use CFAEs as target sites for RF ablations [29]. Nevertheless, there is still no precise guideline justifying culprit and non culprit CFAEs. Today, they are ablated according to the physician expertise.

Chapter 3

Materials and methods

3.1 Study protocol

The ablative protocol was developed in collaboration between Dr. Etienne Pruvot and Dr. Andrei Forclaz from the Cardiology Department of the Hospital Center of Vaud (CHUV) and Andrea Buttu and Dr. Jean-Marc Vesin from the Swiss Institute of Technology of Lausanne (EPFL). It was approved by the Swiss Ethical Committee.

3.1.1 Pre-ablation

Twelve standard leads (V1 to V6 and the three derivations, I, II, and III) are commonly placed on patient chest to continuously record surface ECG during the whole intervention. An extra lead is added on the patient back to improve recording of the antero-posterior activity of atria. Moreover, other catheter is introduced via the right femoral vein and placed at different positions in the atria. The latter records intracardiac electrogram (EGM) signals. Table 3.1 summarizes the intracardiac catethers used during the medical intervention and their position in the atria. Using surface leads and intracardiac electrodes presents a great advantage. Indeed, it brings simultaneously two types of information. The surface ECG returns a global information of the heart activity while EGM signal yields a local information on AF.

The next step consists in reconstructing the LA, the LAA and the PVs of the patient heart in a 3 dimension (3D) model using Lasso catheter and the CARTO 3 Navigation System developed by Biosense Webster, a Johnson & Jonhson compagny. This 3D reconstruction as presented in figure 3.1 is very helpful for the physician. He can identify specific catheter locations in order to record signals at precise positions and perform accurate ablations.

Finally, ECG and EGM signals of about 20 seconds are simultaneously recorded at specific locations in the LA via the surface leads and the Lasso catheter respectively. These acquisitions are necessary in order to define a precise baseline of the patient AF before catheter ablation. Here is the list of the

Intracardiac catheters			
Catheter	**Electrode**	**Location**	**Comment**
CS †	CSd 1-2, CS 3-4, CS 5-6, CS 7-8, CSp 9-10	Coronary sinus vein	CSp 9-10 is placed at the ostium. Decapolar catheter, 5-5-5 mm
Lasso †	Lasso 1-2, Lasso 3-4, Lasso 5-6, Lasso 7-8, Lasso 9-10, Lasso 10-1, Lasso 11-12, Lasso 13-14, Lasso 15-16, Lasso 17-18, Lasso 19-20	Diverse	Circular catheter composed of 20 poles
MAP †	MAPd, MAPp	Diverse	Irrigated and cooled-tip radiofrequency catether for mapping and ablation
HRA ‡	HRAd, HRAp	Right atrial appendix	Quadripolar catheter, 2-5-2 mm

d = distal

p = proxymal

† *Catheter from Biosense Webster, a Johnson & Johnson compagny*

‡ *Catheter from St. Jude Medical*

Table 3.1: *Main features of the intracardiac catheters.*

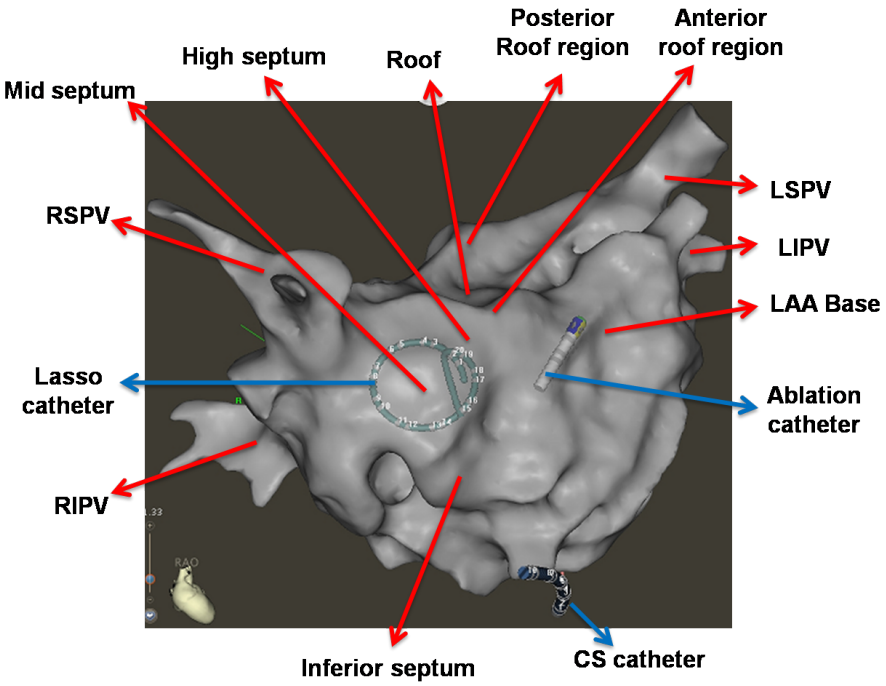

Figure 3.1: *Reconstruction in a 3 dimension of the left atrium, the left atrium appendage, and the pulmonary veins, right anterior view.*

thirteen different locations that the physician has to check during pre-ablation:

- Left superior pulmonary vein (LSPV) ostium
- Left inferior pulmonary vein (LIPV) ostium
- Right superior pulmonary vein (RSPV) ostium
- Right inferior pulmonary vein (RIPV) ostium
- LAA base
- Anterior roof region
- Posterior roof region
- Mid posterior roof region
- Mid inferior roof region
- Mitral isthmus (MI)
- Mid septum
- High septum
- Inferior septum

3.1.2 Ablation

A tag with a specific color is added on the 3D reconstruction depending to the nature of the ablation. For example, if the discrete RF is applied to a pulmonary vein in order to isolate it, a red tag is placed on the 3D reconstruction at the ablation location as illustred on figure 3.2. At the end of the medical intervention, the 3D reconstruction is filled with colored tags. This represents a summary of all the ablations locations performed in the patient atria. It is helpful for the physician if he has to re-operate a patient. Indeed, he already knows where previous ablations were performed.

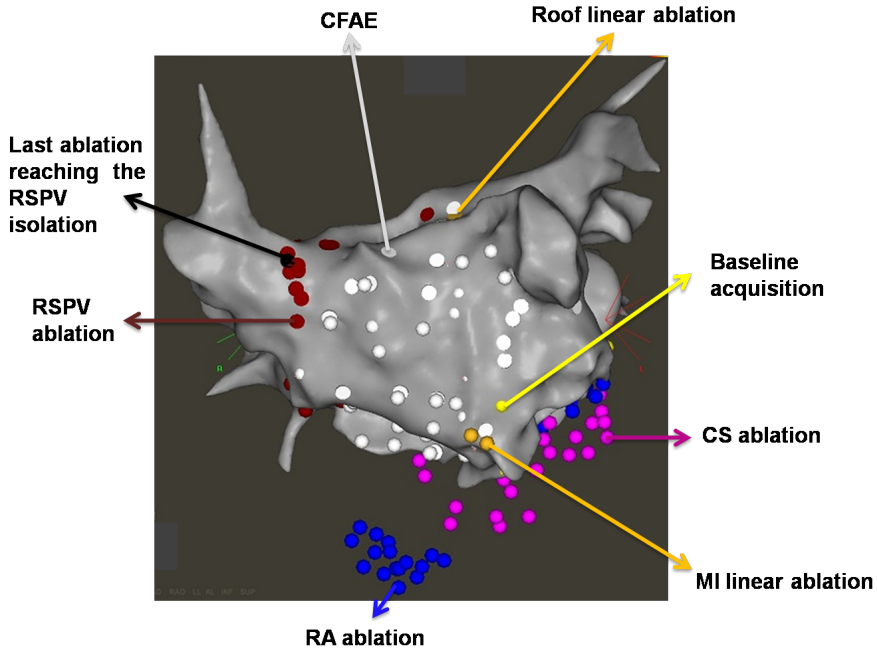

Figure 3.2: *Tags of the ablations performed during the medical procedure in the atria, posterior anterior view.*

If at any step of the ablation protocol the patient reaches sinusal rhythm or atrial tachycardia, the physician stops ablating. Before terminating the medical intervention, the physician has to verify rhythm regularity at the previous ablated locations in order to validate safely the procedural success. Ablation is composed of two main parts:

- Pulmonary veins isolation (PVI)
- Post pulmonary veins isolation (post PVI)

3.1.2.1 Pulmonary veins isolation

PVs are electrically disconnected one by one by specific ablations. The electrodes of the Lasso catheter are placed at the ostium of a PV and they return

to the physician via the computer screen the locations which have to be ablated in order to prevent the propagation of their electrical activity in LA. A PV is considered isolated when the Lasso catheter placed at its ostium does not return any signal on the computer screen. In this case, the Lasso catheter is displaced into the LAA to record signals for a duration of about 30 seconds. During this time, the physician can quantify whether an organization took place by caclulating the AF cycle length (AFCL) and comparing it with a previously computed AFCL. If the new measure is larger than the previous one, it means that the LA is becoming more organized.

3.1.2.2 Post pulmonary veins isolation

The post PVI stage is composed of several types of ablation in order to prevent the propagation of the waves in the atria.

Complex fractionated atrial electrograms ablation After PVI and for the rest of the medical intervention, the Lasso catheter remains in the LAA. Then, the physician removes complex fractionated atrial electrograms (CFAEs) by discrete RF ablations. CFAEs are identified as such according to the physician expertise at the following locations:

- Posterior LA
- Anterior LA
- Septal LA
- Lateral LA
- Inferior along the CS (CS disconnection)
- Base of the LAA / post ridge

Linear ablation The second post PVI ablation consists in performing linear ablations on the roof and the MI in order to prevent wave propagation.

Coronary sinus ablation The next location to disconnect is the epicardial CS which defines the limit between the LA and LV. As for the PVI, discrete RF ablations are applied at the CS until no more activity is are visible on the computer screen for the five electrodes of the CS catheter.

Right atrium ablation The last location to ablate is the RA, if the AFCL in the RAA is shorter than the AFCL in the CSp. In this case, the cavotricuspid isthmus and also CFAEs in the RA are ablated.

At the end of the ablation protocol, if the patient manages to reach sinusal rhythm or atrial tachycardia, the intervention is considered as a success. However, if the patient rhythm remains irregular after the whole ablation protocol, the intervention ends in failure. In this case, the patient is cardioversed. To validate the procedural success or the failure of the medical procedure, the physician

has to verify the electrical activity at the PVI, the LAA, the roof, the MI and also the CS. The figure 3.3 summarizes the main steps of the ablation protocol.

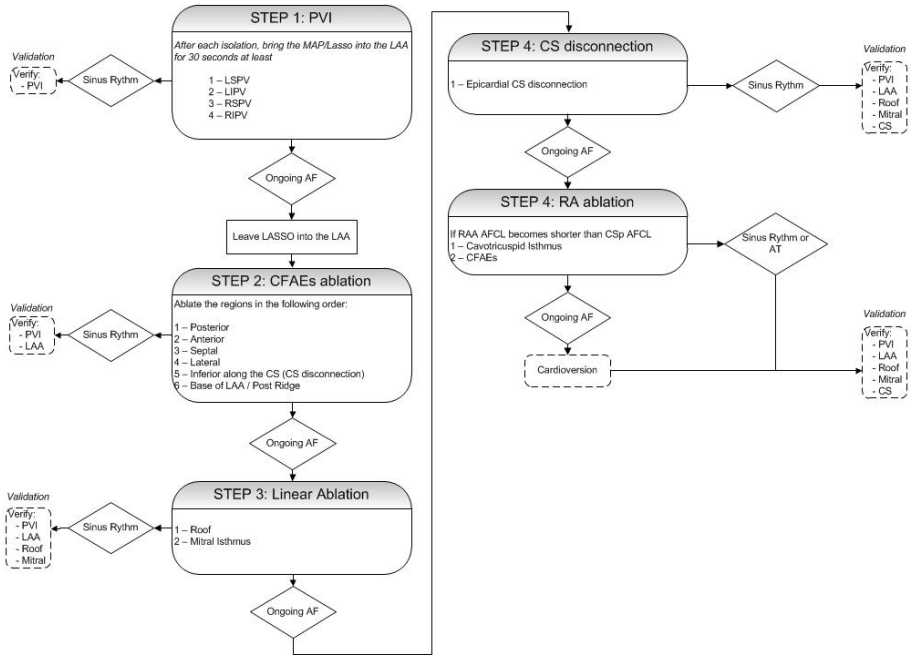

Figure 3.3: *Main steps of the ablative protocol.* [10]

3.2 Patients

Six patients with persistent AF participated in the electrophysiological study. They all approved the study ablation protocol by a written informed consent. The patients were operated by Dr. Etienne Pruvot and Dr. Andrei Forclaz at CHUV. Table 3.2 presents the main features of these six patients.

3.3 Signal processing

ECG and EGM signals were sampled at a frequency of 2 kHz and simultaneously recorded during the intervention. It means that an EGM signal is always associated with the surface ECG. Then, signals were processed by a program written by Andrea Buttu in order to be compatible with the Matlab environment. Moreover, the program not only recorded one signal per catheter but also extracted the name, the time instant (with an accuracy in seconds) and the location of the event. All these informations were used to define the file name of the recording (see the example on figure 3.4). From the ECG file it possible to obtain the signal from any surface lead and from the EGM file, any signal

Main features of the patients					
Number	**Patient identity**	**Age [years]**	**AF duration [months]**	**Termination**	**Success**
1	2746994	64	24	LT	YES
2	43761	55	24	NT	NO
3	340048	67	4	LT	YES
4	2770271	60	24	LT	YES
5	906847	58	6	LT	YES
6	2241998	59	12	RT	YES

LT = termination in the left atrium
NT = no termination
RT = termination in the right atrium

Table 3.2: *Main features of the six patients affected with persistent atrial fibrillation.*

of an intracardiac electrode. Finally, according the ablation type, signals are stored in a database divised in three sections:

- Pre-ablation
- PVI
- post PVI

Therefore, all the database files of a patient can be processed in order to study the evolution of AF organisation and to define more optimal ablative strategies. All signal processing techniques presented in this rapport were implemented and ran with Matlab R2009b from Mathworks®.

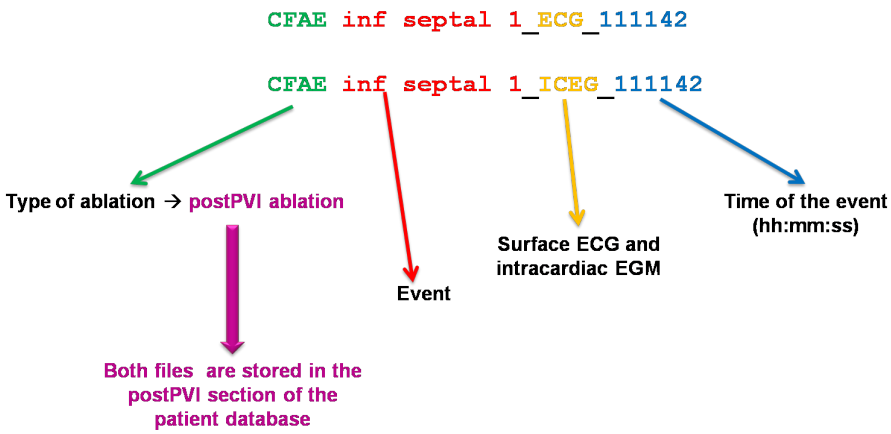

Figure 3.4: *Example of an ECG and an EGM file names.*

Chapter 4

Peak detection

4.1 Introduction

Organization indices based on EGM signals require the determination of the locations of depolarization peaks of interest. Both ventricular and atrial activities are essential to detect correctly and robustly peaks of atrial and ventricular depolarizations in EGM signals and surface ECGs respectively.

4.2 Method

Ventricular depolarizations in surface ECGs are detected via a routine written by Dr. Mathieu Lemay. EGM signal depolarizations are detected by a program developed by Dr. Jean-Marc Vesin and Andrea Buttu. A sliding window of 400 samples duration estimates the upper and lower envelopes of the signal by taking respectively the maximum and the minimum in each time interval. The envelopes of a typical EGM signal are presented in figure 4.1. The upper envelope is used to normalize positive samples between 0 and 1 while the lower envelope normalizes negative samples between 0 and -1. Finally, the outcome is a signal bounded between -1 and 1 as illustrated in figure 4.2. Finally, the atrial peaks of the EGM signal are nothing else than the maximum positive peaks of the bounded signal.

4.3 Results

On the top plot of figure 4.3 the green dots correspond to the ventricular peaks detected of an ECG signal on lead V7 while the red dots of the bottom plot of the same figure described the detected depolarization peaks of an EGM signal.

4.4 Conclusions

In conclusion, by applying these two robust techniques it is possible to detect efficiently atrial and ventricular peaks from EGM and ECG signals. These re-

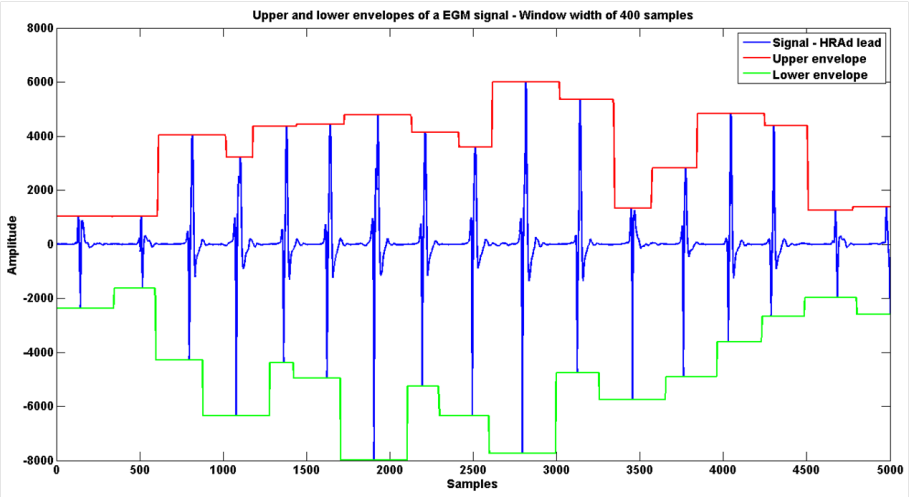

Figure 4.1: *Upper (red curve) and lower (green curve) envelopes of an EGM signal (blue curve) by using a sliding window of 400 samples duration.*

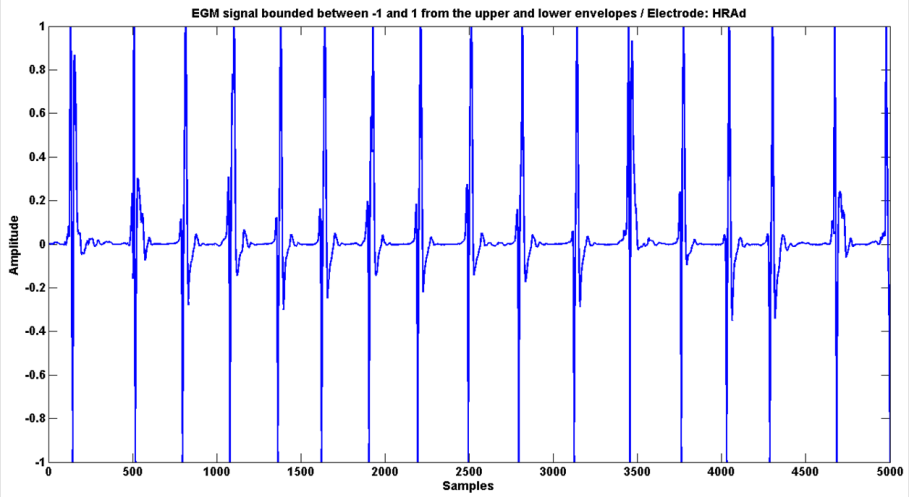

Figure 4.2: *Normalized EGM signal between -1 and 1 from the upper and lower envelopes.*

sults can be used in the development of new methods of intacardiac organization indices.

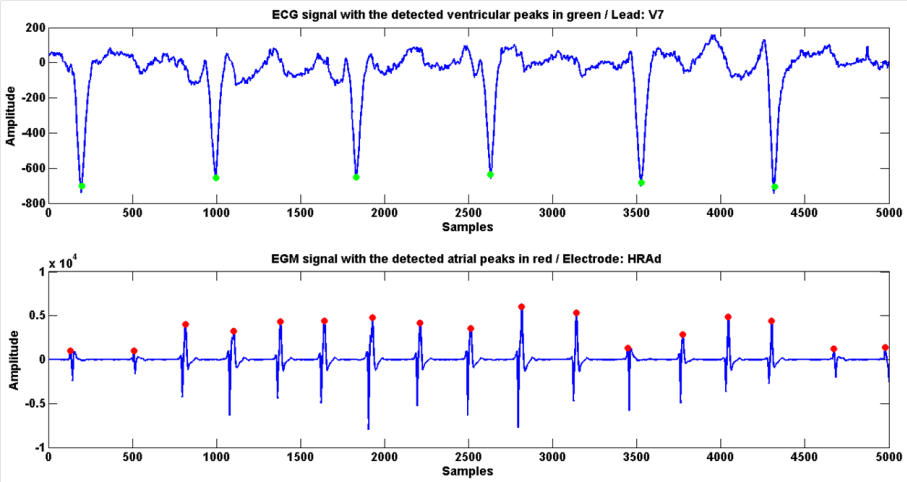

Figure 4.3: ***Top:*** *Peak detection (green dots) performed on an ECG signal.* ***Bottom:*** *Peak detection (red dots) performed on an EGM signal.*

Chapter 5

Dominant frequency analysis

5.1 Introduction

A classical intracardiac organization index is the dominant frequency (DF) which is the inverse of the mean cycle length. This chapter presents three different methods in order to track the DF. Typical DF range of the AF is between 3 Hz and 10 Hz with a particular flutter frequency range between 3 Hz and 5 Hz. Patients affected with persistent AF present high intracardiac DF because of the propagation of numerous wavelengths. By appling discrete RF ablations, the physician tries to prevent the maintenance of these potentials. The consequence is a progressive decrease of the DF. Therefore, AF termination is highly correlated with a low DF.

5.2 Double FFT method

The discrete Fourier transform (DFT) (see equation 5.1) transforms a finite-duration discrete signal in the frequency domain.

$$DFT\{f\}[n] = F[n] = \sum_{n'=0}^{N-1} f[n'] e^{-j2\pi n' \frac{n}{N}} \tag{5.1}$$

The fraction $\frac{n}{N}$ is the discrete frequency. The problem is the time computation of the DFT which is too long. The solution is to use the fast Fourier transform (FFT). It is an algorithm which accelerates condiderably the execution time of the DFT [39]. With the passage in the frequency domain, the signal period (T) in sample is converted to $1/T$ and if the latter is multiplied by the sampling frequency, it gives the DF (see equation 5.2).

$$T_{samples} \quad \overset{\text{DFT via FFT}}{\longleftrightarrow} \quad \frac{1}{T_{samples}} * f_{sampling} = DF \tag{5.2}$$

Classically, the DF of a signal was extracted by first computing the FFT and then applying a window to the FFT covering the frequency range of 3 Hz to 10 Hz. The frequency corresponding to the maximal FFT peak within the

window was considered as the DF of the signal. The method developed in this experiment apply two successive FFTs. The advantage to apply two successive FFTs was to focus the dominant period (DP) of the first FFT at the second peak of the second FFT which limited the zone of investigation. Finally, the DF is just the inverse of the period corresponding to the second peak of the second FFT multiplied by the sampling frequency. The double FFT method was first applied to synthetic EGM signals with a regular interval between adjacent peaks in order to evaluate it before working with real data.

5.2.1 Results

5.2.1.1 Synthetic EGM signal

The top plot of figure 5.1 displays the original regular synthetic signal. The period between two adjacent peaks is 101 samples. The middle plot presents the result after the first FFT. In a window covering the frequency range of 3 Hz to 10 Hz, the frequency for the maximal peak is 19.80 Hz which corresponds to the DF. This value should also be directly extracted from the second FFT. The bottom plot shows the result after the second FFT applied to the modulus of the first FFT. By focusing the research in a narrow window, the second peak of the spectrum can be detected. The dominant period (DP) in sample (DP = 101 samples on the bottom plot) corresponding to the second peak of the second FFT. The inverse of DP multiplied by the sampling frequency (2 kHz) gives the DF of 19.8 Hz as expected.

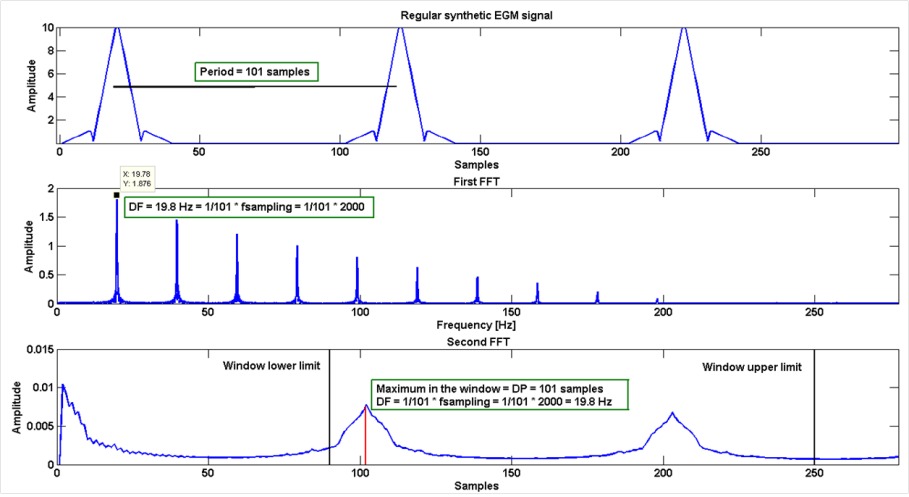

Figure 5.1: *Double FFT method applied to a synthetic EGM signal in order to track the dominant frequency (DF).* ***Top:*** *Original synthetic EGM signal with regular intervals of 101 samples and a sampling frequency of 2 kHz.* ***Middle:*** *Outcome of the first FFT with a DF localized at 19.80 Hz.* ***Bottom:*** *Outcome of the second FFT with a dominant period (DP) equal to 101 samples. The inverse of DP multiplied by the sampling frequency is nothing else than the DF.*

5.2.1.2 Patient 1: 2746994

Figure 5.2 presents the evolution of the DF during the entire procedure of the first patient. The results do not present a constant decrease of the DF as excpected. Moreover, some DF values are lower than the obtained DF when the patient reaches flutter. The method returns good results in the flutter case. Indeed, the detected DF values are about 4.6 Hz which is the typical flutter frequency.

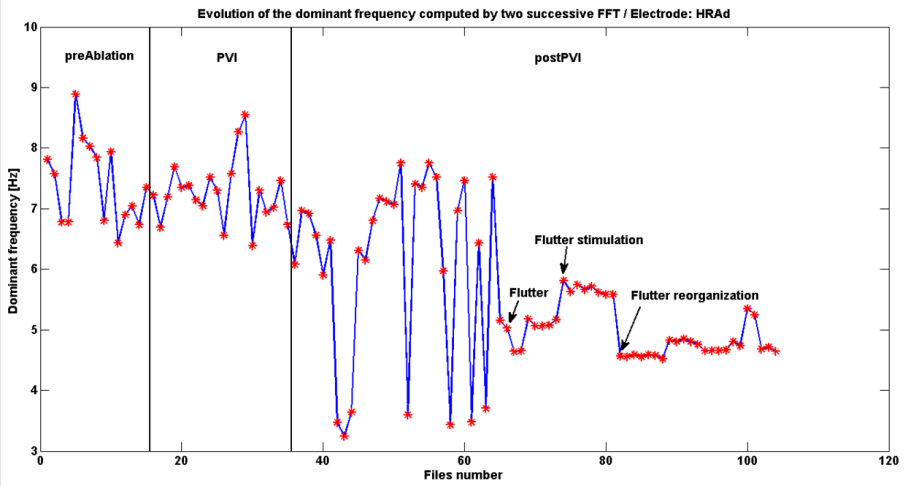

Figure 5.2: *Evolution of the dominant frequency during the procedure with the double FFT method for the first patient.*

5.2.1.3 Patient 2: 43761

Figure 5.3 presents the evolution of DF during the procedure of the second patient. The latter does not manage to reach a regular rhythm, flutter or atrial tachycardia. The failure of the ablation procedure can be observed on the figure. Most of the time, DF values remain very high, around 7 Hz. In addition, the results present a lot of fluctuations as the results of the first patient.

5.2.1.4 Patient 6: 2241998

Evolution of the DF during the intervention of the sixth patient can be observed on figure 5.4. As in the previous patients, the DF values fluctuate a lot. When the patient reaches flutter, there is a sudden decline and a stabilization of the DF value around 4 Hz.

5.2.2 Discussion

The purpose of this experiment was to track the DF of stepwise ablations in order to highlight which ablations were the most beneficial for the patient. However, the results are not conclusive. The DF values fluctuate a lot. Some DF values are even lower than the typical frequency range of flutter (3 Hz to 5

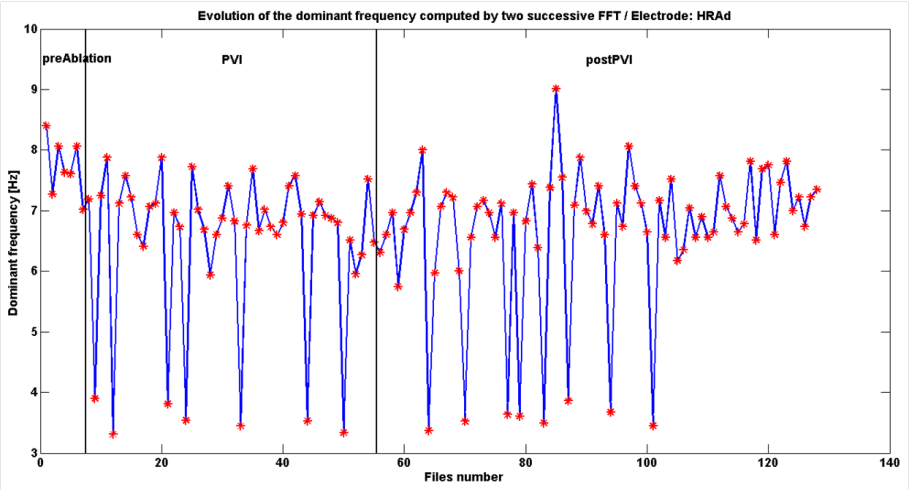

Figure 5.3: *Evolution of the dominant frequency during the procedure with the double FFT method for the second patient.*

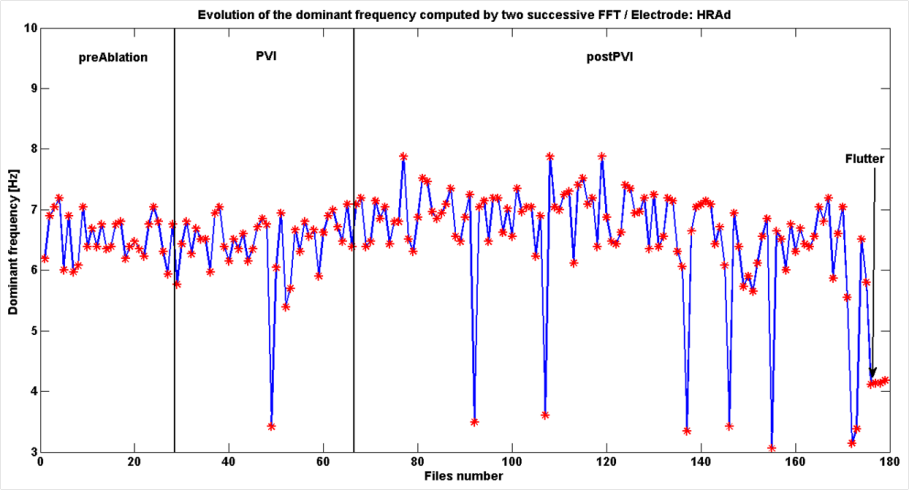

Figure 5.4: *Evolution of the dominant frequency during the procedure with the double FFT method for the sixth patient.*

Hz). It indicates the presence of some circuits in LA with a frequency shorter than the one of the flutter circuit. For the moment, there is no clear explanation. However, the DF values do not progressively decrease until the flutter. There is just a sudden decrease of the DF at the flutter frequency in the successful medical procedures. Therefore, the double FFT method is just only accurate enough to indicate if the medical procedure was a success or a failure but it is not capable to indicate which ablation step was more beneficial for the patient to recover a regular rhythm.

5.3 Autocorrelation method

The discrete autocorrelation is the expectation of the scalar product between a stationnary signal and a delayed version of the latter (see equation 5.3). The delay (τ) of the equation 5.3 is a temporal shift between the samples.

$$R_{x,x}(\tau) = E\left[x(t)x(t-\tau)\right] \tag{5.3}$$

with 2 properties

$$R_{x,x}(-\tau) = R_{x,x}(\tau) \tag{5.4a}$$
$$|R_{x,x}(-\tau)| \leq R_{x,x}(0) \tag{5.4b}$$

The autocorrelation has two important properties (see equations 5.4).It is a pair function and therefore, its representation is symmetric (see equation 5.4a). The second property is that the maximal value is obtained when there is no delay. In other words, the maximum is reached when both signals are perfectly overlapped (see equation 5.4b). [41]

The advantage of performing the autocorrelation on a signal is to highlight the peak corresponding to its dominant period (DP) in a restrictive region. More precisely, the DP is localized at the first maximal peak after those characterizing $R_{x,x}(0)$. To extract the DP value, a narrow window in which the maximum peak is detected is applied to half the autocorrelation in the region of interest. Finally, DF is just the inverse of the DP multiplied by the sampling frequency. The autocorrelation was first applied on synthetic EGM signals with regular intervals between adjacent peaks to assess the accuracy of the routine before processing real data.

5.3.1 Results

5.3.1.1 Synthetic EGM signal

The top plot of figure 5.5 shows the regular synthetic EGM signal with a period of 101 samples. The DF can be computed by multiplying the sampling frequency to the inverse of the period which gives 19.80 Hz as expected. This result should also be found by applying the autocorrelation. The middle plot of figure 5.5 displays the autocorrelation. Because it is symmetric, the DF can be tracking by taking into account only half the autocorrelation. Half the autocorrelation is displayed in the bottom plot of figure 5.5. A narrow window in which the maximum peak is detected is applied to half the autocorrelation. The dominant period (DP) corresponding to the maximal detected peak is inversed and multiplied by the sampling frequency in order to give the DF of 19.80 Hz as expected.

5.3.1.2 Patient 1: 2746994

Figure 5.6 shows the evolution of the DF during the entire procedure. The DF fluctuates a lot. There is not a progressive drecrease of the values until the flutter. When the flutter was reached, the DF becomes more stable which correctly reflects a flutter. However, as in the previous method, some DF values during AF are lower than the typical flutter frequency.

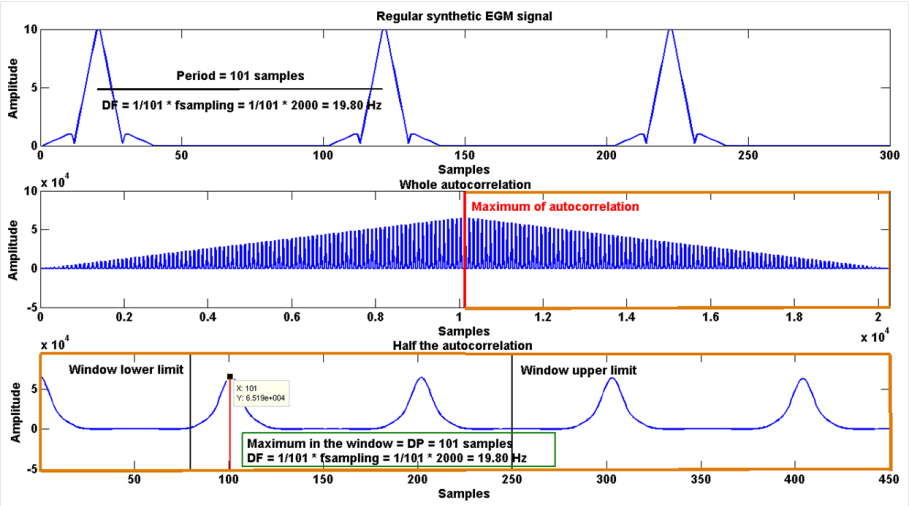

Figure 5.5: *Autocorrelation applied on a regular synthetic EGM signal in order to track the dominant frequency (DF).* ***Top:*** *Original synthetic EGM signal with regular intervals of 101 samples and a sampling frequency of 2 kHz.* ***Middle:*** *Outcome of the autocorrelation.* ***Bottom:*** *Half the autocorrelation with the window in which the DP of the maximal peak is detected. DF is just the inverse of DP multiplied by the sampling frequency.*

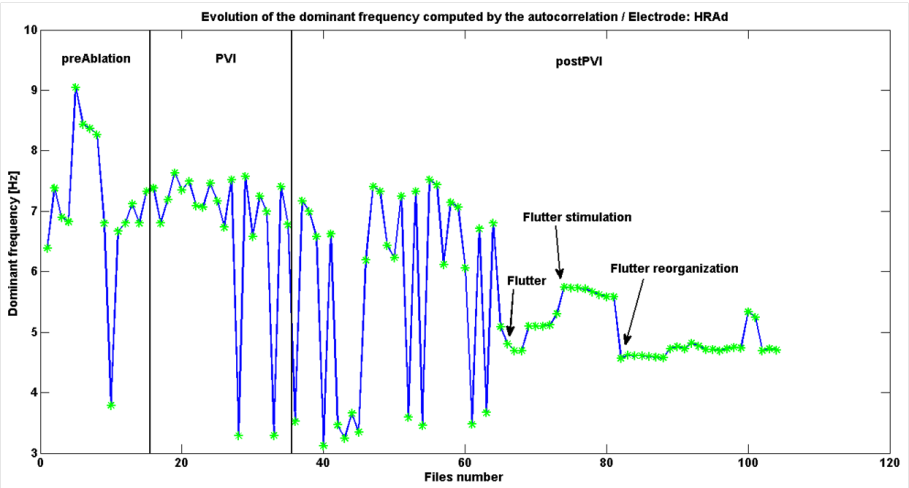

Figure 5.6: *Evolution of the dominant frequency during the procedure with the autocorrelation for the first patient.*

5.3.1.3 Patient 2: 43761

Figure 5.7 shows the he results for the second patient. The non-success of the procedure is reflected on the plot. The DF remains very high, approximatively

around 7 Hz during the whole ablation procedure. There is again the presence of some DF with an unusual low value.

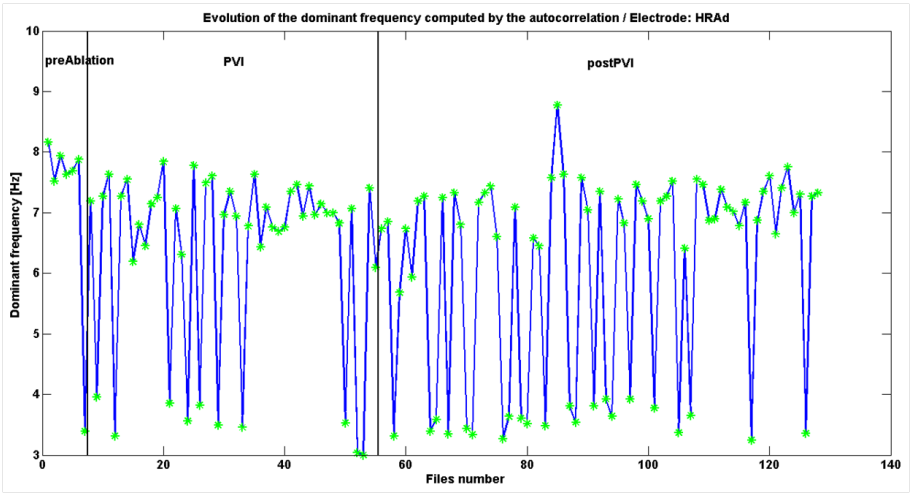

Figure 5.7: *Evolution of the dominant frequency during the procedure with the autocorrelation for the second patient.*

5.3.1.4 Patient 6: 2241998

Figure 5.8 summarizes the DF evolution for the sixth patient. As noticed previously, the DF fluctuates a lot and sometimes reaches values that are lower than those of a flutter. At the end of the procedure, when the flutter is reached, a typical frequency of flutter (around 4 Hz) is correctly detected.

5.3.2 Discussion

The results of the autocorrelation method suggest that the process is not efficient enough to correctly track the DF. Indeed, the DF fluctuates a lot and there is not a progressive decrease of the DF values until flutter or atrial tachycardia for patients who managed to reach a regular rhythm. Moreover, there are values smaller than the typical flutter frequency. This suggests that there are wavelengths which propagate into the LA with a smaller frequency than the flutter. As mentionned previously, there is no clear explanations about this phenomenon for the moment. When atrial tachycardia was reached, the autocorrelation detects an accurate value for the frequency of the of the flutter. However, it is not sufficient to consider this method as robust.

5.4 Peak detection method

As mentionned with the two previous methods, it is difficult to efficiently and robustly extract the DF. The results obtained by the double FFT transformation and the autocorrelation process are not conclusive. The results can

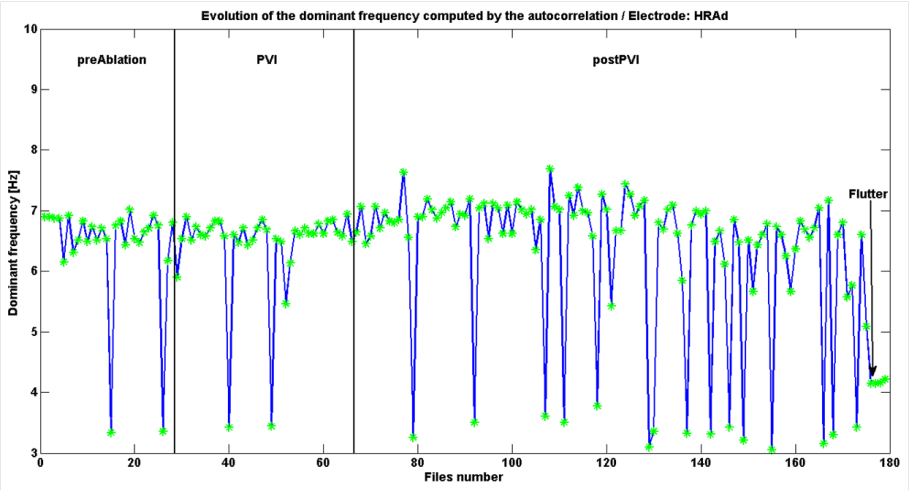

Figure 5.8: *Evolution of the dominant frequency during the procedure with the autocorrelation for the sixth patient.*

be improved if the DF is directly computed via the AF cycle length (AFCL) of a signal. In the previous chapter a robust routine capable to detect atrial peaks of any EGM signal was presented. Knowing the indices of the EGM signal depolarization peaks, the AFCL is nothing else than the mean or the median of their differences. Finally, the DF is the inverse of the AFCL multiplied by the sampling frequency. Therefore, the DF can be calculated in order to track the efficiency of a stepwise catheter ablation. This method was first applied on synthetic signals with regular interval between adjacent depolarizations in order to validate the accuracy of the routine before processing the real data.

5.4.1 Results

5.4.1.1 Variant: mean and median

Synthetic EGM signal Figure 5.9 shows the regular synthetic EGM signal and its detected peaks in red. The mean or the median of the difference between adjacent red peaks gives the dominant period (DP) of 101. Therefore, the DF is nothing else than the inverse of the DP multiplied by the sampling frequency which gives 19.80 Hz as expected.

Patient 1: 2746994 Figure 5.10 shows evolution of the DF during the procedure for the first patient. These results are better, indeed there is no presence of large fluctuations such as in the two previous methods. The decrease of the DF is slightly more progressive until the flutter.

Patient 4: 2770271 Figure 5.11 shows the evolution of the DF for the fourth patient. The DF fluctuates less and it is rather constant (around 5 Hz) during the entire procedure suggesting that the patient intracardiac rhythm was not so

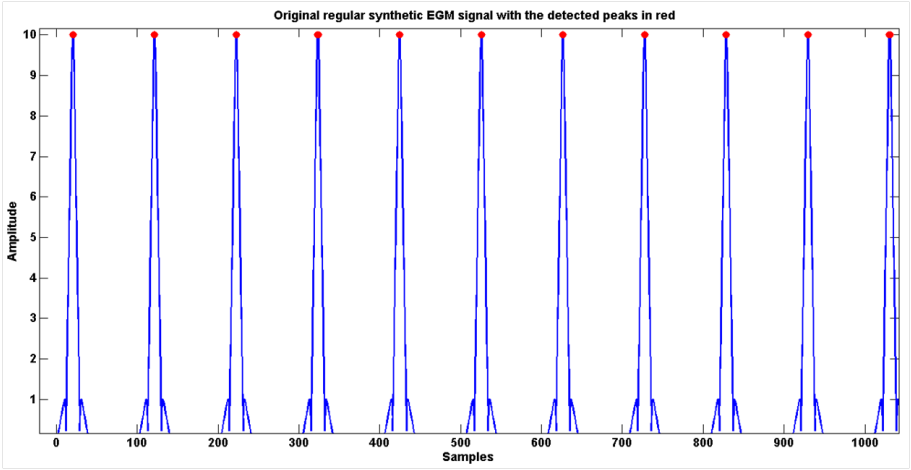

Figure 5.9: *Peak detection applied to a regular synthetic EGM signal. The detected peaks are the red dots.*

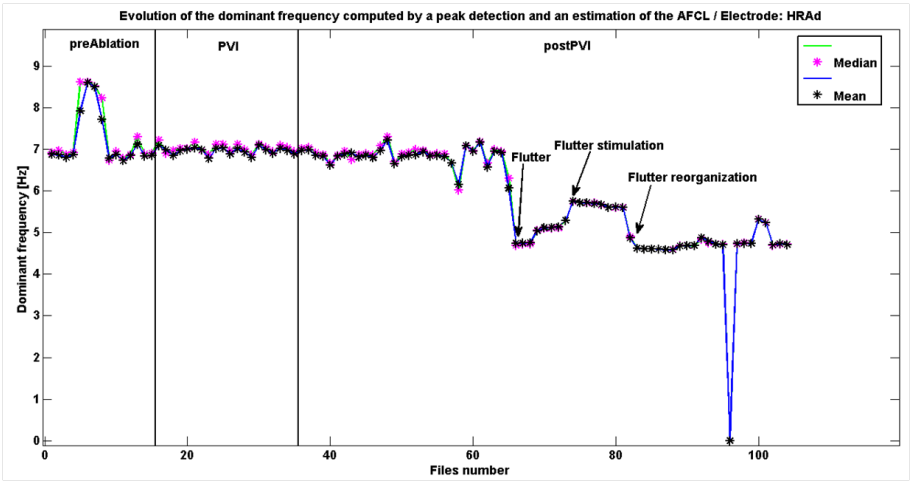

Figure 5.10: *Evolution of the dominant frequency during the procedure for the first patient. DF was computed via a peak detection and an estimation of the AFCL.*

irregular before beginning the procedure despite the presence of AF. In addition, there is no significant decrease of the DF when the patient reached atrial tachycardia.

5.4.1.2 Variant: removal of the extreme values

In order to improve the results, a certain percentage of the largest (12.5%) and smallest(12.5%) differences between the adjacent depolarization peaks were removed before computing the AFCL. After suppression of the extreme values,

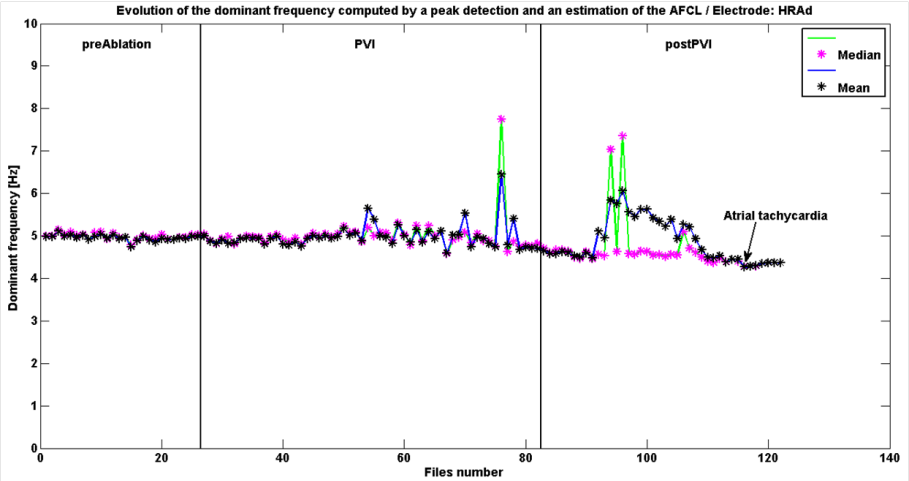

Figure 5.11: *Evolution of the dominant frequency during the procedure for the fourth patient. DF was computed via a peak detection and an estimation of the AFCL.*

the AFCL was computed as explained before.

Patient 4: 2770271 The figure 5.12 presents the DF evolution during the intervention of the fourth patient after the suppression of the 25% of extreme value. There is no significant change in the results compared to the previous figure 5.11.

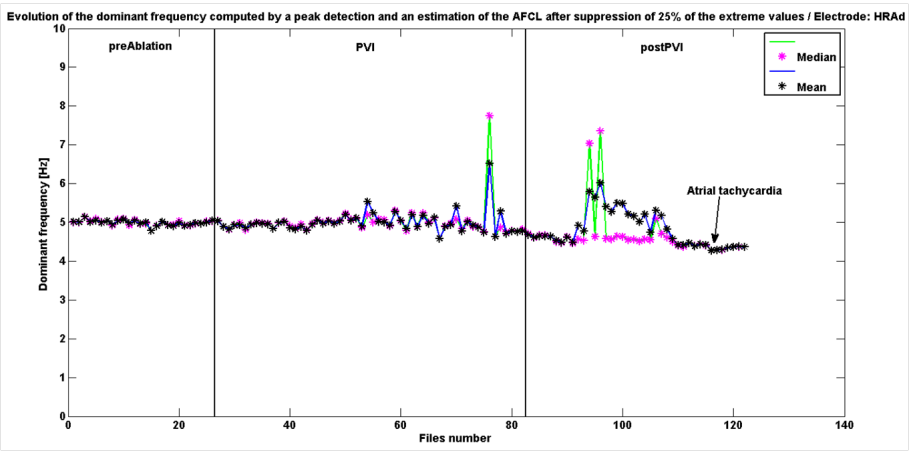

Figure 5.12: *Evolution of the dominant frequency during the procedure for the fourth patient. DF was computed via a peak detection and an estimation of the AFCL after suppression of the extreme values.*

5.4.2 Discussion

The peak detection method presents better results than the two previous methods. Indeed, there is less fluctuations among the DF values. However, it is already the standard method used by physicians during a procedure in order to determine if an improvement of the intracardiac organization takes place after an ablation. Moreover, the DF only decreases when the patient reaches the flutter and not before. It implies that this process is not enough robust for predicting AF termination despite the improvement of the results. The suppression of 25% of the extreme values does not significantly change the results. Even if this variant significantly modified the results, it could not be considered as robust because of the arbitrary choice of the percentage value.

Moreover, the ablations before the flutter do not demonstrate a progressive diminution of DF value but rather a stabilization of the DF value. Would it mean that these ablations are neither negative nor positive for the patient? There are some ablations that can be very positive for the intracardiac organization of the patient as some others which can be non-beneficial for the intracardiac rhythm of the patient. It is just that the method is not enough efficient to highlight which ablations were the most beneficial for the patient in order to reach a regular rythm.

5.5 Conclusions

Globally, the results are not really non conclusive. As demonstrated, the DF as organization index for assessing the efficiency of stepwise ablations is limited. Therefore, there is a strong need for the development of new intracardiac organization indices that would be more efficient for tracking the effect of a stepwise RF ablation.

Chapter 6

Variability of the intracardiac signals

6.1 Introduction

This chapter is mainly focused on the variability of intracardiac AF EGM signals. The variability is defined as the variation of the intracardiac rhythm around the DF. It describes the temporal evolution, that is, the possible accelerations or decelerations of the intracardiac rhythm between adjacent depolarizations. A better knowledge of the intracardiac variability can help to develop new intracardiac organization indices in order to assess stepwise RF catheter ablations.

6.2 Extraction of the ventricular activity

6.2.1 Introduction

It is possible that AF EGM signals variability does not completely represent atrial variability. Indeed, because of the physical connection between atria and ventricles, a mechano-electrical contribution of the ventricular contractions (VC) could affect the AF EGM signals variability. The following method attempts to demonstrate whether such ventricular activity is really present in intracardiac variability signals.

6.2.2 Method

The adaptive filtering method for the quantification and the cancellation of the ventricular mechano-electrical contribution of the VC relies on two preprocessing steps on the EGM and ECG signals.

6.2.2.1 EGM signal preprocessing

The routine written by Andrea Buttu extracts the beat-to-beat intracardiac variability (ICV) of an EGM signal. First, a maximum positive peak detection is performed on AF EGM signals of the HRAd electrode via the method presented

in the fifth chapter (see the top plot of figure 6.1). By nature, the time differences are irregularly sampled. Therefore, by regularly resampling the times differences at 80 Hz, it remains at the end only the intracardiac variability of the EGM signal (see the bottom plot of figure 6.1).

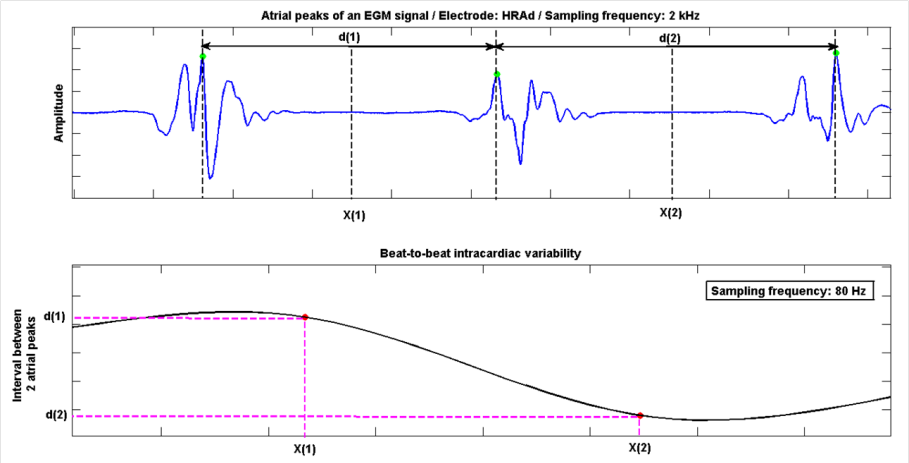

Figure 6.1: *Illustration of the beat-to-beat intracardiac variability.* ***Top:*** *The green dots correspond to the detected atrial depolarizations (sampling frequency of 2 kHz). d(1) and d(2) are the time differences between two adjacent atrial depolarizations. x(1) and x(2) are half the time differences between two adjacent atrial depolarizations.* ***Bottom:*** *Outcome of the regular resampling of the time difference at 80 Hz which is the intracardiac variability of the EGM signal.*

The figure 6.2 summarizes the preprocessing steps done on an EGM signal. The first subplot shows the original EGM signal with the detected peaks in red. The second subplot displays the ICV of the EGM signal resluting from the regular resampling at 80 Hz. A steep decreasing ICV curve between two adjacent peaks suggests an acceleration of the intracardiac rhythm around the DF of the EGM signal while an increasing ICV curve indicates a slowing of the intracardiac rhythm around the DF of the EGM signal.

The goal of the regular resampling operation is the extraction of the ICV signal which is supposed to contain not only the atrial intracardiac varibility (AIVC) but also a mechano-electrical contribution of the VC.

6.2.2.2 ECG signal preprocessing

The ECG signals associated with the EGM signals are also preprocessed. The ventricular depolarizations are detected on lead V1 using the method developed by Dr. Mathieu Lemay (see the top plot of figure 6.3). Then, the detected peaks are converted into a series of impulses (sampling frequency of 80 Hz) as illustrated on the middle plot of figure 6.3.

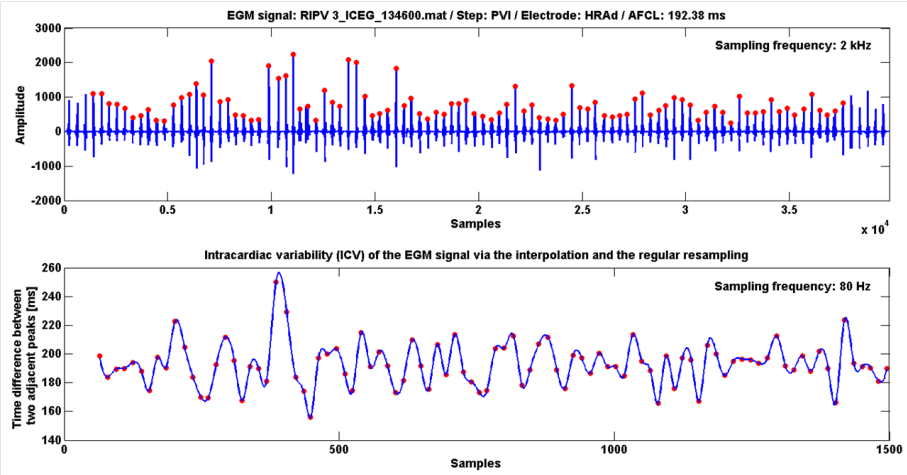

Figure 6.2: *Intracardiac variability of an EGM signal of the fifth patient.* ***Top:*** *EGM signal with the detected atrial peaks in red (sampling frequency of 2 kHz).* ***Bottom*** *Intracardiac variability of the EGM signal (sampling frequency of 80 Hz).*

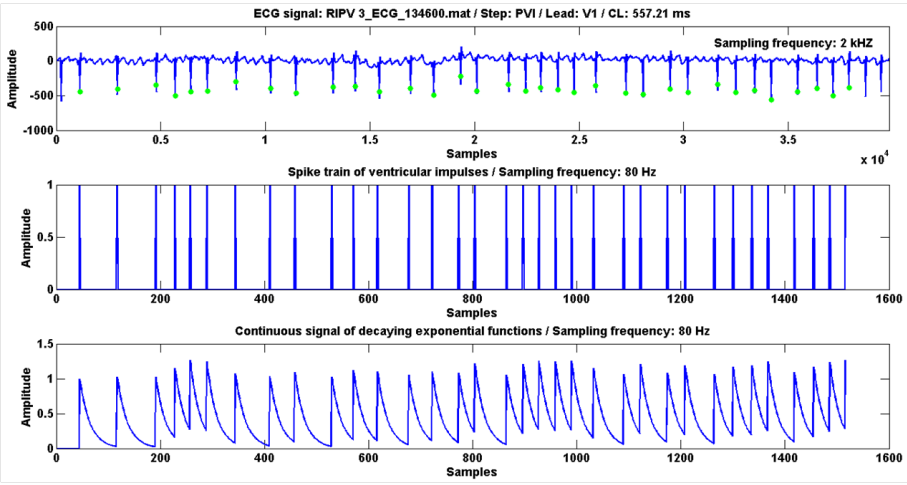

Figure 6.3: *ECG signal preprocessing for the adaptive filtering.* ***Top:*** *Original ECG signal with a sampling frequency of 2 kHz.* ***Middle:*** *ECG signal transformed into a series of ventricular impulses (80 Hz).* ***Bottom:*** *Outcome of the convolution between the series of ventricular impulses and the causal one-pole lowpass filter.*

However, it is technically difficult to handle this series of impulses due to its point-like nature. In addition, it is not very realistic to describe a ventricular depolarization with only one impulse. Therefore, in order to obtain a continuous signal with more realistic depolarizations, the spike train of ventricular impulses

is convoluted with a causal exponential (one-pole lowpass) filter (see figure 6.4) according to the article of Paiva and al. [33]. The outcome of the filtering is displayed on the bottom plot of figure 6.3. The unique pole of this lowpass filter was arbitrarly defined at 0.95.

Figure 6.4: *The convolution between the spike train of ventricular impulses and the causal one-pole lowpass filter resulting in a continuous signal of decaying exponential functions.*

The purpose of this preprocessing is to transform the ECG signal into a continuous 80 Hz signal that summarizes ventricular depolarization.

6.2.2.3 Adaptive filtering using normalized least-mean square algorithm

The adaptive filtering based on the normalized least-mean square (NLMS) algorithm was written by Dr. Jean-Marc Vesin. The schema of figure 7.3 presents the principle of the adaptive filtering which its main purpose is to extract at the filter output a signal as close as possible to the ICV signal. More precisely, an adaptive filter matches its coefficients in order to make the continous signal of decaying exponential functions as similar as possible to the ICV signal by minimizing the error between the prediction and the reference (ICV signal) according to the NLMS criteria. The NLMS algorithm was choosen because it adapts itself well to the structural changes of the filter input signal. Therefore, by using the continuous signal of decaying exponential functions as input of the adaptive filter, the mechano-electrical contribution of VC to ICV signal is extracted at the filter output. Finally, this ventricular activity was substracted from the ICV signal in order to obtain only the atrial intracardiac variability (AICV).

6.2.3 Results

In order to observe the effect of the ventricular mechano-electrical suppression on the IVC signal, the non-parametric power spectral density (PSD) of various signals was computed before filtering, after filtering and after subtraction of the ventricular mechano-electrical contribution. The PSD was estimated using Welch's averaged modified periodogram method of spectral estimation. The signal is divided into an integer number of segments with 50% overlap by default and an equal length as the Hamming window. The remainder of the signal after the division into several segments is not taken into account in the spectral estimation. The periodogram which is an estimation of the PSD is computed in each segment. Finally, the estimated PSDs are averaged. The

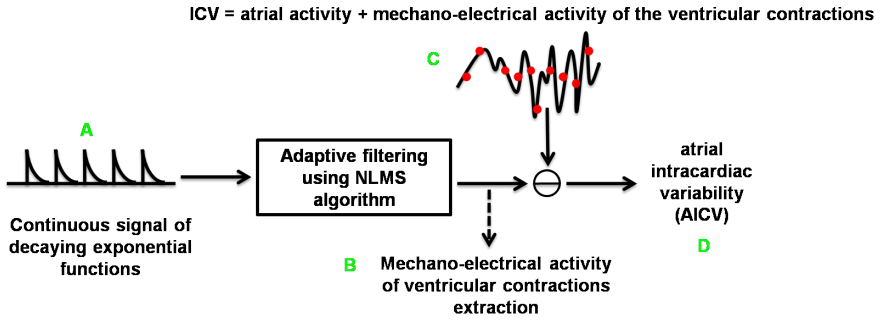

Figure 6.5: *Schema of the adaptive filtering principle. Its purpose is to cancel the ventricular activity from the intracardiac variability signal.*

figures of the results are divised in four subplots. Each subplot refers to a letter A, B, C, or D corresponding to a specific step of the adaptive filtering schema of figure 7.3.

6.2.3.1 Patient 1: 2746994

The figure 6.6 summarizes the results obtained with the adaptive filtering. The PSDs of the filter input and output are respectively represented on the top and middle top plots. The second PSD corresponds to the ventricular mechano-electrical activity. The third subplot presents the PSD of the ICV signal containing the VC contribution, while the fourth subplot shows the same signal devoid of the ventricular mechano-electrical contribution. One can observe that on the middle bottom and the bottom plots, the PSDs change. Indeed, the PSD area of the bottom plot is smaller than those of the middle bottom plot suggesting a non negligeable mechano-electrical contribution of the VC to the ICV signal.

6.2.3.2 Patient 5: 906847

Figure 6.7 shows the four PSDs computed at the different steps of the adaptive filtering (see schema of figure 7.3). The top plot presents the PSD of the adaptive filtering input, which is the continuous signal of decaying exponential functions. The middle top plot shows the PSD of the adaptive filtering output or in other words the mechano-eletrical contribution of VC. The PSD of the ICV signal is on the middle bottom plot. The PSD of the bottom plot is the outcome of the subtraction of the ventricular activity from the ICV, which gives the AIVC. The PSD area of the bottom plot is smaller than that of the middle bottom plot. It means that the ICV signal contained a mechano-electrical VC contribution which was removed by the adaptive filtering.

6.2.3.3 Patient 6: 2241998

The effect of the ventricular mechano-electrical activity cancellation is the most obvious when the patient reached the flutter stage as presented on figure

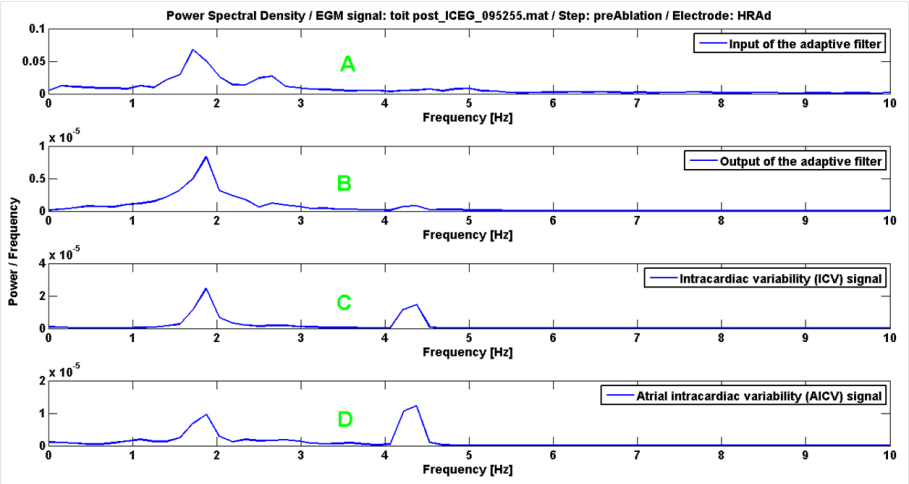

Figure 6.6: *Power spectral density (PSD) of the signals involved in the adaptive filtering for the first patient.* ***Top:*** *PSD of the adaptive filter input which is the continuous signal of decaying exponential functions.* ***Middle top:*** *PSD of the adaptive filter output which is the ventricular contribution to the ICV signal.* ***Middle bottom:*** *PSD of the intracardiac variability (ICV) signal.* ***Bottom:*** *PSD of the ICV signal devoid of VC contribution.*

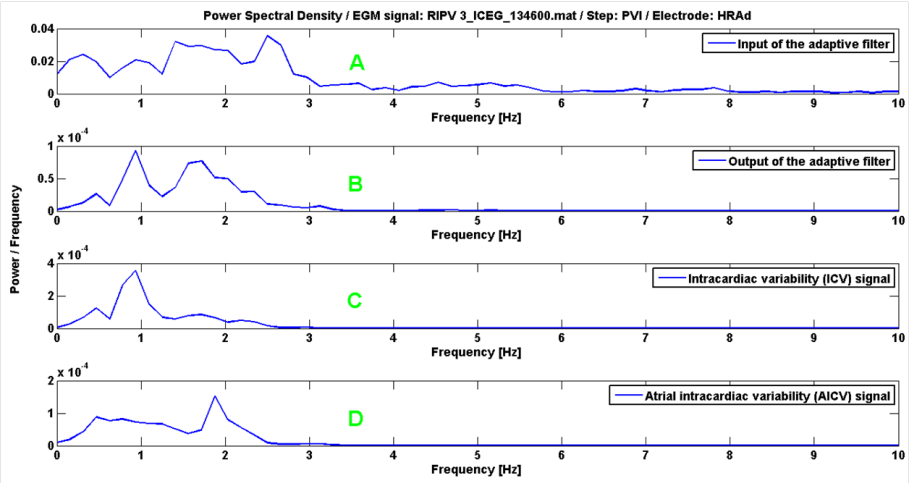

Figure 6.7: *Power spectral density (PSD) of the signals involved in the adaptive filtering for the fifth patient.* ***Top:*** *PSD of the adaptive filter input which is the continuous signal of decaying exponential functions.* ***Middle top:*** *PSD of the adaptive filter output which is the ventricular contribution to the ICV signal.* ***Middle bottom:*** *PSD of the intracardiac variability (ICV) signal.* ***Bottom:*** *PSD of the ICV signal devoid of VC contribution.*

6.8. The PSD of the filter output is similar to that of the input filter and the PSD of the AICV signal is very small. These results are not only logical but also prove the efficiently of the adaptive filtering. Because the patient is in flutter, the EGM signals become very regular. Therefore, they do not contain any atrial variability but only the mechano-electrical activity which is perfectly identified by the adaptive filtering. That is the reason why the PSDs of the middle top and middle bottom plots are similar and the PSD of the AICV signal is quasi null.

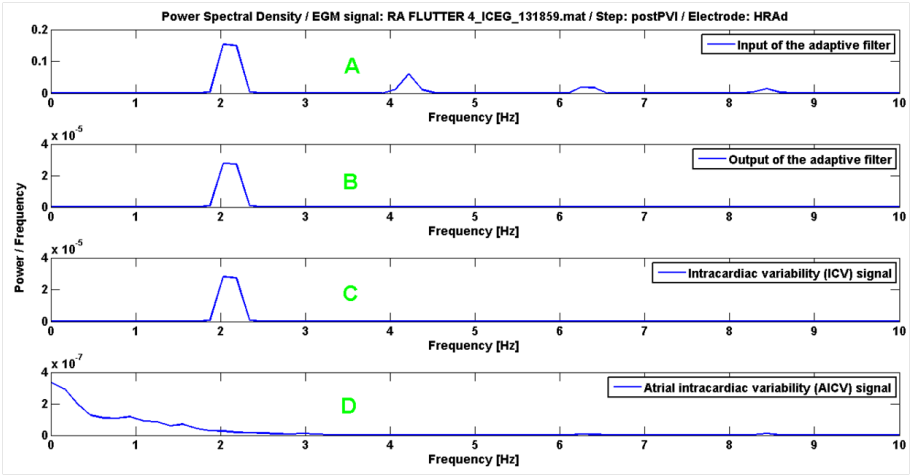

Figure 6.8: *Power spectral density (PSD) of the signals involved in the adaptive filtering for the sixth patient.* ***Top:*** *PSD of the adaptive filter input which is the continuous signal of decaying exponential functions.* ***Middle top:*** *PSD of the adaptive filter output which is the ventricular contribution to the ICV signal.* ***Middle bottom:*** *PSD of the intracardiac variability (ICV) signal.* ***Bottom:*** *PSD of the ICV signal devoid of VC contribution.*

6.2.4 Discussion

The purpose of this experiment was to extract a potential mechano-electrical contribution of the VC present in the ICV signals. The results demonstrated that the ICV signals were significantly affected with ventricular activity, which was efficiently extracted by the adaptive filtering. However, a question remains unanswered. Do the AICV signals contain only atrial activity? In others words, does the adaptive filtering completely cancel the mechano-electrical contribution of the VC? An experiment which could be performed in order to answer this question would be to block briefly the AV node during the medical procedure and compare the results of the adaptive filtering using the signals with and without AV node blocking. A signal recorded during AV node blocking should normally contain only atrial activity even if the patient is not in flutter.

6.3 Selection of the optimal pole value for the exponential filter

6.3.1 Introduction

The presence of a mechano-electrical contribution of VC was demonstrated in the previous section. However, the choice of the pole value at 0.95 for the exponential filter in the preprocessing of the ECG signal was completely arbitrary. It might be possible that a more accurate quantification of the ventricular activity via the adaptive filtering would be obtained larger with an other pole value. Therefore, the goal of this experiment was to find the optimal pole by varying its value in order to maximize the extraction of ventricular activity.

6.3.2 Method

The pole has to be confined inside the unit circle in order to assure filter stability. The closer the real pole to 1 is, the slower the filter impulse response decays. For practical purposes, the largest possible pole value was fixed at 0.95. For each pole value going to 0 to 0.95 by step of 0.5 and signal on the HRAd electrode, the amount of the ventricular suppression was computed as the ratio between the variances of the output filter and the ICV signal. For each signal of a patient database, this ratio was stored in a matrix. To facilitate the interpretation of this matrix, the latter was converted in an image object with a color scale bounded between 0 (dark blue) and 1 (dark red). Finally, the mean percentage of ventricular activity cancellation was calculated for each pole value in the matrix. The pole for which the mean percentage was the largest was considered as the optimal value.

6.3.3 Results

6.3.3.1 Patient 1: 2746994

Figure 6.9 summarizes the results for the research of the optimal pole. The left plot presents the matrix containing all the ratios between the output filter and the ICV signal on the HRAd electrode for each pole value. The ratios become higher at the end of the procedure and especially when the patient reaches the flutter condition. Indeed, whatever the pole value is, the suppression in that case is almost equal to 1. The reason for this phenomenon comes from the high regularity, and thus the weak fluctuations of the ICV signals. The right plot shows the mean ratios of VC contribution to ICV for each pole during. The mean ratios increase progressively until the maximal value reached at 0.95.

6.3.3.2 Patient 2: 43761

The left plot of figure 6.10 shows significant ratios for each pole combined for the forty first EGM and ECG signals. After that, the ratios become smaller and remain almost constant until the end of the intervention. These results suggest that the patient had a more regular rhythm at the beginning of the procedure than at the end of the medical protocol. Besides, the patient did not reach a regular rhythm. The right subplot presents two optimal values for the filter pole

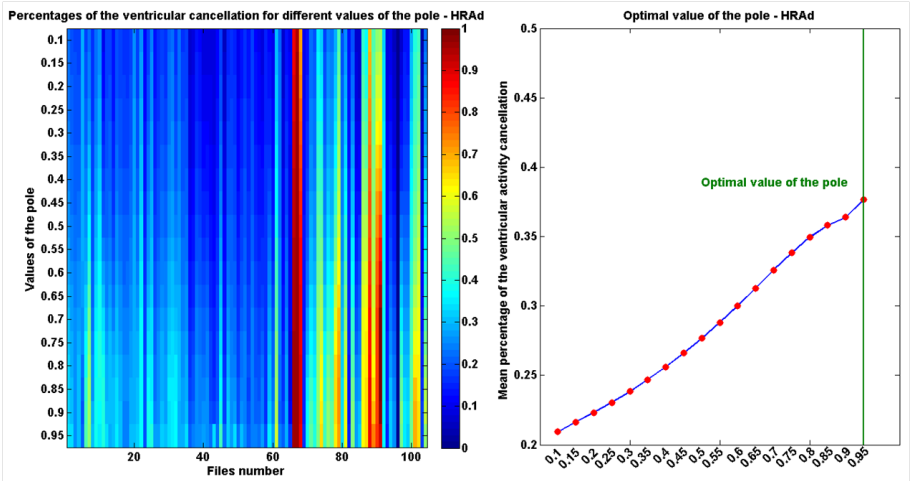

Figure 6.9: *Selection of the optimal pole value for the first patient.* ***Left:*** *Ratios of the ventricular contribution suppression for each pole values and each file of the first patient database.* ***Right:*** *Mean of the ratios corresponding to the poles. The optimal pole value is 0.95*

which are 0.8 and 0.85. The choice of 0.8 was based on the maximization of the filter stability.

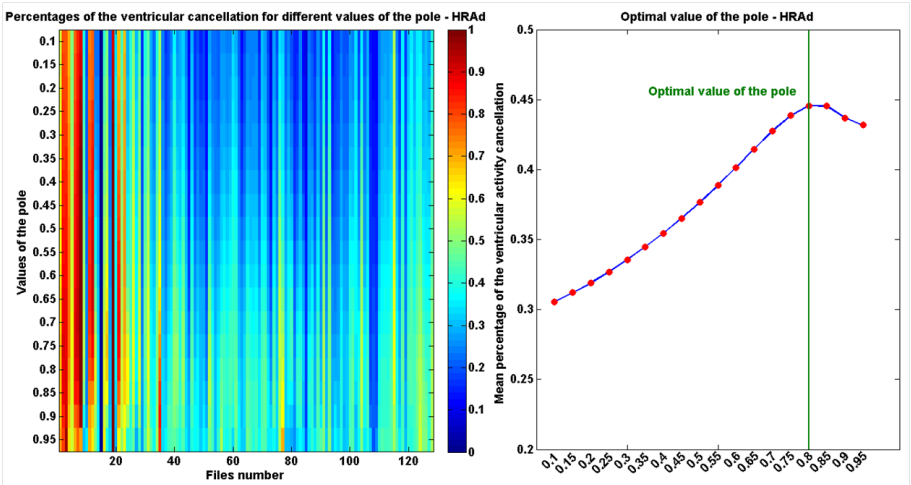

Figure 6.10: *Selection of the optimal pole value for the second patient.* ***Left:*** *Ratios of the ventricular contribution suppression for each pole values and each file of the second patient database.* ***Right:*** *Mean of the ratios corresponding to the poles. The optimal pole value is 0.8.*

6.3.3.3 Patient 3: 340048

The left plot of figure 6.11 shows very high ratios of the cancellation of VC contribution for the first forty EGM and ECG signals. These results are logical with regard to the electrophysiological situation of the patient at the beginning of the medical intervention. Indeed, the patient presented a good intracardiac organization despite the presence of AF. The curve on the right plot is very similar to those of the previous patient (see the right plot on figure 6.10). There is also the presence of a maximum localized around 0.8. In order to maximize the filter stability, the optimal value for the pole was chosen at 0.8.

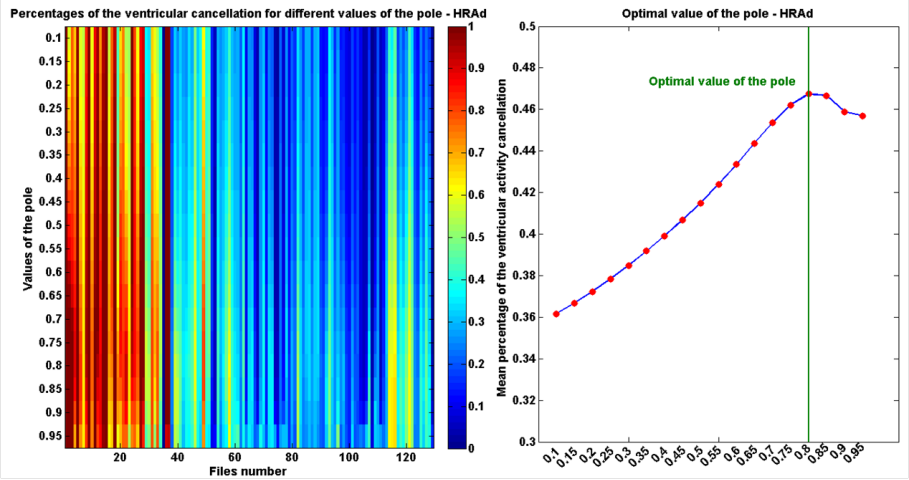

Figure 6.11: *Selection of the optimal pole value for the third patient.* ***Left:*** *Ratios of the ventricular contribution suppression for each pole values and each file of the third patient database.* ***Right:*** *Mean of the ratios corresponding to the poles. The optimal pole value is 0.8.*

6.3.3.4 Patient 4: 2770271

The results presented on figure 6.12 were not expected. Indeed, the patient reached a regular rhythm at the end of the procedure but there is no significant change of the ratios in the color matrix which would confirm the presence of an atrial tachycardia. The right plot shows the mean percentages of the ratios. There curve presents also a maximum localized around a pole value of 0.8 as for the second and the third patients. The optimal value for the pole filter of the fourth patient was defined at 0.75.

6.3.3.5 Patient 5: 906847

The left plot of figure 6.13 displays the ratios calculated between the output of the adaptive filtering and the ICV signals for each pole value. There again, the atrial tachycardia at the end of the intervention is not detectable by higher ratio values. The optimal value for the filter pole is localized at 0.95.

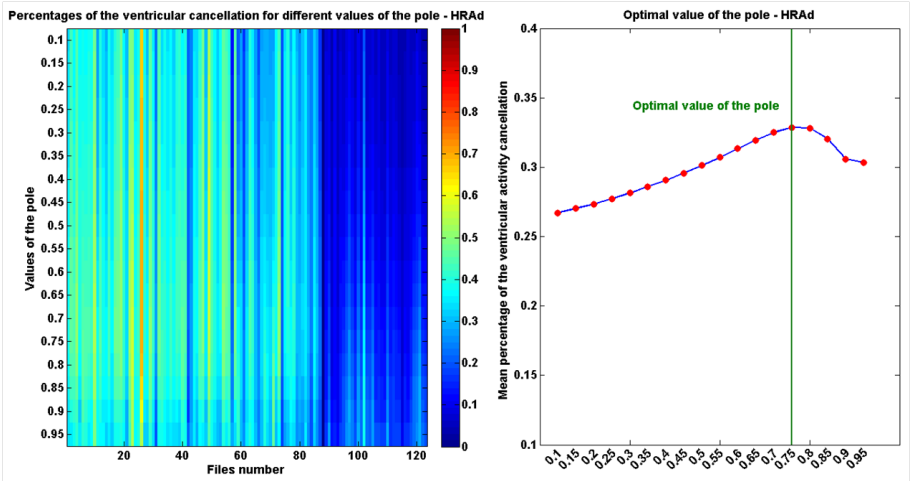

Figure 6.12: *Selection of the optimal pole value for the fourth patient.* ***Left:*** *Ratios of the ventricular contribution suppression for each pole values and each file of the fourth patient database.* ***Right:*** *Mean of the ratios corresponding to the poles. The optimal pole value is 0.75.*

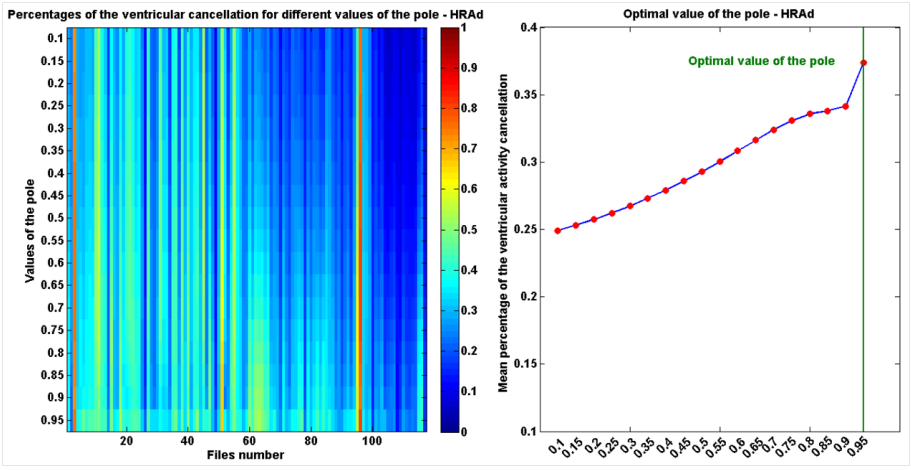

Figure 6.13: *Selection of the optimal pole value for the fifth patient.* ***Left:*** *Ratios of the ventricular contribution suppression for each pole values and each file of the fifth patient database.* ***Right:*** *Mean of the ratios corresponding to the poles. The optimal pole value is 0.95.*

6.3.3.6 Patient 6: 2241998

The right extremity of the color matrix on the left subplot of the figure 6.14 presents high ratio values of the VC contribution to the ICV. As expected in the case of a flutter, the values are close to 1. The optimal value of the filter pole is equal to 0.8 as illustrated on the right plot.

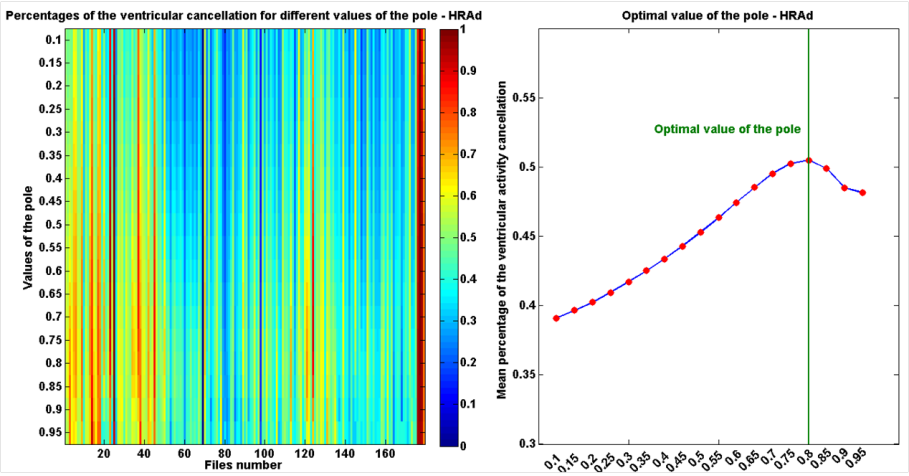

Figure 6.14: *Selection of the optimal pole value for the sixth patient.* ***Left:*** *Ratios of the ventricular contribution suppression for each pole values and each file of the sixth patient database.* ***Right:*** *Mean of the ratios corresponding to the poles. The optimal pole value is 0.8.*

6.3.4 Discussion

The purpose of this experiment was to find the optimal pole value of the exponential filter used for the preprocessing of the ECG signals in order to maximize the extraction of the mechano-electrical contribution of VC to ICV. The optimal values for the filter pole are not the same for all the patients but globally they remain very close. The slight differences among the values can be explained by the fact that the heart and also the AF differ from one patient to another one. The atria remodelling induced by the AF generates particular electrophysiological environnements which can be at the origin of the small differences among the computed results.

In addition, the curves of the right plot of each patient were very similar. Four times out of six, the curves presented a maximum localized around a pole value of 0.8. These maxima were present as well in patients who reached a flutter or an atrial tachycardia state as in the one who failed to reach a regular rhythm. For the moment, there is no explanation of the presence of these maximums.

As expected, the computed ratios of the mechano-electrical contribution of VC to ICV are almost equal to 1 when the patients reached the flutter state. As explained in the previous section, a flutter signal is very regular and so does not contain anymore AICV but a certain amount of mechano-electrical contribution of the VC which is efficiently removed by the adaptive filtering. However, the atrial tachycardia of the fourth and the fifth patient do not present higher ratios of ventricular cancellation despite the regularity of the signals. Is it a coincidence or is there a biological reason behind this phenomenon? A possible reason of this major difference could be the nature of the atrial tachycardia.

Indeed, there are several types of atrial tachycardias. An atrial tachycardia can be due to a macro re-entry or as a focal location of discharge. Therefore, it might be possible that these atrial tachycardias present variability despite their regularity because of the nature of the underlying tachycardia.

Finally, the ratios between the cancellation of the VC contribution and the intracardiac variability power are almost constant for the six patients as illustrated on figure 6.15. Their mean value is 41% ± 6.7%. Therefore, it would suggest that the VC contribution is homogenously present in each patient of the protocol despite the anatomical and electrophysiological differences with regard to the patients heart condition and AF. This hypothesis should be taken with caution because the computations were performed with six patients only.

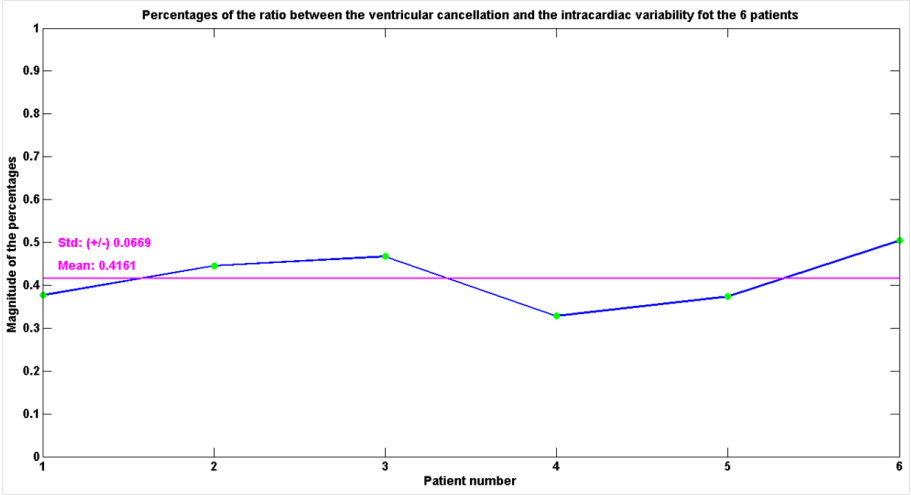

Figure 6.15: *Maxima of mean ratio values of the VC contribution cancellation for the six patients.*

6.4 Evolution of the ventricular contractions contribution

6.4.1 Introduction

The mechano-electrical contribution of ventricular contractions (VC) is supposed to be constant in each ICV signals. In order to confirm this, the variance of the VC contribution can be computed. This experiment was performed by taking into account the optimal pole value of the exponential filter calculated in the previous section.

6.4.2 Method

The discrete variance of a signal x is defined according to the following equation [3]:

$$\sigma^2(x) = \frac{1}{N}\sum_{n=0}^{N-1}|x_n - \mu_x|^2 \tag{6.1}$$

For real signals, it is nothing else than the computation of the signal power of the discrete signal x minus its square mean (see equation 6.2) [3].

$$\sigma^2(x) = P_x - \mu_x^2 \tag{6.2}$$

The variances of the ventricular contribution as those of the AICV were computed for all the signals of each patient database. At the opposite, the AICV variance should not be as constant as the VC contribution variance during the intervention except if the patient reached a regular rhythm. In this case, both variances should be closed to zero.

6.4.3 Results

6.4.3.1 Patient 1: 2746994

Figure 6.16 summarizes the evolution of the variance of the VC contribution and the AIVC during the intervention. As expected, the variance AIVC are quasi null when the patient reaches the flutter. It confirms the results and explanations mentionned in the previous experiments. As expected, the variance of the VC contribution is almost constant during the procedure.

6.4.3.2 Patient 2: 43761

Figure 6.17 shows the variance of the VC contribution and the AICV. This patient failed to reach flutter and this unsuccessful procedure can be observed on the plot. Indeed, both variances do not stop fluctuating. In addition, the variance of the ventricualr contribution is less constant than on the previous figure 6.16 espically in the postPVI step.

6.4.3.3 Patient 3: 340048

The figure 6.18 dispalys the results concerning the variances of the AICV and the VC contribution. The variance of the VC contribution fluctuates a lot during the pre-ablation stage and becomes more constant in the postPVI stage. In addition, the variance of the VC contribution is smaller at the end of the plot confirming a better organization in the RAA.

6.4.3.4 Patient 4: 2770271

Figure 6.19 shows the variances of the VC contribution and AICV. The VC contribution is rather constant during the entire procedure. However, it is not the case for the AICV variance which is more fluctuating especially just before the atrial tachycardia.

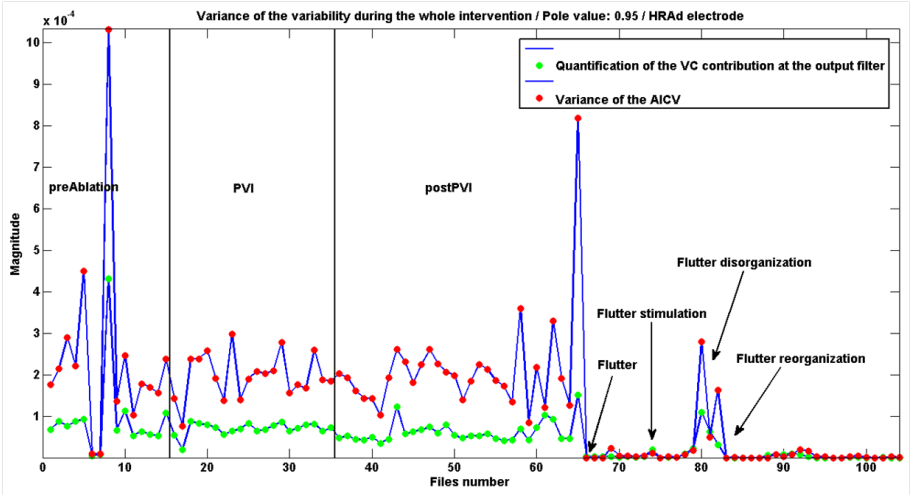

Figure 6.16: *Evolution of the variance of the ventricular contractions contribution and the atrial intracardiac variability during the procedure for the first patient.*

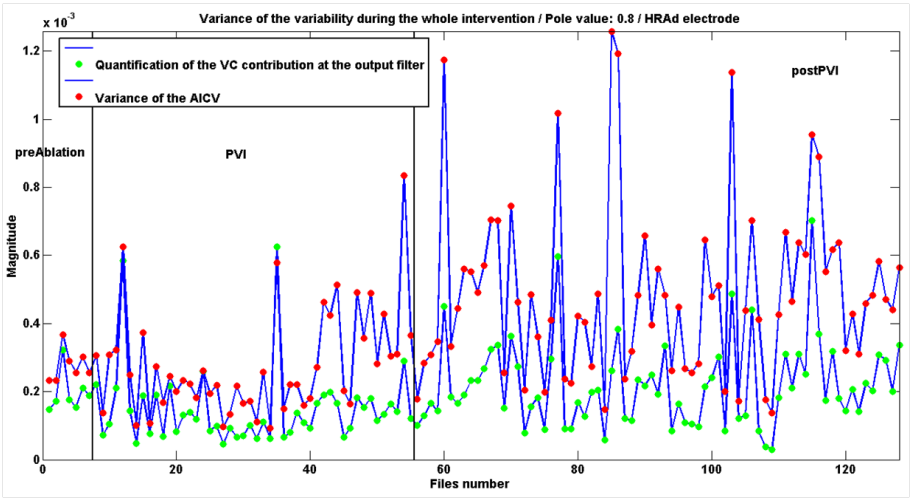

Figure 6.17: *Evolution of the variance of the ventricular contractions contribution and the atrial intracardiac variability during the procedure for the second patient.*

6.4.3.5 Patient 5: 906847

Figure 6.20 shows the results concerning the variances of the VC contribution and the AICV. The variance of the VC contribution is almost constant during the procedure. As expected, both variances become quasi null when the patient reaches atrial tachycardia.

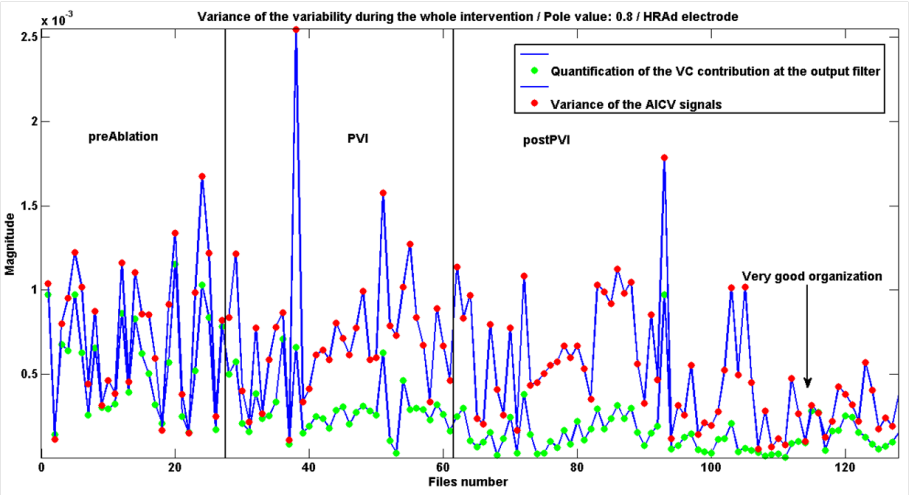

Figure 6.18: *Evolution of the variance of the ventricular contractions contribution and the atrial intracardiac variability during the procedure for the third patient.*

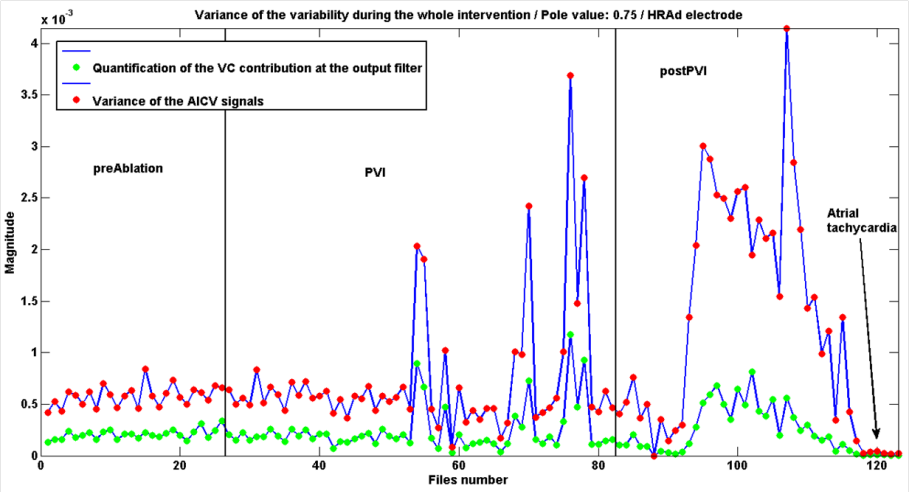

Figure 6.19: *Evolution of the variance of the ventricular contractions contribution and the atrial intracardiac variability during the procedure for the fourth patient.*

6.4.3.6 Patient 6: 2241998

The figure 6.21 displays the variances of the VC contribution and AICV. The VC contribution is almost constant during the procedure while that of AICV presents more fluctuations. But, at the flutter stage, they both become very small and constant because of the regularity of the signals. Indeed, more regular the signals are, smaller the variability and the variance of the variability are.

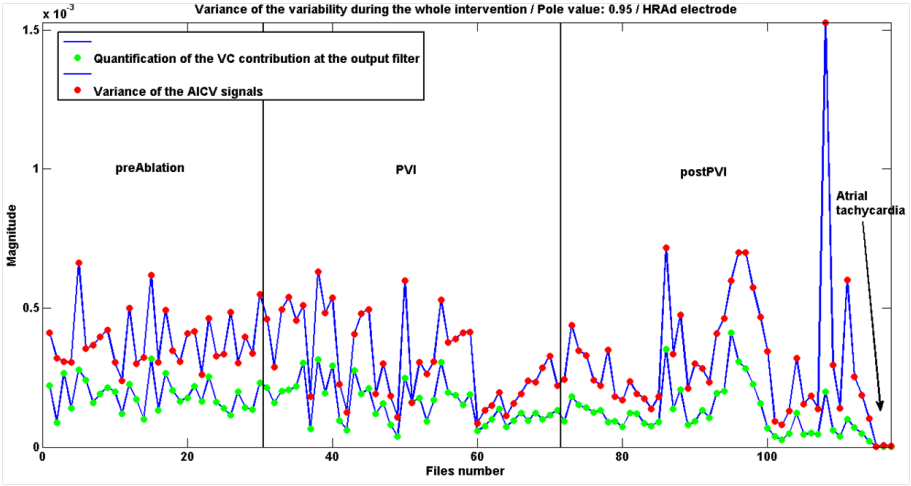

Figure 6.20: *Evolution of the variance of the ventricular contractions contribution and the atrial intracardiac variability during the procedure for the fifth patient.*

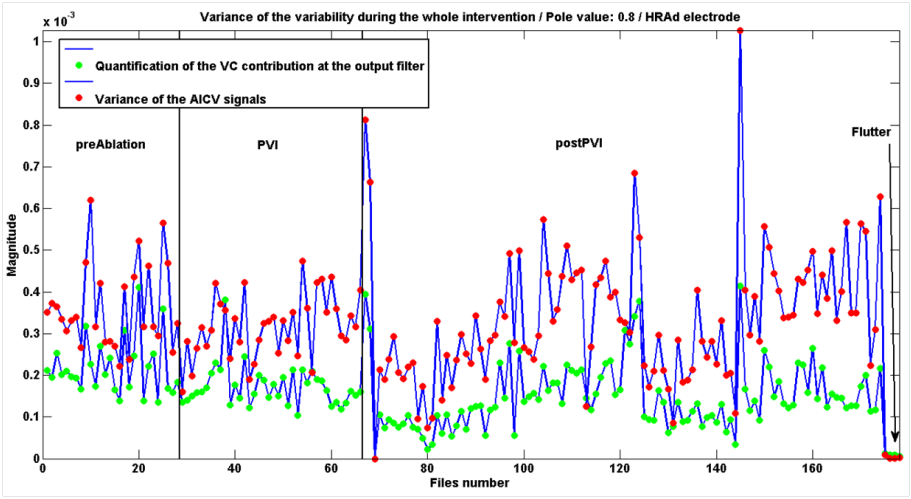

Figure 6.21: *Evolution of the variance of the ventricular contractions contribution and the atrial intracardiac variability during the procedure for the sixth patient.*

6.4.4 Discussion

The goal of this experiment was to confirm the constant VC contribution to ICV signals during the procedure. The results demonstrated that the variance of the mechano-electrical contribution of the VC was almost constant for all the patients. However, this experiment was with only six patients which is not sufficient to conclude definitively that the VC contribution present in the ICV

signals is constant during the procedure.

6.5 Normalized cross-correlation between intracardiac variability and atrial intracardiac variability signals

6.5.1 Introduction

Thanks to the adaptive algorithm presented in the previous sections, it is possible to handle signals containing only AICV. The method presented in this section attempts to determine if the AICV signals become more similar when cancellation of the VC contribution has been performed and, use the similarity of the variabilities among the electrodes as an intracardiac organization index for stepwise RF catheter ablations.

6.5.2 Method

The cross-correlation is a statistical tool often used in signal processing in order to quantify the similarity between two signals. It is defined according to the equation 7.2. It describes the cross-correlation of two stationary discrete-time signals x and y of zero-mean.

$$R_{x,y}(\tau) = E\left[x(t+\tau)y(t)\right] \tag{6.3}$$

The cross-correlation is the expectation of the sample product of the two signals, one of which is delayed. The delay τ of the equation 7.2 is the temporal shift between the samples. To facilitate the interpretation of the cross-correlation, the latter is often normalized between 0 and 1 by the standard deviations σ_x and σ_y of the two signals. The following equation described the normalized cross-correlation:

$$R_{x,y}^{Normalized}(\tau) = \frac{R_{x,y}(\tau)}{\sigma_x * \sigma_y} \tag{6.4}$$

For each pair of catheters, the normalized cross-correlation was computed and the maximum of this cross-correlation was stored in a matrix. As the cross-correlation is anti-symmetric, only half of the matrix was filled. The main diagonal of this matrix represents the normalized autocorrelation which should be equal to 1 for all catheters. Finally, in order to facilitate the reading of the matrix, the latter were displayed in the form of an image object with a color scale bounded between 0 (darke blue) and 1 (dark red). Moreover, the squares of the colored matrix were filled with a number. The latter represent the lag corresponding to this cross-correlation. Lags larger than 1 second (or 80 samples) were described by the symbol X, because such large values were considered as not relevant with respect to AF dynamics.

6.5.3 Results

Each figure of this section is composed of two plots. The left plot shows the similarity of the variability before the cancellation of the VC contribution

while the right plot shows the similarity of the variability after removal of the VC contribution. The signals files presented in the results were selected at the crucial moments during the procedure, for example, just before and after the transition to a regular rythm.

6.5.3.1 Patient 1: 2746994

Figure 7.6 describes the variability similiarity of the ICV signals before and after VC cancellation when the flutter became desorganized. The cross-correlation values are small for both plots and a lot of them are not significant because they correspond to time lags larger than 1 second. The limited similarity of the variability between the ICV and AICV signals was expected.

Figure 7.7 shows the similarity of the variability when the flutter became reorganized. The values are higher than the previous one. However, a lot of them are still unrelevant.

Therefore, there is an improvement of the variability similitude before and after removal of the VC contribution in the transition from a desorganized to an organized flutter but the enhancement is not significant.

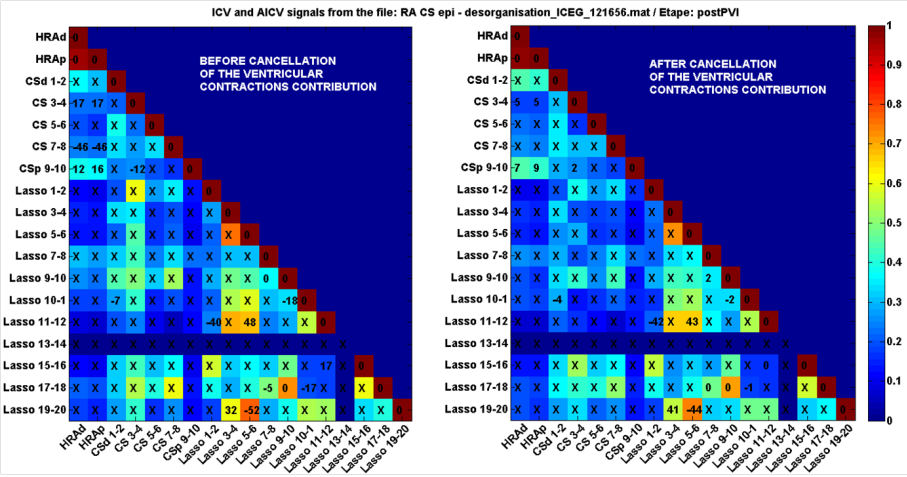

Figure 6.22: *Normalized cross-correlation of the ICV and AICV signals before and after suppression of the VC contribution for the first patient.* ***Part 1.***

6.5.3.2 Patient 5: 906847

Figure 7.9 shows the results of the normalized cross-correlation for the ICV and AICV signals just before atrial tachycardia. The same lag are sometimes repeated within a same column. This phenomenon is amplified with the atrial tachycardia appearance as illustrated on the figure 7.10. For the moment there is no explanation to this phenomenon.

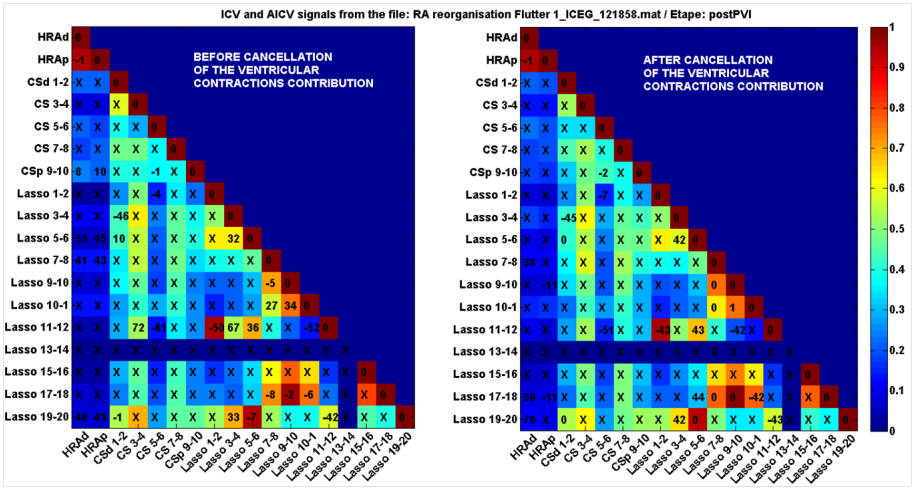

Figure 6.23: *Normalized cross-correlation of the ICV and AICV signals before and after suppression of the VC contribution for the first patient.* ***Part 2.***

The normalized cross-correlaton values on figure 7.10 are larger, suggesting an improvement of the similarity between the signals. Indeed, the values of the CS and Lasso electrodes increased for the atrial tachaycardia.

Figure 6.26 presents the similarity of the variability one minute later, always during the atrial tachycardia. The normalized cross-correlation decreased at the locations of the CS and Lasso leads but is more homogenously distributed compared to the previous figure 7.10.

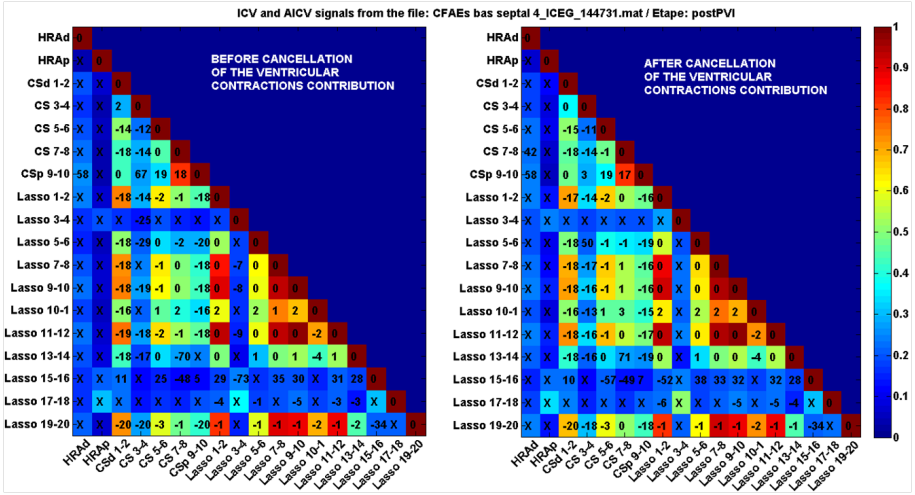

Figure 6.24: *Normalized cross-correlation of the ICV and AICV signals before and after suppression of the VC contribution for the fifth patient.* ***Part 1.***

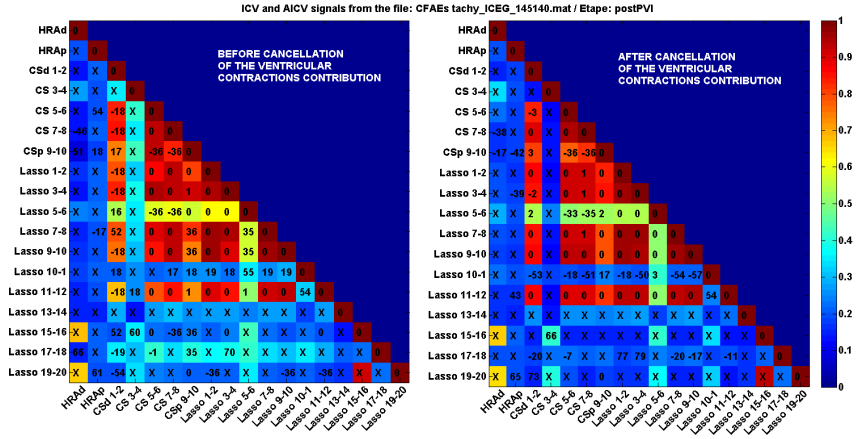

Figure 6.25: *Normalized cross-correlation of the ICV and AICV signals before and after suppression of the VC contribution for the fifth patient.* ***Part 2.***

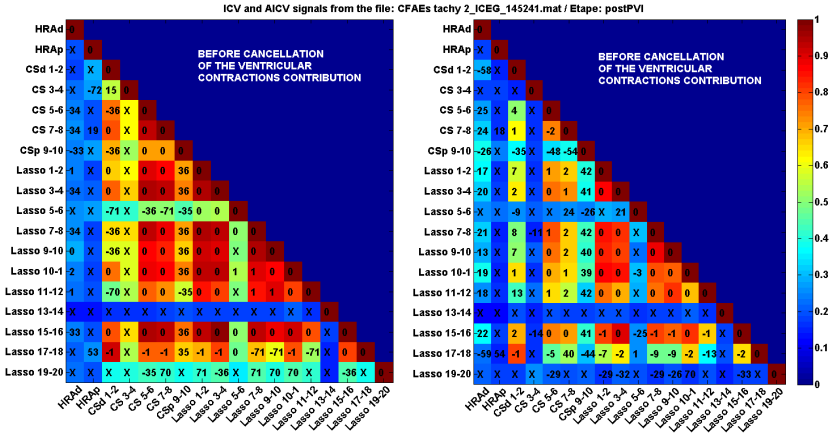

Figure 6.26: *Normalized cross-correlation of the ICV and AICV signals before and after suppression of the VC contribution for the fifth patient.* ***Part 3.***

6.5.4 Discussion

The increase of the similarity of the variability observed before and after the transition to a regular rhythm is broadly small. Besides, the normalized cross-correlation improvement is often localized around a group of electrodes belonging to the same catheter. It was rare that the normalized cross-correlation of two distinct electrodes was large. The results of the Lasso have to be cautiously handled because it is not unlikely that a high cross-correlation value between two electrodes of the Lasso catheter is due to an overlapping of both electrodes. To exclude this situation, it would be helpful to record the Lasso catheter movements in the 3D reconstruction during the procedure. However, this option is not yet available.

It also appeared that the similarity of the variability is higher before VC contribution cancellation than after it. This can be explained by the fact that the adapative filtering removes a regular component present in both signals. Therefore, the normalized cross-correlation becomes smaller because of the removal of this regular component.

The high values of the similarity of the variability are most of the time correlated with a small lag. Moreover, this same lag can appear several times in a column corresponding to a specific electrode. Would it mean that it is the same wave which propagated and reached these electrodes? For the moment, the available data do not permit to answer this question.

Finally, many of the cross-correlation values were considered as not significant because the corresponding lag was too large. More precisely, the lag between the maximum normalized cross-correlation and the reference was larger than 1 second (or 80 samples). A plausible reason which could partially explain this is low quality of the signals at the beginning of the process. The previous experiments were performed with the electrodes of the HRA catheter, and especially with the HRAd electrode. The latter records high quality signals due to its tight location against the endocardiac tissue in the RA during the whole procedure. However, this is not necessarily the case for the signals from the other electrodes. Therefore, if at the beginning the signals present a poor quality, the peak detection can be inaccurate and so, the cross-correlation of the variability cannot return significant results. This issue makes the interpretation of the results yet more difficult.

6.6 Conclusions

In conclusion, the variability of EGM signals is affected by a mechano-electrical contribution of the VC contractions which represents a not negligeable percentage of $41\% \pm 6.7\%$. The normalized least-mean square adaptive filtering cancels very efficiently, but maybe not completely, this VC contribution. These first promising results have to be confirmed with more patients and experiments. They also open the possibility the develop new intracardiac organization indices by handling AICV signals.

Chapter 7

Intracardiac signals

7.1 Introduction

This chapter is mainly focused on the development of intracardiac organization indices from the EGM signals recorded via the intracardiac electrodes. The diversity of the intracardiac electrodes locations during the ablation procedure opens the possibility to develop specific intracardiac organization indices from EGM signals of specific electrodes.

7.2 Extraction of the ventricular activity in the EGM singals

7.2.1 Introduction

The previous chapter clearly demonstrated the presence of a mechano-electrical contribution of the VC in the intracardiac variability signals because of the physical connection between the ventricles and the atria. Most likely, AF EGMs are also affected by the ventricular activity. In order to confirm this assumption, the adaptive filter used for the intracardiac variability signals is also applied to AF EGMs, however the preprocessing is partially modified.

7.2.2 Method

Two preprocessing steps on the EGMs and ECGs are necessary before applying the adaptive filtering.

7.2.2.1 EGM signal preprocessing

The EGMs is transformed in a smoothed version according to the method developed by Botteron and al. [8],[36]. The processing is as follow:

1. Resampling at 1000 Hz
2. Bandpass filtering between 40 Hz and 250 Hz (Kaiser window, order 40)
3. Rectification

4. Lowpass filtering at 20 Hz (Kaiser window, order 40)

5. Resampling at 100 Hz

This last resampling was necessary in order to have a raisonnable time execution with the adaptive filtering. Figure 7.1 illustrates the results of the preprocessing. The top plot shows the original EGM signal resampling at 1 kHz. The bottom plot displays the outcome of the preprocessing (sampling frequency of 1 kHz) which is nothing else than a smoothed version of the EGM signal.

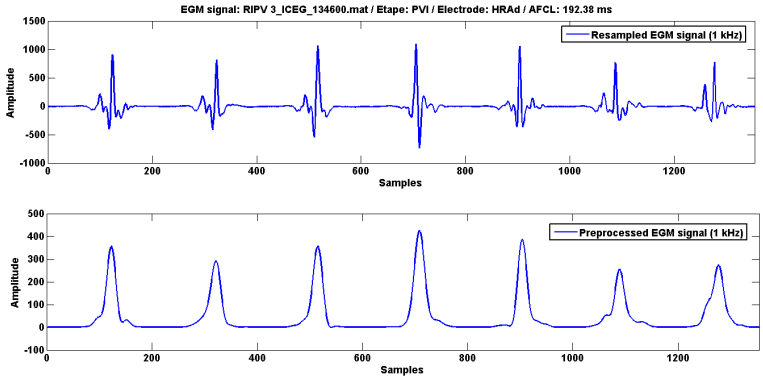

Figure 7.1: *Preprocessing of an EGM signal according the Botteron and al. method [8].* ***Top:*** *Original EGM signal (sampling frequency of 1 kHz).* ***Bottom:*** *Preprocessed EGM signal in a smoothed version (sampling frequency of 1 kHz).*

The purpose of this preprocessing is to obtain a continuous signal of intracardiac times activation at a sampling frequency of 100 Hz which is susceptible to be affected with a ventricular activity.

7.2.2.2 ECG signal preprocessing

The ECG signals are preprocessed in the same way than in the previous chapter. First, the detected ventricular peaks on lead V1 are transformed in a spike train at a sampling frequency of 100 Hz (see top and middle plots of figure 7.2). Then, the spike trains of ventricular impulses are convoluted by a causal exponential filter in order to obtain a continuous signal (see the bottom plot of figure 7.2. The pole of this filter was arbitrarily defined at 0.95.

7.2.2.3 Adaptive filtering

The adaptive filtering algorithm based on the minimization of the normalized least-mean square (NLMS) error was also used in order to extract the ventricular contribution by identifying as close as possible the continuous signal of decaying exponential filter to the preprocessed EGM signal. The extracted ventricular

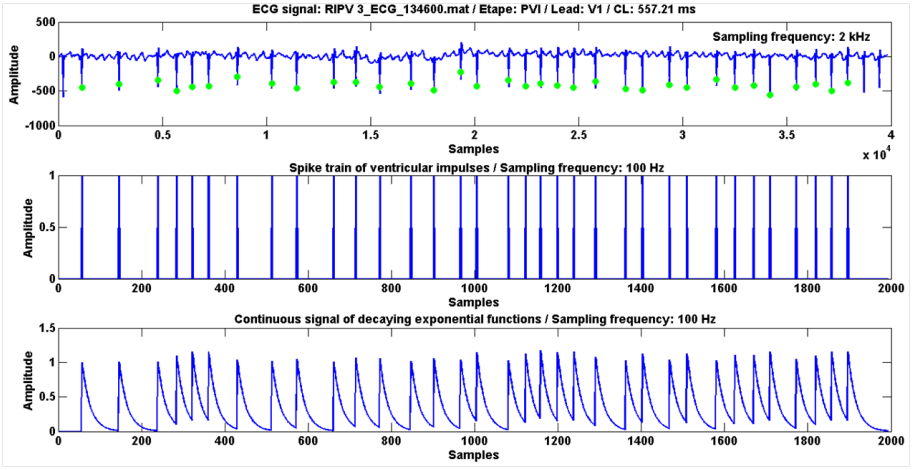

Figure 7.2: *Preprocessing of an ECG signal before the adaptive filtering.* ***Top:*** *ECG signal with the green dots corresponding to the detected ventricular peaks (sampling frequency of 2 kHz).* ***Middle:*** *Spike train of ventricular impulses at 100 Hz.* ***Bottom:*** *Outcome of the convolution between the spike train and the exponential filter (sampling frequency of 100 Hz).*

contribution is then substracted from the preprocessed EGM signal. Figure 7.3 illustrates the main steps of the adaptive filtering.

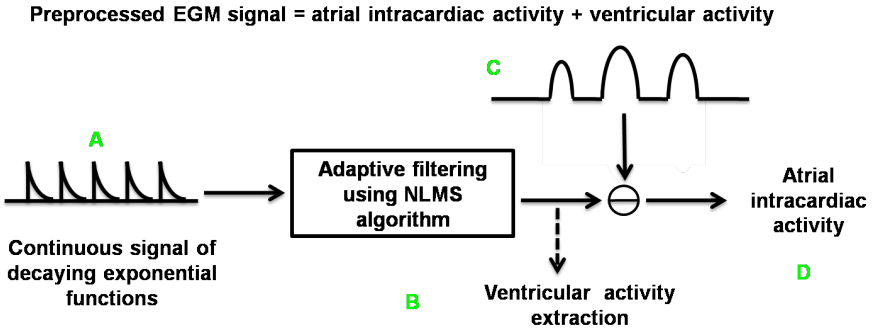

Figure 7.3: *Main steps of the adaptive filtering in order to extract the ventricular contractions contribution to the EGM signals.*

7.2.3 Results

In order to observe the effect of the ventricular mechano-electrical suppression in the ICV signal, the non-parametric power spectral density (PSD) of various signals was computed before filtering, after filtering and after subtraction of the ventricular mechano-electrical contribution. The PSD was estimated using Welch's averaged modified periodogram method of spectral estimation

previously explained in the chapter concerning the intracardiac variability. The figures of the results are divised in four subplots. Each subplot refers to a letter A, B, C, or D corresponding to a specific step of the adaptive filtering schema of figure 7.3.

7.2.3.1 Patient 5: 906847

The figure 7.4 shows the four PSDs performed from the different signals involved in the adaptive filtering. The top plots show respectively the PSDs of the adaptive filtering input and output. The PSD of the output filter is principally concentrated around 5 Hz and which reflects the atrial activity and quasi nothing around the typical range of the ventricular activity (1.5 to 2.5 Hz). Therefore, the adpative filtering extracts not only the ventricular activity but also a non negligeable atrial activity. The bottom plots display respectively the PSD of the EGM signal and the PSD of this same EGM signal at which the ventricular contribution extracted from the PSD of the output filter was subtracted. As atrial activity and ventricular activity were extracted by the adaptive filtering, the consequence is a non desirable suppression of the atrial activity in the PSD of the EGM signal.

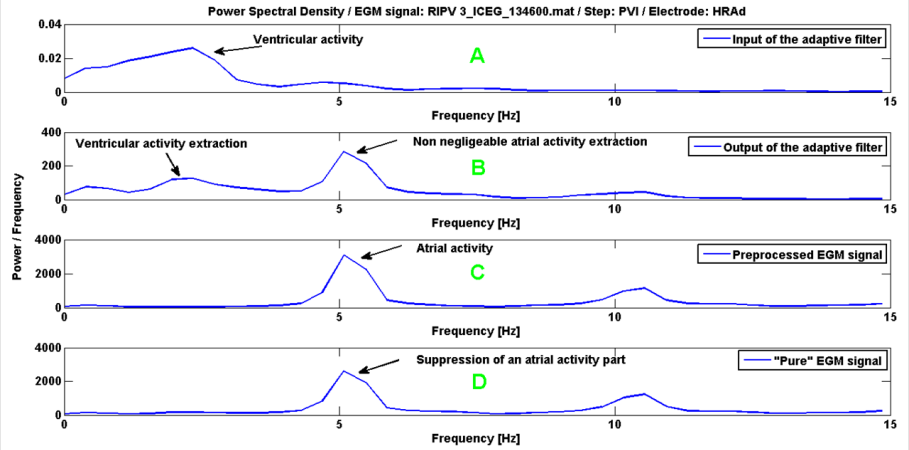

Figure 7.4: *Power spectral density (PSD) of the signals involved in the adaptive filtering for the fifth patient.* ***Top:*** *PSD of the adaptive filter input which is the continuous signal of decaying exponential functions.* ***Middle top:*** *PSD of the adaptive filter output which is the ventricular contribution.* ***Middle bottom:*** *PSD of the EGM signal.* ***Bottom:*** *PSD of the EGM signal devoid of the ventricular contribution.*

7.2.3.2 Patient 6: 2241998

The effect of this non desirable atrial activity suppression via the adaptive filtering is more obvious when the patient is in flutter. The top plots of figure 7.5 display respectively the PSDs of the input and output of the adaptive filtering. The PSD of the adaptive filter output extracted a large part of the atrial activity (around 4 Hz) and a negligeable ventricular activity (around 2 Hz). The bottom

plots display respectively the PSD of the EGM signal with a main atrial activity around 4 Hz and the PSD of this same EGM signal at which the ventricular contribution extracted from the PSD of the output filter was subtracted. The PSD of the bottom plot shows a PSD where quasi all the atrial activity was removed.

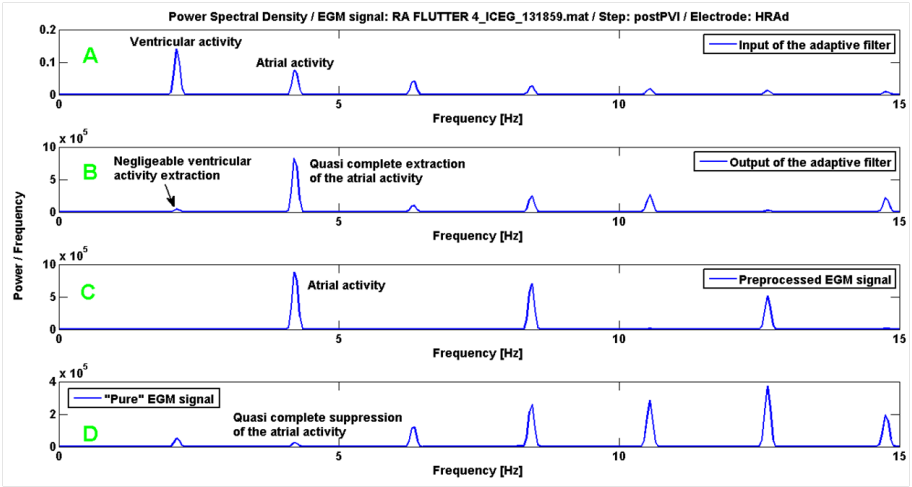

Figure 7.5: *Power spectral density (PSD) of the signals involved in the adaptive filtering for the fifth patient.* ***Top:*** *PSD of the adaptive filter input which is the continuous signal of decaying exponential functions.* ***Middle top:*** *PSD of the adaptive filter output which is the ventricular contribution.* ***Middle bottom:*** *PSD of the EGM signal.* ***Bottom:*** *PSD of the EGM signal devoid of the ventricular contribution.*

7.2.4 Discussion

The purpose of this method was to extract a possible ventricular contribution present in the EGM signals. The results demonstrated that the EGM signals do not contain a ventricular activity or at least a very negligeable one and the adaptive filtering has the tendancy to remove a part of the atrial activity of the preprocessed EGM signal. Therefore, by comparing these results with those concerning the variability in the previous chapter, it is principally the variability of the EGMs which is affected by a mechano-electrical contribution of the VC and not the EGM signals themselves.

7.3 Normalized cross-correlation of EGM signals of all possible pair of electrodes

7.3.1 Introduction

The pairwise method presented in this section attempts to estimate the normalized cross-correlation of the EGM signals of all possible pair of electrodes

and to determine if there is an evolution of their similarity during the procedure.

7.3.2 Method

The method used to calculate the normalized cross-correlation was the same as the one presented in the previous chapter in the section dedicating to the normalized cross-correlation of ICV and AICV signals. Here, the normalized cross-correlation is performed via the EGM signals (1 kHz) preprocessed by the method of Botteron and al. [8],[36]. This preprocessing is necessary because if the normalized cross-correlation was performed with spike trains, the results would have almost null because the probability that two spikes perfectly overlap is low. In order to take into account the possible lag between the spikes correlation, the EGM signals were transformed into smoothed versions which confer a certain slack in the peak-to-peak correlation. For each pair of electrodes, the smoothed versions of the EGM signals were cross-correlated and the maximum was stored in a matrix. In order to facilitate the interpretation of the matrix, the latter was displayed in the form of an image object with a color scale bounded between 0 (dark blue) and 1 (dark red). Each square of the matrix contains a number or the symbol X. Lags larger than 1 second (or 1000 samples) were described by the symbol X, because such large values were considered as not relevant with respect to AF dynamics.

7.3.3 Results

The signals files presented in the results were selected at the crucial moments during the procedure, for example, just before and after the transition to a regular rythm.

7.3.3.1 Patient 1: 2746994

Figure 7.6 displays the normalized cross-correlation between all possible pair of electrodes. The similarity is rather low except the one for the Lasso catheter. Therefore, it would seem that the LAA is much more organized than the rest of both atria.

Figure 7.7 shows the results a few minutes later. The similarity of the signals on the Lasso catheter is again more important than in the previous figure suggesting an improvement of the intracardiac organization in the LAA. In addition, there is also an increase of the similarity between the EGM signals on the CS catheter. Therefore, the improvement of the intracardiac organization was maybe not only localized at the LAA but at the LA.

Figure 7.8 displays the results of the normalized cross-correlation a few minutes after the figure 7.7. Globally, the similarity of the EGM signals is much better between any pairwise catheter. It implies a global improvement of the intracardiac organization in both atria. Therefore, the ablation related to these results was maybe an appropriate CFAE to ablate.

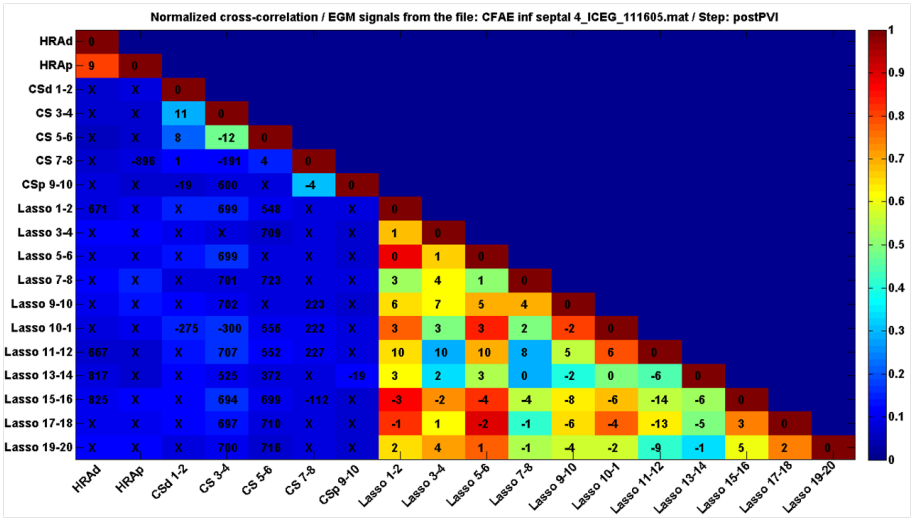

Figure 7.6: *Normalized cross-correlation between the EGM signals of all possible pair of electrodes for the first patient,* ***Part 1.***

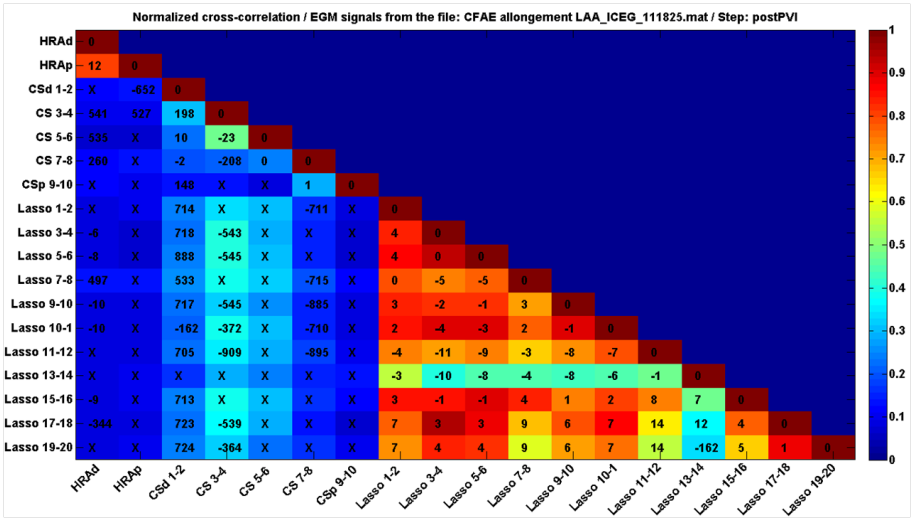

Figure 7.7: *Normalized cross-correlation between the EGM signals of all possible pair of electrodes for the first patient,* ***Part 2.***

7.3.3.2 Patient 5: 906847

Figure 7.9 displays the normalized cross-correlation performed between all EGMs of all pairs of electrodes. The normalized cross-correlation values of the EGMs in the LA are very high. It is not the case for the signals of the HRA catheter. It suggests that the LA and the LAA are more organized than the RAA.

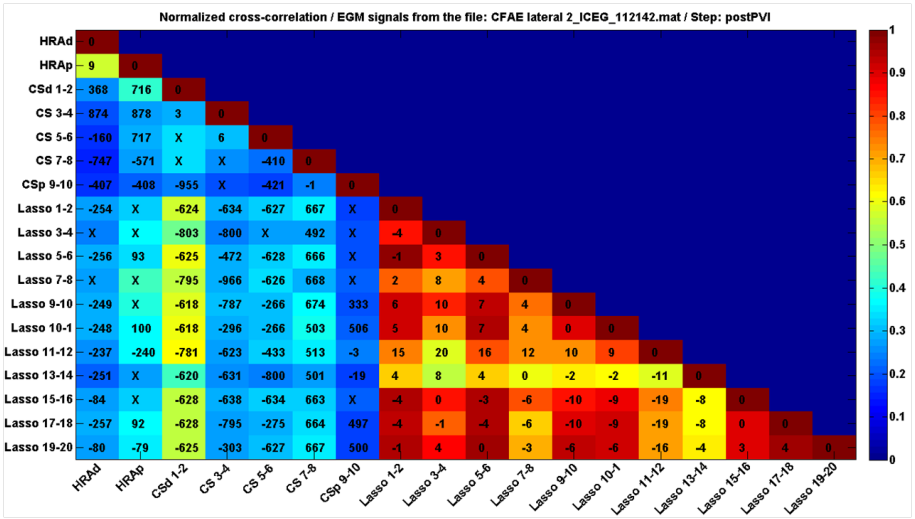

Figure 7.8: *Normalized cross-correlation between the EGM signals of all possible pair of electrodes for the first patient,* ***Part 3.***

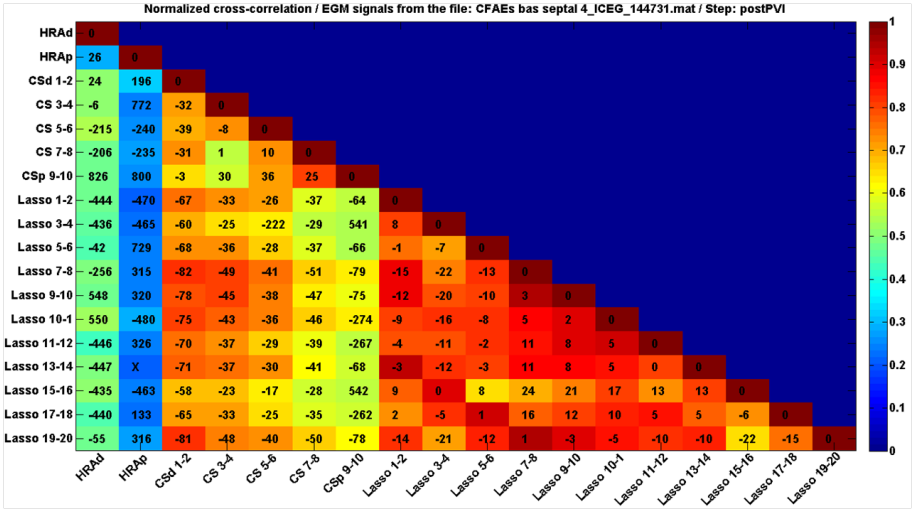

Figure 7.9: *Normalized cross-correlation between the EGM signals of all possible pair of electrodes for the fifth patient,* ***Part 1.***

Figure 7.10 shows the normalized cross-correlation values of the EGM signals in atrial tachycardia. Only a few minutes separate the results between this figure and the previous one. All the values are closed or equal to 1 suggesting the presence of a unique wave propagating in both atria and so, the presence of an atrial tachycardia.

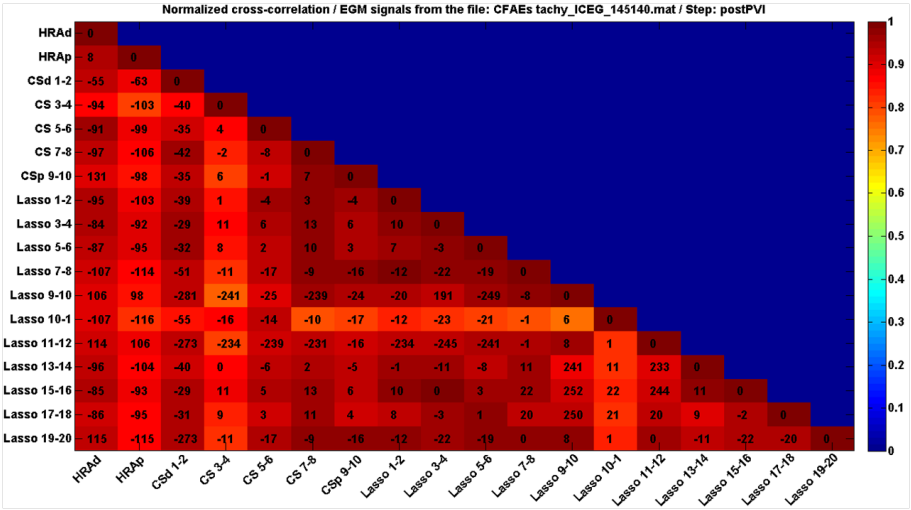

Figure 7.10: *Normalized cross-correlation between the EGM signals of all possible pair of electrodes for the fifth patient,* ***Part 2.***

7.3.4 Discussion

The goal of this experiment was to assess the similarity of the EGM signals in a pairwise catheters process via the estimation of the normalized cross-correlation. The obtained results were rather good. However, the results have to be taken with caution concerning the Lasso catheter. As mentionned previously, it is possible that the normalized cross-correlation performed on the EGM signals from the Lasso catheter are large because the electrodes of the Lasso catheter overlap. The main advantage of this method is that there is no need to detect the atrial depolarizations before computing the normalized cross-correlation. Therefore, the possible issues coming from the peak detection because of the poor signal quality can be excluded in this method. Finally, the main disadvantage of this method is to have a too large temporal resolution. One way to reduce the temporal resolution is to insert a window in which the correlation is estimated as described in the next subsections.

7.4 Clipped cross-intensity function

7.4.1 Introduction

Hahnloser developed a method for measuring the cross-intensity function (CIF). The CIF can be understood as the probability of observing spikes in source (S) signal at some time lag t of spikes in target (T) signal. Figure 7.11 illustrates the CIF. Therefore, the CIF is the conditional spike probability (CSP).

In order to confer a certain slack in the spike-to-spike correlation, the CIF can be clipped by a window τ in which the CSP is estimated. Therefore, the

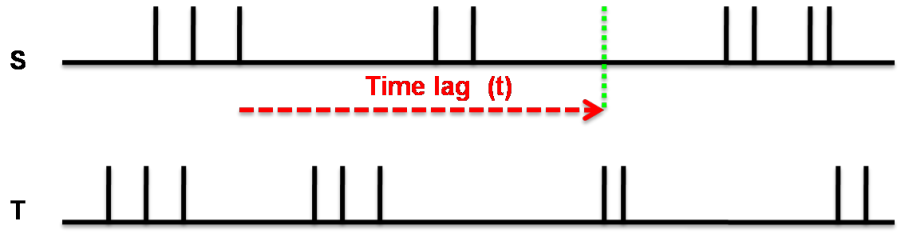

Figure 7.11: *Illustration of the cross-intensity function which is the probability of observing spikes in signal S at som time lag t of spikes in signal T.*

clipped CIF represents the fraction of S spikes for which target fires at least one T spike in the window. The clipped CIF is illustrated on figure 7.12.

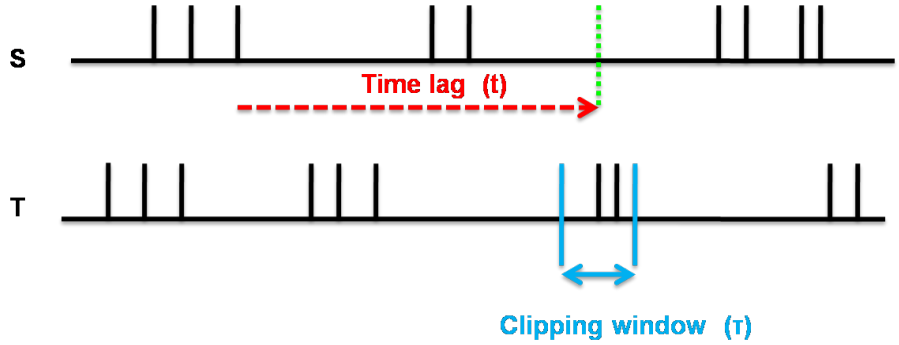

Figure 7.12: *Illustration of the clipped cross-intensity function which is the fraction of S spikes for which target T fires at least one T spike in the window τ.*

The method developed by Hahnloser was transposed to synchronized AF EGMs from two different electrodes in order to explore if there is a natural time scale between depolarizations and if it the case use it as an intracardiac organization indice.

7.4.2 Method

The clipped CIF is function of two parameters, t and τ. The risk in this method is to choose a τ window too wide. Indeed, for values of τ too large, the probability to find at least one T spike is almost equal to 1. The statistic is overestimated in this case. Therefore, a tradeoff has to be done in order to find the optimal values of the time lag t and the window width τ.

The following statistics is divided into two parts. The first part attempts to find a significant time lag t. The second part investigates in the research of the optimal window width τ by taking into account the previously defined time lag t.

7.4.2.1 Spike-train correlation

AF EGMs can be easily transformed into a spike train by a sum of delta functions

$$\rho(t) := \sum_{i=1}^{N} \delta(t - t_i) \tag{7.1}$$

where N variable corresponds to the number of the spikes up to time T which is the total recording time. T is composed of discrete steps Δt. The discrete delta function is defined as $\delta(k\Delta t) = 0$ for all integers $k \neq 0$ and $\delta(0) = 1/\Delta t$.

Cross-correlation function The method is applied on two synchronizd spike trains S and T with spike times $t_i^{\mathrm{T}}(i = 1, \ldots, N_{\mathrm{T}})$, and $t_i^{\mathrm{S}}(i = 1, \ldots, N_{\mathrm{S}})$ recorded from two different electrodes. Do not be confused with the parameters T which defines the time and T which corresponds to the target signal. The following equation describes the cross-correlation function $P_{\mathrm{TS}}(t)$ between these two spike trains,

$$P_{\mathrm{TS}}(t) := \langle \rho_{\mathrm{T}}, \rho_{\mathrm{S}} \rangle (t) = \frac{1}{T} \int_0^T ds \quad \rho_{\mathrm{T}}(t+s)\rho_{\mathrm{S}}(s) \tag{7.2}$$

Because the cross-correlation function is commutative ($P_{\mathrm{TS}}(t) = P_{\mathrm{ST}}(-t)$), it can be thought of as the joint probability density of observing a spike in signal S separated by time t from a spike in signal T.

Cross-intensity function The conditional probability between two random variables is defined as the joint probability divided by the marginal probability. According to this definition, the CIF function is

$$P_{\mathrm{T|S}} := \langle \rho_{\mathrm{T}} | \rho_{\mathrm{S}} \rangle (t) = \frac{1}{\langle \rho_{\mathrm{S}} \rangle} \langle \rho_{\mathrm{T}}, \rho_{\mathrm{S}} \rangle (t) \tag{7.3}$$

where $\langle \rho_{\mathrm{S}} \rangle := N_{\mathrm{S}}/T$ and N_{S} is the total number of spikes S. However, the CIF function is nothing else than an estimation of the conditional spike probability (CSP). Therefore, the CIF function can be simplified. Indeed, as mentionned at the beginning of this section, it corresponds to the number of S spikes separated by time t of a T spike. Therefore, the CIF between the spike trains S and T can be calculated according to the following equation

$$P_{\mathrm{T|S}} = \langle \rho_{\mathrm{T}} | \rho_{\mathrm{S}} \rangle (t) = \frac{\#\text{ S spikes separated by } t \text{ of a T spike}}{N_{\mathrm{S}}} \tag{7.4}$$

The standard error $S_{\mathrm{T|S}}(t)$ evaluates the uncertainity of the CIF at a time lag t

$$S_{\mathrm{T|S}}(t) := \sqrt{\frac{P_{\mathrm{T|S}}(t)\left(1 - P_{\mathrm{T|S}}(t)\right)}{N_{\mathrm{S}}}} \tag{7.5}$$

First significance test In order to test the significance of the CIF maximum, $\hat{p} = max_t P_{\mathrm{T|S}}(t)$, a z-test iss performed with the null hypothesis that the target spike train is conditionally independant of the source spike train, $H_0 := \hat{p} = P_{\mathrm{T}}$. P_{T} is the probability that the target spikes appears in a random fashion,

$$P_{\mathrm{T}} := \frac{N_{\mathrm{T}}}{T/\Delta t} = \frac{N_{\mathrm{T}}\Delta t}{T} \tag{7.6}$$

where N_{T} is equal to the total number of target spikes and $T/\Delta t$ is equal to the total number of time bins include in T. The hypothesis is rejected if the estimator of P_{T} which is $\hat{p}$ falls into in the α-tail of the estimator density 7.7. Therfore, H_0 is rejected if

$$\text{z-value} := \frac{|\hat{p} - P_{\mathrm{T}}|}{\sqrt{\frac{P_{\mathrm{T}}(1-P_{\mathrm{T}})}{N_{\mathrm{S}}}}} > z_\alpha \tag{7.7}$$

where $z_\alpha = 2.33$ corresponds to a one-sided test at a confidence level $\alpha = 1\%$. If the H_0 is rejected, it means that the estimator of P_{T} which is $\hat{p}$ is considered as significant. More precisely, the time lag t of the estimator $\hat{p}$ is significant and corresponds to a natural time scale for which the clipped CIF can be computed.

7.4.2.2 Clipped cross-intensity function

According to the significant time lag t defined in the first part of the statistics, the clipped CIF can be calculated. The clipped CIF estimates the probability that at least one target spike is detected in a window $[t - \tau/2, t + \tau/2]$ from a source spike delayed by a time lag t (see figure 7.12). The clipped CIF equation is

$$P^{\tau}_{\mathrm{T|S}} := \frac{1}{N_{\mathrm{S}}} \sum_{i=1}^{N_{\mathrm{S}}} \Theta\Big(\frac{\tau}{2} - min_j \left|t^{\mathrm{S}}_i + t - t^{\mathrm{T}}_j\right|\Big), \tag{7.8}$$

where the Heaviside function is given by

$$\Theta(x) = \begin{cases} 1 & \text{if } x \geq 0 \\ 0 & \text{otherwise} \end{cases} \tag{7.9}$$

The standard error $S^{\tau}_{\mathrm{T|S}}$ of the clipped CIF function is computed according the following equation

$$S^{\tau}_{\mathrm{T|S}} := \sqrt{\frac{P^{\tau}_{\mathrm{T|S}}\left(1 - P^{\tau}_{\mathrm{T|S}}(t)\right)}{N_{\mathrm{S}}}} \tag{7.10}$$

Marginal probability The marginal spike probability P^{τ}_{T} corresponds to the probability that a random time window of width τ applying to the T spike train contains at least one spike.

$$P^{\tau}_{\mathrm{T}} := \frac{\tau}{T} \sum_{k=1}^{T/\tau} \Theta\Big(\frac{\tau}{2} - min_j \left|k\tau - t^{\mathrm{T}}_j\right|\Big) \tag{7.11}$$

where T/τ is equal to the total number of clipping window which can be include in the target signal. The standard error of the marginal probability is

$$S_{\mathrm{T}}^{\tau} := \sqrt{\frac{P_{\mathrm{T}}^{\tau}\left(1 - P_{\mathrm{T}}^{\tau}\right)}{N_{\mathrm{S}}}} \tag{7.12}$$

Second significance test The clipped CIF $P_{\mathrm{T|S}}^{\tau}(t)$ is significantly larger than the marginal spike probability P_{T}^{τ} if it satisfies

$$\text{z-value function} = z^{\tau}(t) = \frac{\left|P_{\mathrm{T|S}}^{\tau}(t) - P_{\mathrm{T}}^{\tau}\right|}{S_{\mathrm{T}}^{\tau}} > z_{\alpha} \tag{7.13}$$

Finally, the optimal clippling window for the time lag t is the maximum of $z^{\tau}(t)$ and the clipped CIF related to this window width can be stored.

7.4.3 Results

The clipped CIF was computed on EGM signals of 10 seconds duration. The EGM signal recorded from the HRAd electrode was considered as the source while the EGM signal recorded from the HRAp electrode was defined as the target.

7.4.3.1 Patient 4: 2770271

Figure 7.13 displays the clipped CIF percentages obtained via the method of Hahnloser. Globally, the results are not good. Instead of having a progressive increase of the clipped CIF values, there are fluctuations. In addition because the first z-test failed by accepting H_0 hypothesis, there are numerous gaps on the plot. At the end of the procedure, the clipped CIF increases progressively and stabilizes around the value 0.8 confirming the atrial tachycardia state of the patient.

7.4.4 Discussion

The purpose of this method was to assess the clipped CIF during the procedure for both synchronized spike trains, the source (EGM signals of the HRAd electrode) and the target (EGM signals of the HRAp electrode). The results were not good for all the patients. However, Hahnloser applied his method to real spike trains from neurons recorded in the sleeping songbirds. Therefore, it might be possible that this method is not convenient for the structure of the EGM signals. Indeed, the waves collision in the atria during AF could maybe modify the natural time scale of the EGM signals.

7.5 Cross-correlation of EGM signals of a pair of electrodes

7.5.1 Introduction

The following method attempts to assess the similarity between simultaneous EGM spike trains of pairwise electrodes by computing the cross-correlation

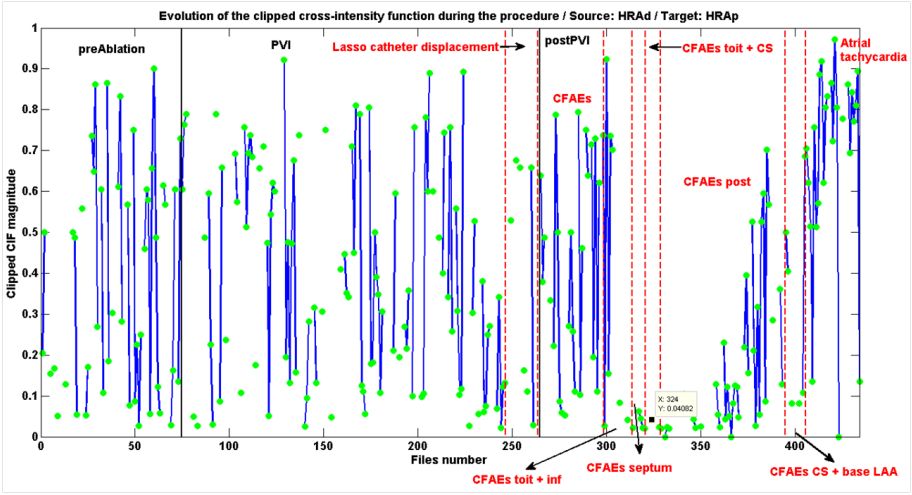

Figure 7.13: *Evolution of the clipped CIF during the procedure for the fourth patient.*

within a window. The cross-correlation calculation performed in this process is similar as a standard cross-correlation but the fact to reduce its time resolution by applying a window gives the possibility to extract a sparseness information which can be used as an intracardiac organization index. Finally, the evolution of this cross-correlation within the window can be also assessed during the procedure.

7.5.2 Method

This method is applied on all synchronized EGM signals of a pair of electrodes for each patient. The source (S) is defined as the reference signal (HRAd lead) and the target (T) is considered as the signal (HRAp lead) on which the spike detection is performed. A window of width equal to the AFCL of the source spike train is applied around each S spikes (red windows on figure 7.14. In each window, a spike detection is performed in the T spike train. The number and the position of the detected T spikes are stored in a window (purple windows on figure 7.14). Finally, the purple windows on figure 7.14 are adding to a final window (blue window on figure 7.14). From the final window two informations are extracted:

- The evolution of the final window during the entire procedure
- A sparseness measure according the following equation

$$\text{sparseness}(w) := \frac{\arg_{max}(w) + 2 \text{ values before and after } \arg_{max}(w)}{\sum_{i=1}^{N_w} w_i} \quad (7.14)$$

In order to facilitate the interpretation, the successive final windows were stored in a matrix. The latter were converted in an image object with a color

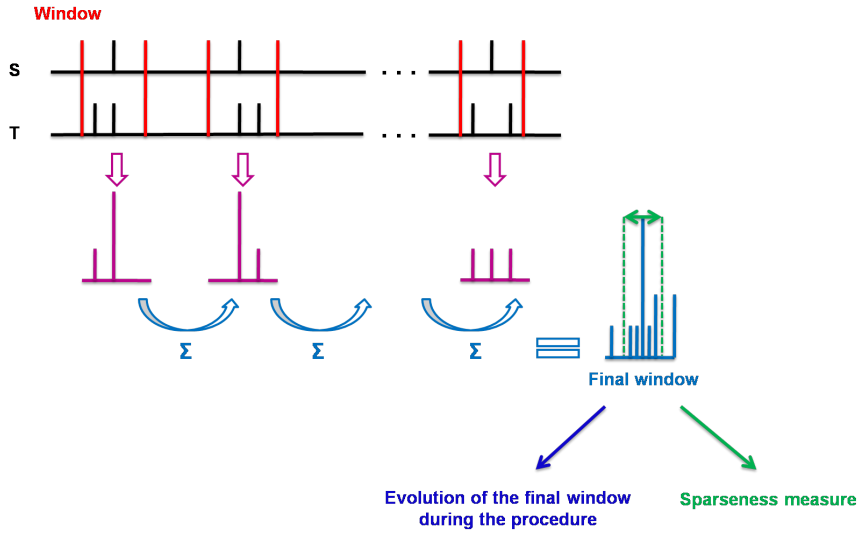

Figure 7.14: *Cross-correlation of EGM signals of a pair of electrodes. The source is the reference signal while the target is the signal on which a spike detection is performed within a window. The way how the cross-correlation between the source and the target is computed permits to extract two types of informations, the sparseness and the final window evolution.*

scale bounded between 0 (dark blue) and 1 (dark red). In addition, the sparseness values were only considered if the ratio between the total number of the T spikes and the total number of S spikes was between 0.8 and 1.2. It implies that both spikes trains contained more or less the same number of peaks and therefore the sparseness computation was not overestimated or underestimated. More close to 1 the sparseness value is, more local was the spike detection whitin the final window and inversly as illustrated on figure 7.15. If the sparseness value is close to 1, it suggests that the T spikes are very close correlated to the S spikes during the detection. This means that the S and T spike trains are more similar and therefore, it implies a higher intracardiac organization.

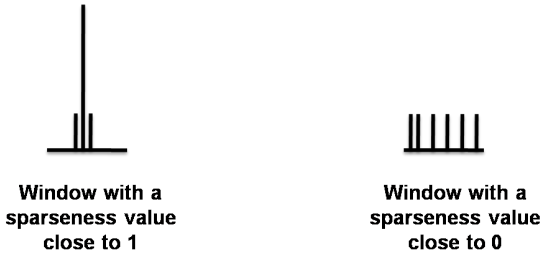

Figure 7.15: *Illustration of the sparseness which is almost equal to 1 when the detected spikes whitin the final window are very close each other and 0 when the detected spikes are dispersed within the final window.*

7.5.3 Results

The two informations extracted from the final window were performed for all the patients but only one of both informations per patient are presented.

7.5.3.1 Patient 1: 2746994

Figure 7.16 displays the evolution of the sparseness during the procedure. The PVI was beneficial because the sparseness becomes larger. The sparseness related to the CFAEs ablations shows fluctuations which suggests that were are some ablated CFAEs which were more beneficial than others. The sparseness became very high when the patient reached flutter state which confirm the very good intracardiac organization in the RAA.

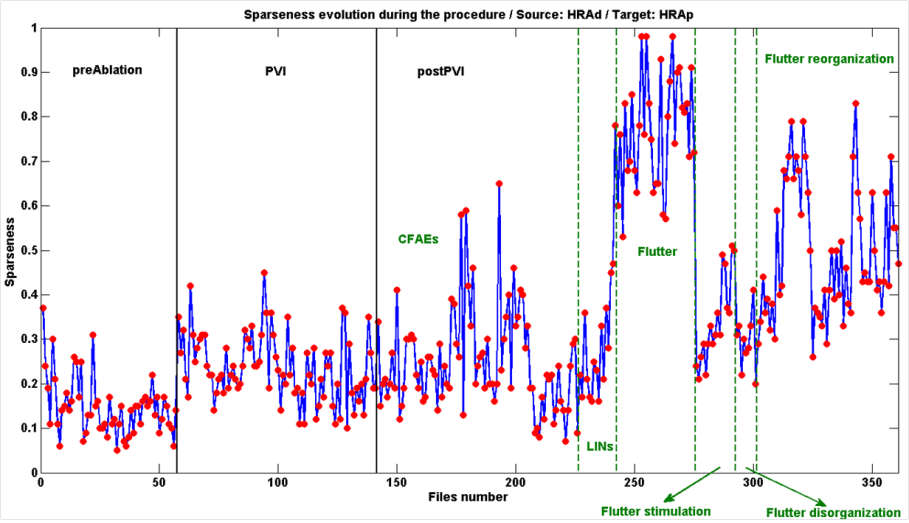

Figure 7.16: *Evolution of the sparseness during the procedure for the first patient.*

7.5.3.2 Patient 2: 43761

The evolution of the final window during the procedure is displayed on figure 7.17. The latter correctly reflects the non success of the procedure. Indeed, the detected spike whithin the successive final windows were always dispersed. There was no regrouping of the detected spike at a local position in the final window which would suggest a better intracardiac organization.

7.5.3.3 Patient 3: 340048

Figure 7.18 shows the evolution of the sparseness during the procedure. The sparseness remained rather constant around 0.25 except when the intracardiac organization became better where it was approximatively between 0.5 and 0.7. The sparseness also fluctuated during the CFAEs ablations suggesting the presence of beneficial as non beneficial ablations for the patient.

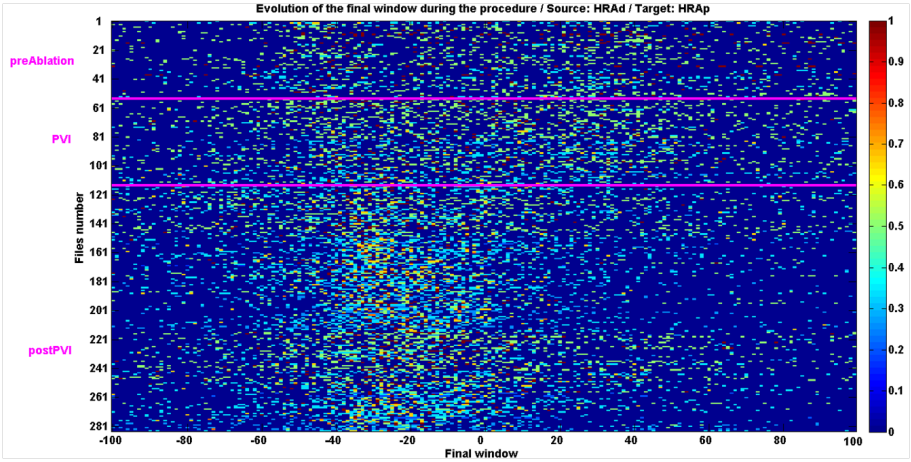

Figure 7.17: *Evolution of the final window during the procedure for the second patient.*

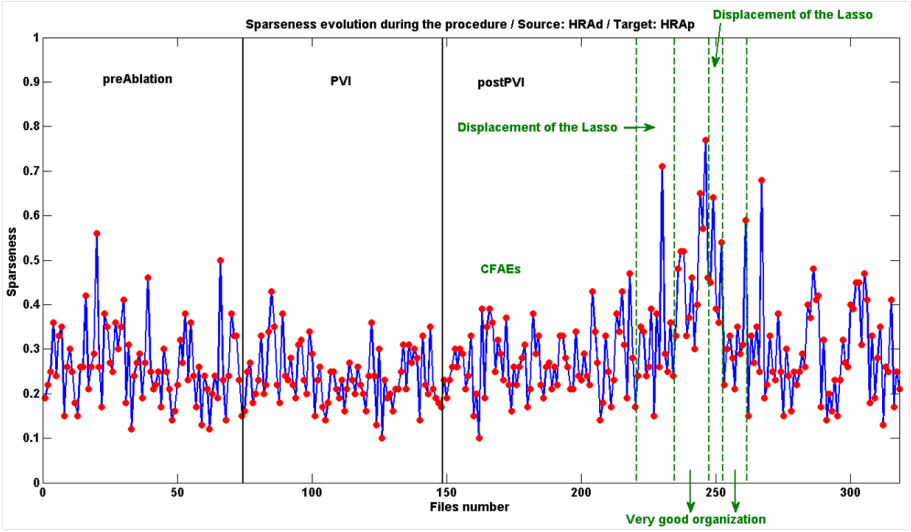

Figure 7.18: *Evolution of the sparseness during the procedure for the third patient.*

7.5.3.4 Patient 4: 2770271

Figure 7.19 presents the evolution of the final window vector during the procedure. At the beginning of the procedure, the detected spikes were mostly localized in the left part of the final window and they were rather dispersed whithin the final window. After the CFAEs ablations, the detected spikes progressively shifted at the center of the final window until becoming very close each other suggesting a high intracardiac organization like an atrial tachycardia.

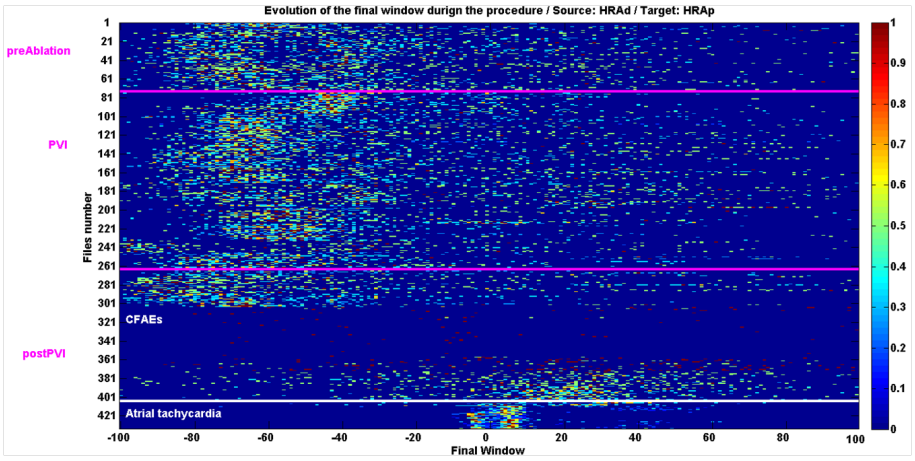

Figure 7.19: *Evolution of the final window during the procedure for the fourth patient.*

7.5.3.5 Patient 5: 906847

The evolution of the final window during the procedure can be observed on figure 7.20. The detected spikes were very dispersed at the pre-ablation and especially during PVI suggesting a disorganized intracardiac rhythm. The first CFAEs ablations improved the situation. Indeed, the detected spikes were less dispersed. Indeed, they were mainly localized in the left part of the final window. The last CFAEs ablations at the posterior inferior roof and septal regions greatly improved the intracardiac rhythm of the patient. The detected spikes shifted and became more close each other compared to previously. When the patient reached atrial tachycardia, the detected spikes were very close each other, suggesting a very organized intracardiac rhythm.

7.5.3.6 Patient 6: 2241998

Figure 7.21 presents the sparseness evolution during the procedure. Globally, the sparseness was very low compared to the previous figures 7.16 and 7.18. Despite this low sparseness suggesting a dispersed detected spikes in the final window, the patient managed to be in flutter. The sparseness equal to 1 reflected well the presence of the flutter in the RAA.

7.5.4 Discussion

The purpose of this experiment was to evaluate the similarity between EGM signals from a pair of electrodes by computing the cross-correlation. The used of a window permitted to extract a sparseness measure concerning the location of the detected spikes within the final window. The fluctuations of the sparseness during the procedures demonstrated that some CFAEs ablations were more beneficial than some other. Therefore, a deeper investigation of these CFAEs seems to be the logical follow of this experiment. If the "good", the "bad" and the "neutral" CFAEs could be identified, it could help to better understand their

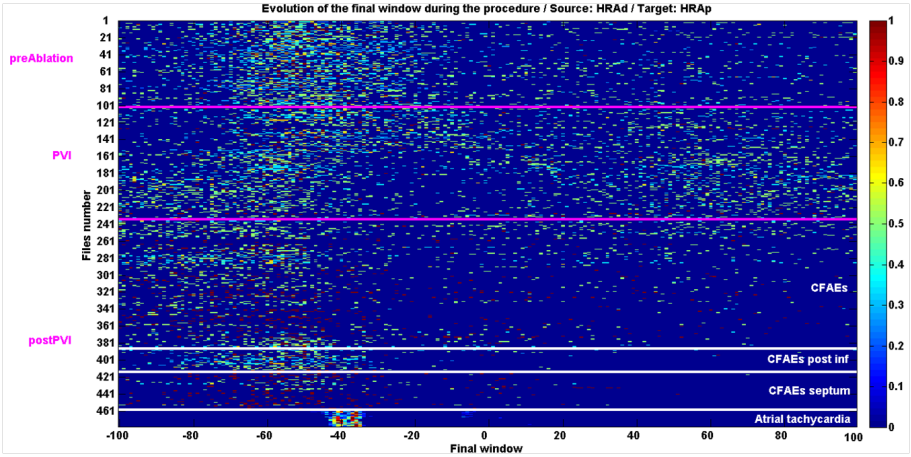

Figure 7.20: *Evolution of the final window during the procedure for the fifth patient.*

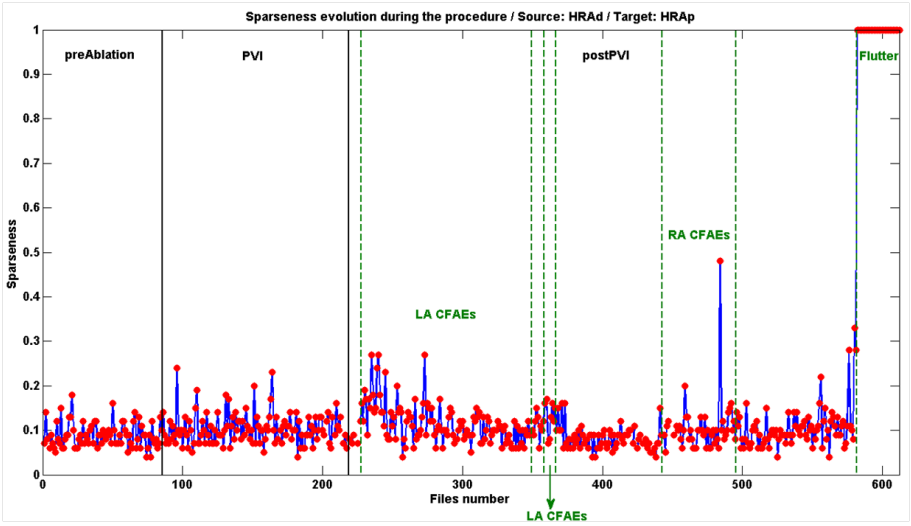

Figure 7.21: *Evolution of the sparseness during the procedure for the sixth patient.*

structural complexity. A next interesting experiment would be the comparison of the intracardiac organization in the RAA and LAA via the sparseness evolution respectively computing from the HRAd and HRAp electrodes for the RAA and two electrodes of the Lasso or CS catheter for the LAA.

The evolution of the final window opens the possibility to assess step by step the effect of an ablation during the procedure. Indeed, more the detected spikes were close each other in the final window, more organized was the intracardiac rhythm in the RAA. It could be helpful for the physician if this method was

implemented in real time. He could have a global view of the evolution of the intracardiac organization.

7.6 Cross-correlation of EGM signals of the Lasso electrodes

7.6.1 Introduction

The principles of the previous method were extended to the signals of the Lasso catheter. The following method computes the cross-correlation of the signals from the Lasso catheter within a window in order to estimate the intracardiac organization in the LAA.

7.6.2 Method

For the first run, the source (S) is the signal on the Lasso1-2 electrode and the remaining signals on the other electrodes of the Lasso catheter are considered as the matrix target (T) on which a spike detection is performed (green target matrix on figure 7.23). A window width equal to the mean of the AFCLs of the signals recorded on the Lasso electrodes was centered around each S spike (red windows on figure 7.23). Within each window, a spike detection is performed in the target matrix. The number and the position of the detected T spikes are stored in a window (purple windows on figure 7.23). Finally, the purple windows on figure 7.23 are adding to a final window which is symmetric (blue window on figure 7.23).

For the second run, the idea remains the same. However, the source is the signal of the Lasso3-4 electrode and the remainder constitutes the target matrix. For the third run, it is the signal on the Lasso5-6 electrode which is the source and the other signals of the Lasso catheter are the target matrix. And this process continues until each signal of the Lasso electrodes were once considered as the source. At the end of the algorithm, a final symmetric window is obtained.

7.6.3 Results

For each patient, the method was applied to all EGM signals recorded on the Lasso catheter. Each EGM signal were split in segment of 10 seconds duration. In order to facilitate the interpretation of the results, only half of the final symmetric window was displayed in the form of an image object with a color scale bounded between 0 (dark blue) and 1 (dark red).

7.6.3.1 Patient 1: 2746994

Figure 7.24 represents the successive final windows corresponding to the cross-correlation of the EGM signals of the Lasso electrodes. Globally, there was a clear evolution of the organization between the pre-ablation and postPVI steps. The CFAEs ablations at the septum region brought a significant improvement of the intracardiac organization in the LAA. Indeed, the detected spikes

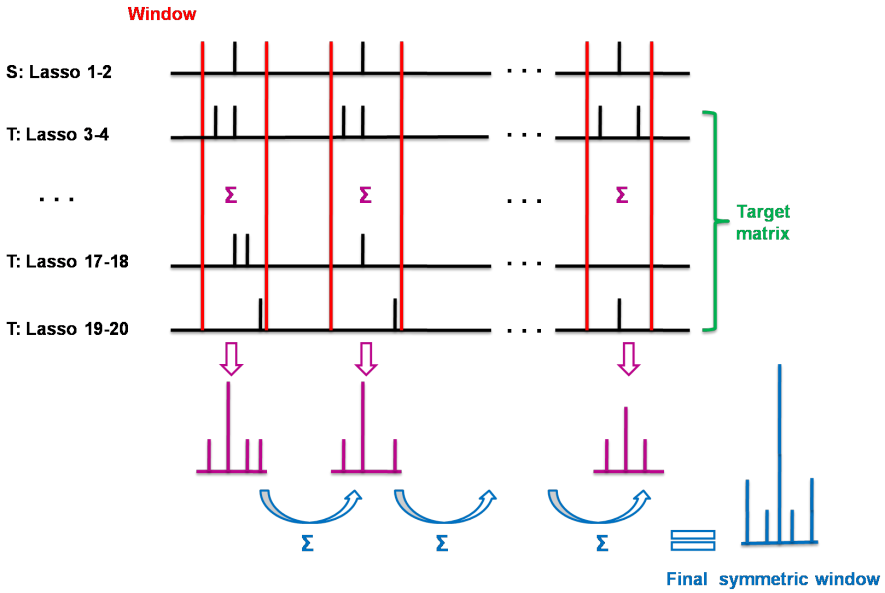

Figure 7.22: Principles of the cross-correlation between EGM signals from the Lasso catheter.

Figure 7.23: *Cross-correlation of EGM signals of Lasso electrodes. The schema present only the first run of the algorithm. EGM signal of Lasso 1-2 electrode is considered as the source while the EGM signals of the Lasso electrodes are defined as the target matrix in which a spike detection is performed whithin a window. At the end of the algorithm, a final symmetric window is obtained.*

were more concentrated at the center of the window. The flutter was composed of two barycenters which became disorganized with the stimulation. After the flutter stimulation, the flutter reorganized showing two barycenters. However, the flutter shifted with the stimulation compared to its previous position.

7.6.3.2 Patient 2: 43761

Figure 7.25 represents the successive final windows for the second patient. Globally, there is no significant evolution of the intracardiac organization in the LAA. Each detected spikes in the final window was very dispersed. It confirms the non success of ablation procedure. In addition, this method is very efficient in order to detect the displacement of the Lasso catheter during the medical procedure.

7.6.3.3 Patient 3: 340048

The signals between the 80^{th} and 100^{th} lines of figure 7.26 suggest an intracardiac organization. Indeed, there is a concentration of the detected spikes around the 10^{th} position from the center of the final window.

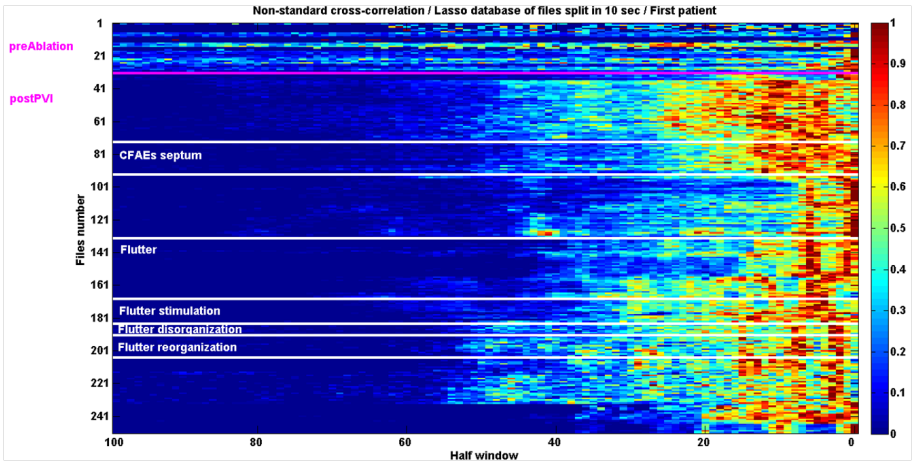

Figure 7.24: *Evolution of the final window during the procedure for the first patient. The results concerning the PVI are not present on the figure because of the poor quality EGM signals.*

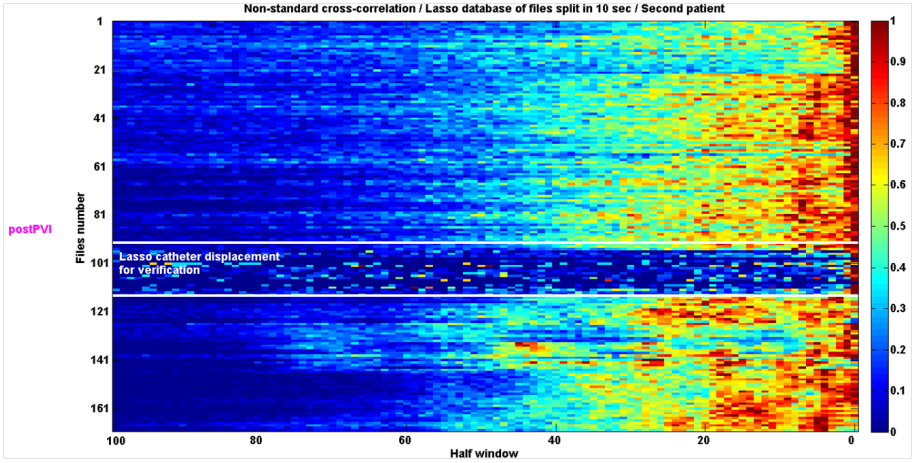

Figure 7.25: *Evolution of the final window during the procedure for the second patient. The results concerning the pre-ablation and the PVI stage are not present on the figure because EGM signals were recorded on the MAP catheter instead of the Lasso catheter.*

7.6.3.4 Patient 4: 2770271

Figure 7.27 shows the results obtained for the fourth patient. Globally, there is a significant positive evolution of the intracardiac organization in the LA until the atrial tachycardia at the end of the procedure. The CFAEs ablations in the septum region involved an important improvement of the intracardiac organisation. Indeed, these ablations concentrated the detected spikes in three distinct regions. These three regions are tranformed with the CFAEs ablations

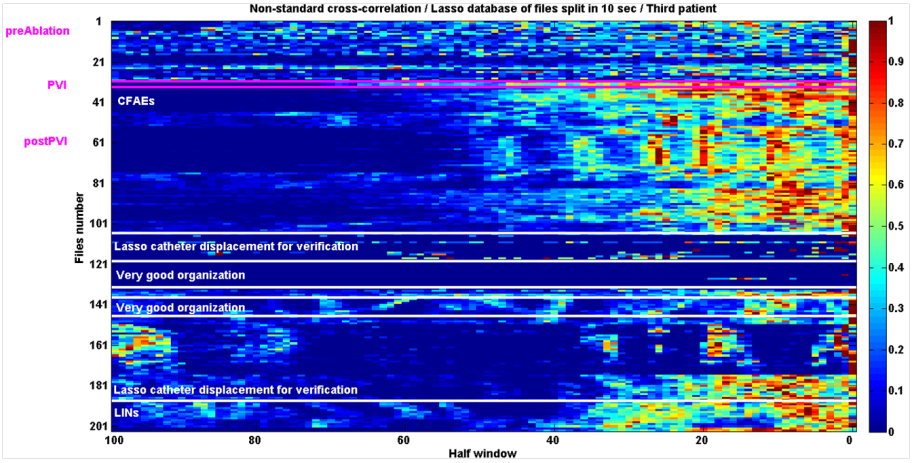

Figure 7.26: *Evolution of the final window during the procedure for the third patient.*

at the base of the LAA into a unique region where the spikes are detected. This corresponds to the apparition of the atrial tachycardia.

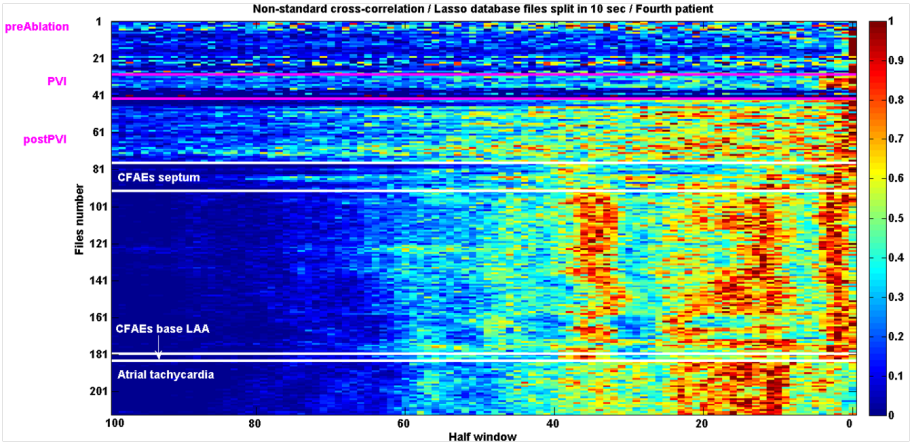

Figure 7.27: *Evolution of the final window during the procedure for the fourth patient.*

7.6.3.5 Patient 5: 906847

Figure 7.28 displays the evolution of the intracardiac organization in LAA. The first CFAEs ablations shifted the detected spikes to the right extremity of the final window center. The CFAEs at the septal region seem to bring a determining improvement of the intracardiac organization. Indeed after CFAEs ablation in the septum regions, all the spikes are detected in the final window center leading the patient to atrial tachaycardia.

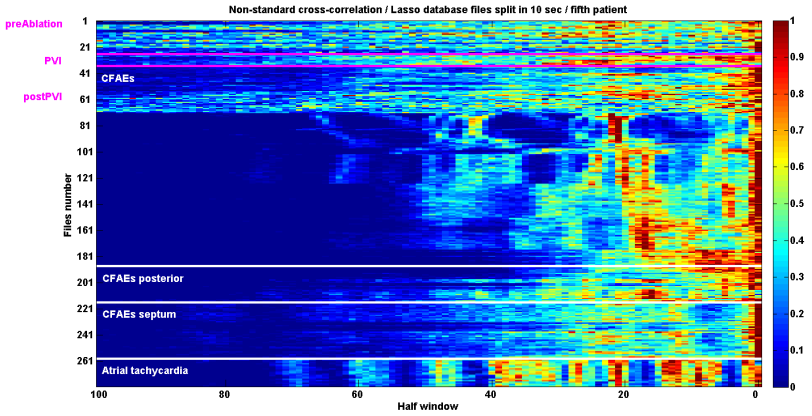

Figure 7.28: *Evolution of the final window during the procedure for the fifth patient.*

7.6.3.6 Patient 6: 2241998

Figure 7.29 displays the cross-correlation evolution via the final window. Globally, there is a constant progression of the intracardiac organization until the flutter. The CFAEs and the LIN ablations significantly improved the intracardiac organization. The detected spikes are more concentrated at the center of the final window.

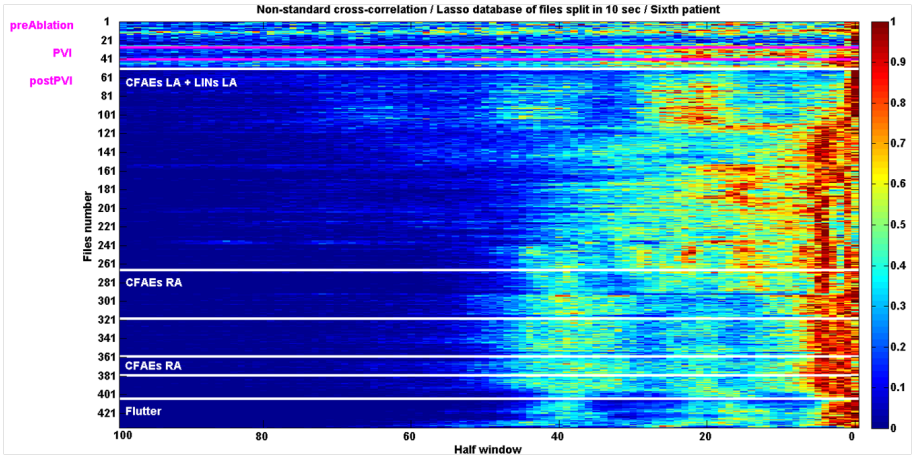

Figure 7.29: *Evolution of the final window during the procedure for the sixth patient.*

7.6.4 Discussion

This method gives concluant results. They reflect well what happened during the medical procedure. The manner how the cross-correlation is computed is very advantageous because it opens the possibility to follow the evolution of the intracardiac organization in the LAA inside a window of a certain width during the entire procedure. It is not the case with a standard computation of the cross-correlation. Moreover, this method can help to identify which ablated region contributed more to terminate AF. Among the results, the ablations at the septal region seem to be very efficient. Very often they improve the intracardiac organization as illustrated on the figure 7.24, 7.27, and 7.28. It is a coincindence? It is less likely that it is just a coincidence because the physicians noticed that the septal region presented a lot of CFAEs and its ablation was generally beneficial for the patients. Therefore, these results seem to confirm what the physicians observed during the medical procedures. The further step of this method would be to investigate the CFAEs signals recorded on the septal region in order to find a possible recurrent pattern which could help to better understand their structural complexity. Finally, it should be very interesting to place also a Lasso catheter in the RAA in order to assess simultaneously the evolution of the intracardiac organization in the RAA and in the LAA during the entire procedure.

7.7 Conclusions

In this chapter, among the diverse developed intracardiac organization indices, two give promising results. The first one was based on the cross-correlation between signals on HRAd and HRAp electrodes while the second one was focused on the cross-correlation of signals from the Lasso electrodes. The results returned by both methods were rather favourable but the experiments were only performed on six patients which is too few in order to perform a statistical analysis.

Chapter 8

Conclusions

8.1 Summary

In the first chapter, the tracking of the dominant frequency (DF) during the procedure was shown to return not conclusive results. The methods developed in this first chapter were not efficient enough to highlight which ablations were the most beneficial for the patient in order to recover a regular rhythm. The best method was the one which computed the DF via the peak detection and the AF cycle length (AFCL). However, it is already the standard method used by physicians during a procedure in order to determine if an improvement of the intracardiac organization takes place after an ablation.

The second part of the project was focused on the variability of the EGM signals. It appeared that the intracardiac variability (ICV) signals were affected by a mechano-electrical contribution of ventricular contractions, which was efficiently removed by an adaptive filtering based on the normalized least-mean square error. The results for the six patients demonstrated that the ICV signals contained about $41\% \pm 6.7\%$ of ventricular activity. Therefore, these promising results open the possibility to develop new intracardiac organization indices from ICV signals devoid of ventricular influence.

Finally, the last part of the projet was centered on the EGM signals and the evolution of their similarity during the ablative procedure. The clipped cross-intensity function as an intracardiac organization index returned very poor results and was certainly not well suited to the EGM signals. However, the method computing the cross-correlation within a window for signals on pairs of catheters returned interesting results, especially the sparseness measure. Indeed, it was possible to judge the efficiency of a particular complex fractionated atrial electrogram (CFAE) ablation on the intracardiac organization according to the sparseness value. Finally, the same method was transposed to the signals of the Lasso electrodes. The image-object containing the successive windows in which the cross-correlation was calculated permitted to assess the evolution of the intracardiac organization during the procedure and localized which part of the ablative protocol was the most beneficial for the patient.

8.2 Outlook

In the short term, a deeper investigation of the CFAEs should be carried on in order to better understand their structure, and to detect a particular pattern which could cluster the CFAEs ablations as "good", "bad" or "neutral".

In the long term, other intracardiac organization indices have to be developed and combined with those presented in this rapport in order to find the best combination of indices, which would predict efficiently if an ablation at a specific location would be beneficial or non beneficial for the patient.

Appendix A

Generation of synthetic EGM signals

A.1 Introduction

Synthetic signals are very helpful in signal processing in order to validate methods before applying them to real data. The advantage is that all parameters of the synthetic signal are known. Therefore, it is possible to predict the outcome and assess the accuracy of a particular method.

A.2 Method

Fischer and al. developed a method to generate synthetic EGM signals [14]. A pulse shape was characterized by a tri-phase morphology obtained as the sum of two triangular pulses with identical areas but opposite sign (see the top and the middle plots of figure A.1). Then, the synthetic pulse was rectified by taking its absolute value as illustrated on the bottom plot of figure A.1.

Finally, an synthetic EGM signal was generated by the convolution between a Dirac comb and a rectified synthetic pulse (see figure A.2). The method include also the possibility to introduce irregular intervals between adjacent pulses. Indeed, the interval between ajacent pulses was computed as the length of the pulse in samples plus a number randomly picked between 0 and a maximal limit defined by the program user.

A.3 Results

Figure A.3 presents a regular synthetic EGM signal generated by the convolution of a Dirac comb and a rectified synthetic pulse. Figure A.4 shows a synthetic EGM signal in which the intervals between adjacent pulses are irregular.

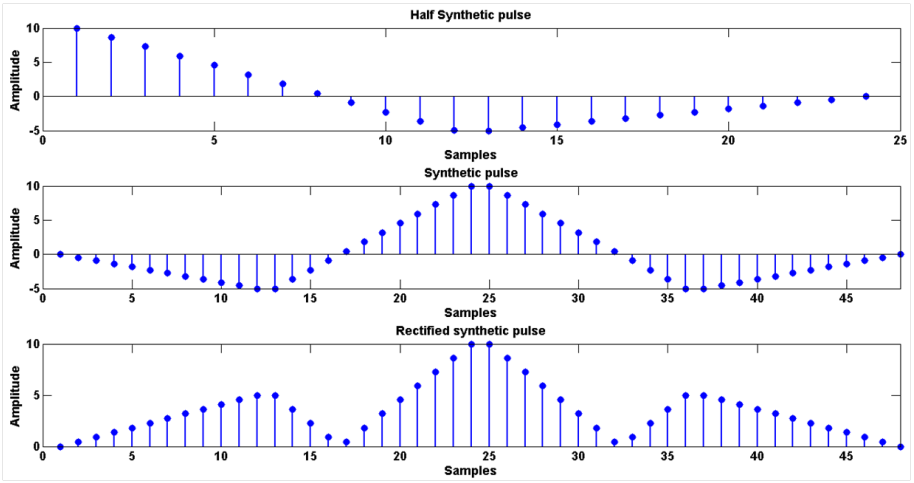

Figure A.1: ***Top:*** *Half synthetic pulse (top).* ***Middle:*** *Synthetic pulse.* ***Bottom:*** *Rectified synthetic pulse.*

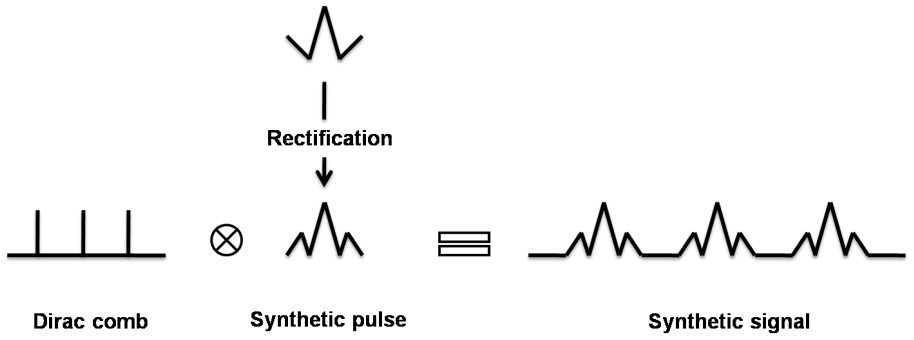

Figure A.2: *Generation of a synthetic EGM signal by the convolution between a Dirac comb and a rectified synthetic pulse.*

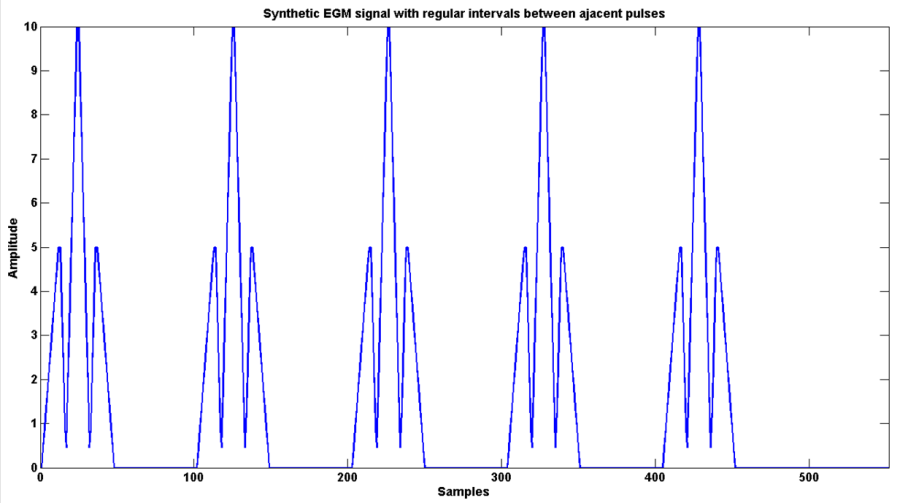

Figure A.3: *Example of the generation of a synthetic EGM signal with regular intervals between adjacent pulses.*

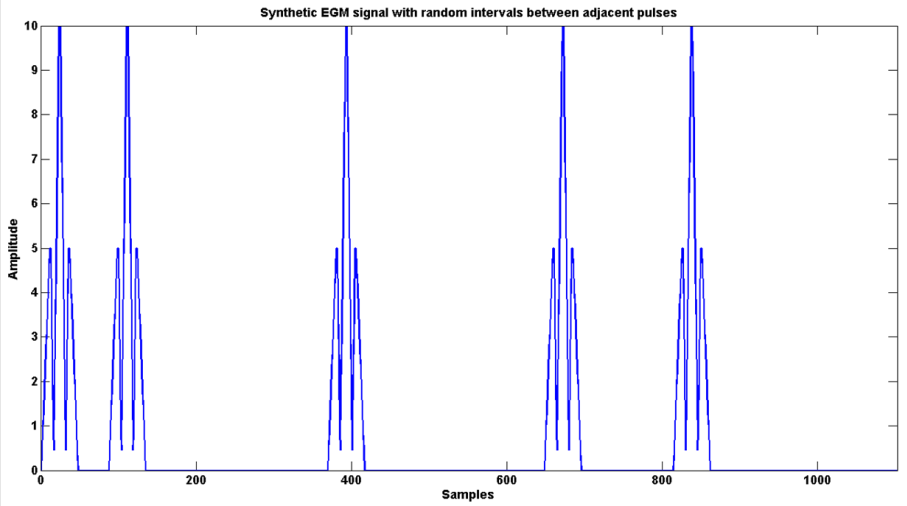

Figure A.4: *Example of the generation of a synthetic signal with irregular intervals between adjacent pulses.*

Bibliography

[1] *http://chen2820.pbworks.com/w/page/11951479/Skeletal-muscle-tissue-engineering*.

[2] *http://ocw.tufts.edu/Content/50/lecturenotes/634463/634544*.

[3] *https://ccrma.stanford.edu/~jos/st/Signal_Metrics.html*.

[4] *http://www.swissheart.ch*.

[5] B. Alberts and al. *Molecular Biology of the Cell*. Garland Science, 4$^{\text{th}}$ edition edition, 2002.

[6] M. A. Allessie and al. Circus movement in rabbit atrial muscle as a mechanism of tachycardia. iii. the "leading circle" concept: a new model of circus movement in cardiac tissue without the involvement of an anatomical obstacle. *Journal of the American Heart Association – Circulation research*, 41:9–18, 1977.

[7] E. J. Benjamin and al. Impact of atrial fibrillation on the risk of death: The framingham heart study. *Journal of the American Heart Association – Circulation research*, 98:946–952, 1998.

[8] GW. Botteron and al. A technique for measurement of the extent of spatial organization of atrial activation during atrial fibrillation in the intact human heart. *Institute of Electrical and Electronics Engineer – Transaction on Biomedical Engineering*, 42:579–586, 1995.

[9] G. L. Botto and al. Atrial fibrillation: the remodelling phenomenon. *European Heart Journal Supplements*, 3:H1–H7, 2003.

[10] A. Buttu and al. Defining ablative strategies for persistent atrial fibrillation based on organization indexes - study protocol. Technical report, Signal Processing Institute - ASPG, 2010.

[11] H. Calkins and al. Hrs/ehra/ecas expert consensus statement on catheter and surgical ablation of atrial fibrillation: Recommendations for personnel, policy, prodedures and follow-up. *Heart Rhythm Society and the European Heart Rhythm Association*, 92:335–379, 2007.

[12] R. Cappato and al. Worlwide survey on the methods, efficacy, and safety of catheter ablation for human atrial fibrillation. *Journal of the American Heart Association – Circulation research*, 111:1100–1105, 2005.

[13] C. S. Elayi and al. Left superior vena cava isolation in patients undergoing pulmonary vein antrum isolation: Impact on atrial fibrillation recurrence. *Journal of the Heart Rhythm*, 3:1019–1023, 2006.

[14] G. Fischer and al. On computing dominant frequency from bipolar intracardiac electrograms. *Institute of Electrical and Electronics Engineer – Transaction on Biomedical Engineering*, 54:165–169, 2007.

[15] A. C. Guyton and J. E. Hall. *Textbook of Medical Physiology.* Elsevier Saunders, 11$^{\text{th}}$ edition edition, 2006.

[16] M. Haïssaguerre and al. Radiofrequency catheter ablation in unusual mechanisms of atrial fibrillation: Report of three cases. *Journal of Cardiovascular Electrophysiology*, 5:743–751, 1994.

[17] M. Haïssaguerre and al. Spontaneous initiation of atrial fibrillation by ectopic beats originating in the pulmonary veins. *The New England Journal of Medicine*, 339:659–666, 1998.

[18] M. Haïssaguerre and al. Catheter ablation of chronic atrial fibrillation targeting the reinitiating triggers. *Journal of Cardiovascular Electrophysiology*, 11:2–10, 2000.

[19] M. Haïssaguerre and al. Changes in atrial fibrillation cycle length and inducibility during catheter ablation and their relation to outcome. *Journal of the American Heart Association – Circulation research*, 109:3007–3013, 2004.

[20] M. Haïssaguerre and al. Impact of catheter ablation of the coronary sinus on paroxysmal or persistent atrial fibrillation. *Journal of Cardiovascular Electrophysiology*, 18:378–386, 2007.

[21] M. Hocini and al. Techniques, evaluation, and consequences of linear block at the left atrial roof in paroxysmal atrial fibrillation: A prospective randomized study. *Journal of the American Heart Association – Circulation research*, 112:3688–3696, 2005.

[22] P. Jais and al. A focal source of atrial fibrillation treated by discrete radiofrequency ablation. *Journal of the American Heart Association – Circulation research*, 95:572–576, 1997.

[23] P. Jais and al. Technique and results of linear ablation at the mitral isthmus. *Journal of the American Heart Association – Circulation research*, 110:2996–3002, 2004.

[24] J. Jalife, , and al. Mechanisms of atrial fibrillation: Mother rotors or multiple daughter wavelets, or both? *Journal of Cardiovascular Electrophysiology*, 9:2–12, 1998.

[25] U. B. Kaupp and R. Seifert. Molecular diversity of pacemker ion channels. *Annual Review of Physiology*, 63:235–257, 2001.

[26] Y. Khaykin. Cost-effectiveness of catheter ablation for atrial fibrillation. *Current Opinion in Cardiology*, 22:11–17, 2007.

[27] R. Mandapati and al. Stable microreentrant sources as a mechanism of atrial fibrillation in the isolated sheep heart. *Journal of the American Heart Association – Circulation research*, 101:194–199, 2000.

[28] M. D. Moe and al. A computer model of atrial fibrillation. *Journal of the American Heart Association*, 67:200–220, 1964.

[29] K. Nademanee and al. A new approach for catheter ablation of atrial fibrillation: Mapping of the electrophysiologic substrate. *Journal of the American College of Cardiology – Electrophysiology*, 43:2044–2053, 2004.

[30] A. Natale and al. Propective randomized comparison of antiarrhythmic therapy versus first-line radiofrequency ablation in patients with atrial flutter. *Journal of the American College of Cardiology*, 35:1898–1904, 2000.

[31] S. Nattel. New ideas about atrial fibrillation 50 years on. *Nature*, 415:219–226, 2002.

[32] P. G. Novak. Effectiveness of catheter ablation versus antiarrhythmic drug therapy for atrial fibrillation. *Current Opinion in Cardiology*, 24:9–17, 2009.

[33] A. R. C. Paiva and al. Spectral clustering of synchronous spike trains. *Institute of Electrical and Electronics Engineers*, 2007.

[34] C. Pappone and al. A randomized trial of circumferential pulmonary vein ablation versus antiarrhytmic drug therapy in paroxysmal atrial fibrillation – the apaf study. *Journal of the American College of Cardiology*, 48:2340–2347, 2006.

[35] A. Perez-Lugones and al. Evidence of specialized conduction cells in human pulmonary veins of patients with atrial fibrillation. *Journal of Cardiovascular Electrophysiology*, 14:803–809, 2003.

[36] L. Sandrini and al. Morphology-based measurement of activation time in human atrial fibrillation. *Computers in Cardiology*, 29:593–596, 2002.

[37] A. J. Shah and al. Comparison of rhythm restoration strategies in paroxysmal atrial fibrillation. *Expert Review of Cardiovascular Therapy*, 8:903–906, 2010.

[38] S. Stewart and al. Population prevalence, incidence, and predictors of atrial fibrillation in the renfrew/paisley study. *Journal of the American Heart Association*, 86:516–521, 2001.

[39] Pr. P. Vandergheynst. Signaux et systèmes – volume 2. Technical report, Laboratoire de Traitement des Signaux, 2007.

[40] A. Verma and al. Why atrial fibrillation ablation should be considered first-line therapy for some patients. *Journal of the American Heart Association – Circulation research*, 112:1214–1222, 2005.

[41] Dr. J.-M. Vesin. Signal processing in biomedical signals. Technical report, Signal Processing Institute - ASPG, 2010.

[42] O. M. Wazni and al. Radiofrequency ablation vs antiarrhythmic drugs as first-line treatment of symptomatic atrial fibrillation – a randomized trial. *Journal of the American Medical Association*, 293:2634–2640, 2005.